Long-term health risk of climate change associated surface PM2.5 concentration variation:

Multiple ACCMIP model data under different emission scenarios (RCP2.6, 4.5, 6.0, 8.5) and population scenarios (SSP1, SSP2, SSP3)

A Thesis Presented for the

Master of Science

Degree

The University of Tennessee, Knoxville

Xiufen Zhu

August 2016

Copyright © 2016 by Xiufen Zhu.

All rights reserved.

ACKNOWLEDGEMENTS

I would like to thank my research group and my advisor Dr. Joshua Fu for their assistance.

ABSTRACT

In this study, multiple models from Atmospheric Chemistry and Climate Model Intercomparison Project (ACCMIP) are utilized to derive the global burden of disease of chronic obstructive pulmonary disease (COPD), lung cancer (LNC), and lower respiratory infection (LRI) derived from surface $PM_{2.5}$ elevation. Various Representative Concentration Pathways and Shared Socio-economic Pathways scenarios are compared as well as various models to deduct the impact from various scenarios. The time series variation and seasonal variation are also illustrated in this study. Multi-model ensemble was conducted to reduce the deviation in model projection output.

Projection shows increase in the population normalized relative risk for COPD, LNC, and LRI disease between 2030 and 2000 for developed countries and northern Africa for various population scenarios using the average value for different emission scenarios from GISS-E2-R model output. MIROC-CHEM actually predicts a much lower normalized PM concentration or relative risk level than GISS-E2-R model. Black carbon adjusted relative risk results show that LNC derived relative risk might be much more sensitive for black carbon compared with COPD or LRI. LAC region is more sensitive to black carbon surface pollution compared with other regions for LRI relative risk.

Dust storms in the Saharan regions can be a major contribution to risk elevation in Saharan and adjacent regions. Australia dust storm in the central Australia can also be responsible to the exposure at coastal areas. The emission increase in East Asia since 1980s can be responsible to the widespread risk elevation in recent years.

Key words: relative risk; $PM_{2.5}$; exposure; region; model; scenario;

TABLE OF CONTENTS

CHAPTER ONE INTRODUCTION AND GENERAL INFORMATION 1
1.1 $PM_{2.5}$ POLLUTION DEFINITION 1
1.3 $PM_{2.5}$ AND ITS RELATED HEALTH IMPACT 1
1.4CLIMATE CHANGE AND EMISSION RELATED $PM_{2.5}$ CAUSED HEALTH IMPACT 2
1.41ACCMIP MODELS 2
1.42 Chronic health impact 3
1.5 GLOBAL BURDEN OF DISEASE STUDIES 3
CHAPTER TWO LITERATURE REVIEW 5
CHAPTER THREE METHODOLOGY 10
3.1 PARTICULATE CONCENTRATION 10
3.2 POPULATION DATASETS 10
3.2.1 SSPs scenarios 10
3.2.2 The advantage of SSPs 11
3.3 $PM_{2.5}$ DERIVED RRS AND MORTALITY BASED UPON IER MODEL 11
3.3.1 RRs value 11
3.3.2 Mortality value 12
3.4 INTEGRATION AND COMPARISON 14
3.4.1 The world regions and related integrated data 14
3.4.2 The reason for using three year average data 14
3.4.3 Time series 14
3.4.4 Comparison 14
3.5 UNCERTAINTY MEASUREMENT 16
3.5.1 Uncertainty in concentration data 16
3.5.2 Uncertainty in population data 17
CHAPTER FOUR RESULTS 18
4.1 SEASONAL DISTRIBUTION OF RR_S FROM GISS-E2-R MODEL OUTPUT 18
4.2 ANNUAL PLOT OF GISS-E2-R MODEL OUTPUT 22
4.3 MIROC-CHEM MODEL OUTPUT 37
4.4 RCP SCENARIO COMPARISON 38
4.5 COMPARISON BETWEEN MODELS 61

4.6 POPULATION VARIANCE BETWEEN MODELS 69
4.7 GRID AVERAGE DATA FROM PRE-INDUSTRIAL TIME TO PRESENT 72
4.8 POPULATION NORMALIZED OUTPUT 72
CHAPTER FIVE CONCLUSION AND RECOMMENDATIONS 95
LIST OF REFERENCES 97
APPENDIX 104
VITA 133

LIST OF TABLES

TABLE 1 POPULATION NORMALIZED $PM_{2.5}$ CONCENTRATION FOR GISS-E2-R MODEL UNDER POPULATION SCENARIO SSP1 AND DIFFERENT RCP SCENARIOS (RCP2.6, RCP4.5, RCP6.0 and RCP8.5) FOR THE TIME PERIOD OF 2000S,2030S,2050S AS MEASURING THE EFFECT OF BOTH POPULATION SCENARIO AND GREENHOUSE GAS EMISSION SCENARIOS UPON REGIONAL DISTRIBUTION OF POPULATION NORMALIZED RELATIVE RISK. 74
TABLE 2 POPULATION NORMALIZED $PM_{2.5}$ CONCENTRATION FOR GISS-E2-R MODEL UNDER POPULATION SCENARIO SSP2 AND DIFFERENT RCP SCENARIOS (RCP2.6, RCP4.5, RCP6.0 and RCP8.5) FOR THE TIME PERIOD OF 2000S,2030S,2050S AS MEASURING THE EFFECT OF BOTH POPULATION SCENARIO AND GREENHOUSE GAS EMISSION SCENARIOS UPON REGIONAL DISTRIBUTION OF POPULATION NORMALIZED RELATIVE RISK. 75
TABLE 3 POPULATION NORMALIZED $PM_{2.5}$ CONCENTRATION FOR MIROC-CHEM MODEL UNDER POPULATION SCENARIO SSP1 AND DIFFERENT RCP SCENARIOS (RCP2.6, RCP6.0 and RCP8.5) FOR THE TIME PERIOD OF 2000S,2030S,2050S AS MEASURING THE EFFECT OF BOTH POPULATION SCENARIO AND GREENHOUSE GAS EMISSION SCENARIOS UPON REGIONAL DISTRIBUTION OF POPULATION NORMALIZED RELATIVE RISK. 76
TABLE 4 POPULATION NORMALIZED COPD RELATIVE RISK FOR GISS-E2-R MODEL UNDER POPULATION SCENARIO SSP1 AND DIFFERENT RCP SCENARIOS (RCP2.6, RCP4.5, RCP6.0 AND RCP8.5) FOR THE TIME PERIOD OF 2000S,2030S,2050S AS MEASURING THE EFFECT OF BOTH POPULATION SCENARIO AND GREENHOUSE GAS EMISSION SCENARIOS UPON REGIONAL DISTRIBUTION OF POPULATION NORMALIZED RELATIVE RISK. 77
TABLE 5 POPULATION NORMALIZED COPD RELATIVE RISK FOR GISS-E2-R MODEL UNDER POPULATION SCENARIO SSP2 AND DIFFERENT RCP SCENARIOS (RCP2.6, RCP4.5, RCP6.0 AND RCP8.5) FOR THE TIME PERIOD OF 2000S,2030S,2050S AS MEASURING THE EFFECT OF BOTH POPULATION SCENARIO AND GREENHOUSE GAS EMISSION SCENARIOS UPON REGIONAL DISTRIBUTION OF POPULATION NORMALIZED RELATIVE RISK. 78
TABLE 6 POPULATION NORMALIZED LNC RELATIVE RISK FOR GISS-E2-R MODEL UNDER POPULATION SCENARIO SSP1 AND DIFFERENT RCP SCENARIOS (RCP2.6, RCP4.5, RCP6.0 AND RCP8.5) FOR THE TIME PERIOD OF 2000S,2030S,2050S AS MEASURING THE EFFECT OF BOTH POPULATION SCENARIO AND GREENHOUSE GAS EMISSION SCENARIOS UPON REGIONAL DISTRIBUTION OF POPULATION NORMALIZED RELATIVE RISK. 80
TABLE 7 POPULATION NORMALIZED LNC RELATIVE RISK FOR GISS-E2-R MODEL UNDER POPULATION SCENARIO SSP2 AND DIFFERENT RCP SCENARIOS (RCP2.6, RCP4.5, RCP6.0 AND RCP8.5) FOR THE TIME PERIOD OF 2000S,2030S,2050S AS MEASURING THE EFFECT OF BOTH POPULATION

SCENARIO AND GREENHOUSE GAS EMISSION SCENARIOS UPON REGIONAL DISTRIBUTION OF POPULATION NORMALIZED RELATIVE RISK. 81
TABLE 8 POPULATION NORMALIZED LRI RELATIVE RISK FOR GISS-E2-R MODEL UNDER POPULATION SCENARIO SSP1 AND DIFFERENT RCP SCENARIOS (RCP2.6, RCP4.5, RCP6.0 AND RCP8.5) FOR THE TIME PERIOD OF 2000S,2030S,2050S AS MEASURING THE EFFECT OF BOTH POPULATION SCENARIO AND GREENHOUSE GAS EMISSION SCENARIOS UPON REGIONAL DISTRIBUTION OF POPULATION NORMALIZED RELATIVE RISK. 82
TABLE 9 POPULATION NORMALIZED LRI RELATIVE RISK FOR GISS-E2-R MODEL UNDER POPULATION SCENARIO SSP2 AND DIFFERENT RCP SCENARIOS (RCP2.6, RCP4.5, RCP6.0 AND RCP8.5) FOR THE TIME PERIOD OF 2000S,2030S,2050S AS MEASURING THE EFFECT OF BOTH POPULATION SCENARIO AND GREENHOUSE GAS EMISSION SCENARIOS UPON REGIONAL DISTRIBUTION OF POPULATION NORMALIZED RELATIVE RISK. 83
TABLE 10 POPULATION NORMALIZED $PM_{2.5}$ CONCENTRATION, COPD RISK, LNC RISK, LRI RISK RESPECTIVELY FOR GISS-E2-R MODEL UNDER POPULATION SCENARIO SSP3 FOR THE TIME PERIOD OF 2000S AS MEASURING THE EFFECT OF BOTH POPULATION SCENARIO AND GREENHOUSE GAS EMISSION SCENARIOS UPON REGIONAL DISTRIBUTION OF POPULATION NORMALIZED RELATIVE RISK. 84
TABLE 11 POPULATION NORMALIZED $PM_{2.5}$ CONCENTRATION, COPD RISK, LNC RISK, LRI RISK RESPECTIVELY FOR GISS-E2-R MODEL UNDER POPULATION SCENARIO SSP3 AND EMISSION SCENARIOS (RCP2.6,RCP4.5,RCP6.0,RCP8.5) FOR THE TIME PERIOD OF 2030S AS MEASURING THE EFFECT OF BOTH POPULATION SCENARIO AND GREENHOUSE GAS EMISSION SCENARIOS UPON REGIONAL DISTRIBUTION OF POPULATION NORMALIZED RELATIVE RISK. 85
TABLE 12 POPULATION NORMALIZED $PM_{2.5}$ CONCENTRATION, COPD RISK, LNC RISK, LRI RISK RESPECTIVELY FOR GISS-E2-R MODEL UNDER POPULATION SCENARIO SSP3 AND EMISSION SCENARIOS (RCP2.6,RCP4.5,RCP6.0,RCP8.5) FOR THE TIME PERIOD OF 2050S AS MEASURING THE EFFECT OF BOTH POPULATION SCENARIO AND GREENHOUSE GAS EMISSION SCENARIOS UPON REGIONAL DISTRIBUTION OF POPULATION NORMALIZED RELATIVE RISK. 86
TABLE 13 POPULATION NORMALIZED $PM_{2.5}$ CONCENTRATION, COPD RISK, LNC RISK, LRI RISK RESPECTIVELY FOR NCAR-CAM5.1 MODEL UNDER POPULATION SCENARIO SSP1,SSP2,SSP3 FOR THE TIME PERIOD OF 2000S AS MEASURING THE EFFECT OF BOTH POPULATION SCENARIO AND GREENHOUSE GAS EMISSION SCENARIOS UPON REGIONAL DISTRIBUTION OF POPULATION NORMALIZED RELATIVE RISK. 89
TABLE 14 POPULATION NORMALIZED BLACK CARBON ADJUSTED NEW $PM_{2.5}$ CONCENTRATION, COPD RISK, LNC RISK, LRI RISK RESPECTIVELY FOR NCAR-CAM5.1 MODEL UNDER POPULATION SCENARIO SSP1 FOR THE TIME PERIOD OF 2000S AS MEASURING THE EFFECT OF BOTH POPULATION SCENARIO AND

GREENHOUSE GAS EMISSION SCENARIOS UPON REGIONAL DISTRIBUTION OF POPULATION NORMALIZED RELATIVE RISK. 90
TABLE 15 COPD MORTALITY FROM GISS-E2-R OUTPUT UNDER POPULATION SCENARIO SSP1, SSP2 and SSP3 FOR THE TIME PERIOD OF 2000S 92
TABLE 16 COPD MORTALITY FROM GISS-E2-R OUTPUT UNDER POPULATION SCENARIO SSP1, SSP2 AND SSP3 FOR THE TIME PERIOD OF 2030S UNDER THE RCP2.6 EMISSION SCENARIO 93
TABLE 17 POPULATION FOR VARIOUS REGIONS IN 2000 PREDICTED BY POPULATION SCENARIOS INCLUDING SSP1, SSP2 AND SSP3 93
TABLE 18 POPULATION FOR VARIOUS REGIONS IN 2030 PREDICTED BY POPULATION SCENARIOS INCLUDING SSP1, SSP2 AND SSP3 94

LIST OF FIGURES

Figure 1 UN regions 15
Figure 2 Global relative risk for cardiopulmonary disease from January to June of the three year average data from 1850 to 1852 with the ambient $PM_{2.5}$ concentration output from GISS-E2-R model based on the integrated risk function developed for GBD(Burnett et al., 2014b) for each figure, vertical axes indicate latitude and horizontal axes indicate longitude. The map plot indicate the monthly level of relative risk over a global terrain by applying the concentration-risk function from IER model for COPD disease endpoint. 19
Figure 3 Global relative risk for cardiopulmonary disease from July to December of the three year average data from 1850 to 1852 with the ambient $PM_{2.5}$ concentration output from GISS-E2-R model based on the integrated risk function developed for GBD(Burnett et al., 2014b) for each figure, vertical axes indicate latitude and horizontal axes indicate longitude. The map plot indicate the monthly level of relative risk over a global terrain by applying the concentration-risk function from IER model for COPD disease endpoint. 20
Figure 4 Global relative risk for cardiopulmonary disease from January to June of the three year average data from 2050 to 2052 with the ambient $PM_{2.5}$ concentration output from GISS-E2-R model based on the integrated risk function developed for GBD(Burnett et al., 2014b) for each figure, vertical axes indicate latitude and horizontal axes indicate longitude. The map plot indicate the monthly level of relative risk over a global terrain by applying the concentration-risk function from IER model for COPD disease endpoint. 23
Figure 5 Global relative risk for cardiopulmonary disease from July to December of the three year average data from 2050 to 2052 with the ambient $PM_{2.5}$ concentration output from GISS-E2-R model based on the integrated risk function developed for GBD(Burnett et al., 2014b) for each figure, vertical axes indicate latitude and horizontal axes indicate longitude. The map plot indicate the monthly level of relative risk over a global terrain by applying the concentration-risk function from IER model for COPD disease endpoint. 24
Figure 6 Global relative risk for cardiopulmonary disease for 6 time periods from 1850s to 1900s with the ambient $PM_{2.5}$ concentration output from GISS-E2-R model based on the integrated risk function developed for GBD(Burnett et al., 2014b) for each figure, vertical axes indicate latitude and horizontal axes indicate longitude. The map plot indicate the level of relative risk over a global terrain by applying the concentration-risk function from IER model for COPD disease endpoint. Note that the Saharan dust regions might present an elevated relative risk all through 6 decades and there is no other obvious increase of risk in other regions. 25
Figure 7 Global relative risk for cardiopulmonary disease for 6 time periods from 1910s to 1960s with the ambient $PM_{2.5}$ concentration output from GISS-E2-R model based on the integrated risk function developed for GBD(Burnett et al., 2014b) for each figure, vertical axes indicate latitude and horizontal axes indicate longitude. The map plot

indicate the level of relative risk over a global terrain by applying the concentration-risk function from IER model for COPD disease endpoint. Note that the peak value might be higher than previous decades. 26
Figure 8 Global relative risk for cardiopulmonary disease for 6 time periods from 1970s to 2020s with the ambient $PM_{2.5}$ concentration output from GISS-E2-R model based on the integrated risk function developed for GBD(Burnett et al., 2014b) for each figure, vertical axes indicate latitude and horizontal axes indicate longitude. The map plot indicate the level of relative risk over a global terrain by applying the concentration-risk function from IER model for COPD disease endpoint. Note that eastern Asia and other parts of Asia are associated with risk elevation since 2000s. 27
Figure 9 Global relative risk for cardiopulmonary disease for 7 time periods from 2030s to 2090s with the ambient $PM_{2.5}$ concentration output from GISS-E2-R model based on the integrated risk function developed for GBD(Burnett et al., 2014b) for each figure, vertical axes indicate latitude and horizontal axes indicate longitude. The map plot indicate the level of relative risk over a global terrain by applying the concentration-risk function from IER model for COPD disease endpoint. Note that the elevation in Asia start to decrease since 2040s with peak value in Saharan and Australia consistent all through the time period. 28
Figure 10 Global relative risk for lung cancer for 6 time periods from 1850s to 1900s with the ambient $PM_{2.5}$ concentration output from GISS-E2-R model based on the integrated risk function developed for GBD(Burnett et al., 2014b) for each figure, vertical axes indicate latitude and horizontal axes indicate longitude. The map plot indicate the level of relative risk over a global terrain by applying the concentration-risk function from IER model for LNC disease endpoint. 29
Figure 11 Global relative risk for lung cancer for 6 time periods from 1910s to 1960s with the ambient $PM_{2.5}$ concentration output from GISS-E2-R model based on the integrated risk function developed for GBD(Burnett et al., 2014b) for each figure, vertical axes indicate latitude and horizontal axes indicate longitude. The map plot indicate the level of relative risk over a global terrain by applying the concentration-risk function from IER model for LNC disease endpoint. 30
Figure 12 Global relative risk for lung cancer for 6 time periods from 1970s to 2020s with the ambient $PM_{2.5}$ concentration output from GISS-E2-R model based on the integrated risk function developed for GBD(Burnett et al., 2014b) for each figure, vertical axes indicate latitude and horizontal axes indicate longitude. The map plot indicate the level of relative risk over a global terrain by applying the concentration-risk function from IER model for LNC disease endpoint. 31
Figure 13 Global relative risk for lung cancer for 7 time periods from 2030s to 2090s with the ambient $PM_{2.5}$ concentration output from GISS-E2-R model based on the integrated risk function developed for GBD(Burnett et al., 2014b) for each figure, vertical axes indicate latitude and horizontal axes indicate longitude. The map plot indicate the level of relative risk over a global terrain by applying the concentration-risk function from IER model for LNC disease endpoint. 32

Figure 14 Global relative risk for lower respiratory infection for 6 time periods from 1850s to 1900s with the ambient $PM_{2.5}$ concentration output from GISS-E2-R model based on the integrated risk function developed for GBD(Burnett et al., 2014b) for each figure, vertical axes indicate latitude and horizontal axes indicate longitude. The map plot indicate the level of relative risk over a global terrain by applying the concentration-risk function from IER model for LRI disease endpoint. 33
Figure 15 Global relative risk for lower respiratory infection for 6 time periods from 1910s to 1960s with the ambient $PM_{2.5}$ concentration output from GISS-E2-R model based on the integrated risk function developed for GBD(Burnett et al., 2014b) for each figure, vertical axes indicate latitude and horizontal axes indicate longitude. The map plot indicate the level of relative risk over a global terrain by applying the concentration-risk function from IER model for LRI disease endpoint. 34
Figure 16 Global relative risk for lower respiratory infection for 6 time periods from 1970s to 2020s with the ambient $PM_{2.5}$ concentration output from GISS-E2-R model based on the integrated risk function developed for GBD(Burnett et al., 2014b) for each figure, vertical axes indicate latitude and horizontal axes indicate longitude. The map plot indicate the level of relative risk over a global terrain by applying the concentration-risk function from IER model for LRI disease endpoint. 35
Figure 17 Global relative risk for lower respiratory infection for 7 time periods from 2030s to 2090s with the ambient $PM_{2.5}$ concentration output from GISS-E2-R model based on the integrated risk function developed for GBD(Burnett et al., 2014b) for each figure, vertical axes indicate latitude and horizontal axes indicate longitude. The map plot indicate the level of relative risk over a global terrain by applying the concentration-risk function from IER model for LRI disease endpoint. 36
Figure 18 Global relative risk annual plot for cardiopulmonary disease from 1850s to 2050s of the three year average data from the ambient $PM_{2.5}$ concentration output from MIROC-CEHM model based on the integrated risk function developed for GBD(Burnett et al., 2014b) for each figure, vertical axes indicate latitude and horizontal axes indicate longitude. The map plot indicate the monthly level of relative risk over a global terrain by applying the concentration-risk function from IER model for COPD disease endpoint. . 39
Figure 19 Global relative risk annual plot for lower respiratory infection disease from 1850s to 2050s of the three year average data from the ambient $PM_{2.5}$ concentration output from MIROC-CEHM model based on the integrated risk function developed for GBD(Burnett et al., 2014b) for each figure, vertical axes indicate latitude and horizontal axes indicate longitude. The map plot indicate the monthly level of relative risk over a global terrain by applying the concentration-risk function from IER model for LRI disease endpoint. 40
Figure 20 Global relative risk annual plot for lung cancer disease from 1850s to 2050s of the three year average data from the ambient $PM_{2.5}$ concentration output from MIROC-CEHM model based on the integrated risk function developed for GBD(Burnett et al., 2014b) for each figure, vertical axes indicate latitude and horizontal axes indicate longitude. The map plot indicate the monthly level of relative risk over a global terrain by applying the concentration-risk function from IER model for LNC disease endpoint. 41

Figure 21 Emissions of main greenhouse gases CO_2, CH_4, N_2O from 2000 to 2100 across all RCPs. The four RCPs, RCP2.6, RCP4.5, RCP6.0, and RCP8.5, refer to a possible range of radiative forcing values in the year 2100 compared with pre-industrial values (+2.6, +4.5, +6.0, and +8.5 W/m^2, respectively) For CO_2 and N_2O, the emission amount increase from 2000 to 2100 from highest to lowest is RCP8.5, RCP6.0, RCP4.5, RCP2.6. For methane emissions, RCP4.5 and RCP 6 share similar trajectory all through the time. 42
Figure 22 RCP scenarios (RCP2.6, RCP6.0, RCP8.5) comparison for $PM_{2.5}$ surface concentration from MIROC-CHEM model output in 2030s. The ambient $PM_{2.5}$ concentration is the three year average of 2030, 2031, 2032 with unit of $\mu g/m^3$. RCP8.5 depicts the worst scenario, especially in Asia. 43
Figure 23 RCP scenarios (RCP2.6, RCP6.0, RCP8.5) comparison for cardiopulmonary disease relative risk from MIROC-CHEM model output in 2030s. The relative risk output is the three year average of 2030, 2031, 2032. RCP8.5 depicts the worst scenario, especially with a widespread elevation in relative risk over Asia. 46
Figure 24 RCP scenarios (RCP2.6, RCP6.0, RCP8.5) comparison for lower respiratory infection disease relative risk from MIROC-CHEM model output in 2030s. The relative risk output is the three year average of 2030, 2031, 2032. RCP8.5 depicts the worst scenario, especially with a widespread elevation in relative risk over Asia. 47
Figure 25 RCP scenarios (RCP2.6, RCP6.0, RCP8.5) comparison for lung cancer relative risk from MIROC-CHEM model output in 2030s. The relative risk output is the three year average of 2030, 2031, 2032. RCP8.5 depicts the worst scenario, especially with a widespread elevation in relative risk over Asia..... 48
Figure 26 RCP scenarios (RCP2.6, RCP6.0, RCP8.5) comparison for $PM_{2.5}$ surface concentration from MIROC-CHEM model output in 2050s. The ambient $PM_{2.5}$ concentration is the three year average of 2050, 2051, 2052 with unit of $\mu g/m^3$. RCP8.5 depicts the worst scenario, especially in Asia. 49
Figure 27 RCP scenarios (RCP2.6, RCP6.0, RCP8.5) comparison for cardiopulmonary disease relative risk from MIROC-CHEM model output in 2050s. The relative risk output is the three year average of 2050, 2051, 2052. RCP8.5 depicts the worst scenario, especially with a widespread elevation in relative risk over Asia. 50
Figure 28 RCP scenarios (RCP2.6, RCP6.0, RCP8.5) comparison for lung cancer relative risk from MIROC-CHEM model output in 2050s. The relative risk output is the three year average of 2050, 2051, 2052. RCP8.5 depicts the worst scenario, especially with a widespread elevation in relative risk over Asia..... 51
Figure 29 RCP scenarios (RCP2.6, RCP6.0, RCP8.5) comparison for lower respiratory infection relative risk from MIROC-CHEM model output in 2050s. The relative risk output is the three year average of 2050, 2051, 2052. RCP8.5 depicts the worst scenario, especially with a widespread elevation in relative risk over Asia. 52
Figure 30 RCP scenarios (RCP2.6, RCP4.5, RCP6.0, RCP8.5) comparison for $PM_{2.5}$ concentration (unit:$\mu g/m^3$) from GISS-E2-R model output in 2030s. The relative risk output is the three year average of 2030, 2031, 2032. 53

Figure 31 RCP scenarios (RCP2.6, RCP4.5, RCP6.0, RCP8.5) comparison for cardiopulmonary disease relative risk from GISS-E2-R model output in 2030s. The relative risk output is the three year average of 2030, 2031, 2032. RCP6.0 scenario predicts the highest risk level in eastern Asia. 54
Figure 32 RCP scenarios (RCP2.6, RCP4.5, RCP6.0, RCP8.5) comparison for lung cancer relative risk from GISS-E2-R model output in 2030s. The relative risk output is the three year average of 2030, 2031, 2032. RCP6.0 scenario predicts the highest risk level in eastern Asia. 55
Figure 33 RCP scenarios (RCP2.6, RCP4.5, RCP6.0, RCP8.5) comparison for lower respiratory infection disease relative risk from GISS-E2-R model output in 2030s. The relative risk output is the three year average of 2030, 2031, 2032. RCP6.0 scenario predicts the highest risk level in eastern Asia. 56
Figure 34 RCP scenarios (RCP2.6, RCP4.5, RCP6.0.0, RCP8.5) comparison for $PM_{2.5}$ concentration (unit: $\mu g/m^3$) from GISS-E2-R model output in 2050s. The relative risk output is the three year average of 2050, 2051, 2052. 57
Figure 35 RCP scenarios (RCP2.6, RCP4.5, RCP6.0.0, RCP8.5) comparison for cardiopulmonary disease relative risk from GISS-E2-R model output in 2050s. The relative risk output is the three year average of 2050, 2051, 2052. RCP6.0.0 scenario predicts the highest risk level in eastern Asia. 58
Figure 36 RCP scenarios (RCP2.6, RCP4.5, RCP6.0.0, RCP8.5) comparison for lung cancer disease relative risk from GISS-E2-R model output in 2050s. The relative risk output is the three year average of 2050, 2051, 2052. RCP6.0.0 scenario predicts the highest risk level in eastern Asia. 59
Figure 37 RCP scenarios (RCP2.6, RCP4.5, RCP6.0.0, RCP8.5) comparison for lower respiratory infection relative risk from GISS-E2-R model output in 2050s. The relative risk output is the three year average of 2050, 2051, 2052. RCP6.0.0 scenario predicts the highest risk level in eastern Asia. 60
Figure 38 The comparison of ambient $PM_{2.5}$ concentration between various models (CICERO-OsloCTM2, MIROC-CHEM, NCAR-CAM3.5, NCAR-CAM5.1 and GISS-E2-R) in 1850s. CICERO-OsloCTM2 predicts surface concentration in an obvious different way compared with other models while NCAR-CAM3.5 has a generally higher prediction. 61
Figure 39 multi-ensemble results for COPD relative risk for 1850s with the unweighted average of cardiopulmonary relative risk from models including MIROC-CHEM, NACR-CAM3.5, NCAR-CAM5.1 and GISS-E2-R. 62
Figure 40 multi-ensemble results for LNC relative risk for 1850s with the unweighted average of lung cancer relative risk from models including MIROC-CHEM, NACR-CAM3.5, NCAR-CAM5.1 and GISS-E2-R. 62
Figure 41 Multi-ensemble results for lower respiratory infection relative risk for 1850s with the unweighted average of lung cancer relative risk from models including MIROC-CHEM, NACR-CAM3.5, NCAR-CAM5.1 and GISS-E2-R. 63
Figure 42 The comparison of ambient $PM_{2.5}$ concentration between various models (CICERO-OsloCTM2, MIROC-CHEM, NCAR-CAM3.5, NCAR-CAM5.1, GISS-E2-R,

GFDL-AM3) in 2000s. CICERO-OsloCTM2 predicts surface concentration in an obvious different way compared with other models while GFDL-AM3 has a generally higher prediction..... 64
Figure 43 Multi-ensemble results for cardiopulmonary disease relative risk for 2000s with the unweighted average from models including MIROC-CHEM, NACR-CAM3.5, NCAR-CAM5.1, GISS-E2-R and GFDL-AM3. 65
Figure 44 Multi-ensemble results for lung cancer relative risk for 2000s with the unweighted average output from models including MIROC-CHEM, NACR-CAM3.5, NCAR-CAM5.1, GISS-E2-R and GFDL-AM3. 66
Figure 45 Multi-ensemble results for lower respiratory infection relative risk for 2000s with the unweighted average output from models including MIROC-CHEM, NACR-CAM3.5, NCAR-CAM5.1, GISS-E2-R and GFDL-AM3. 66
Figure 46 Multi-ensemble results for dust concentration for 2000s with the unweighted average from models including MIROC-CHEM, NACR-CAM3.5, NCAR-CAM5.1, GISS-E2-R and GFDL-AM3. 67
Figure 47 The variance of the prediction of ambient $PM_{2.5}$ concentration derived relative risk for cardiopulmonary disease, lung cancer and lower respiratory infection between various models (MIROC-CHEM,NCAR-CAM3.5,NCAR-CAM5.1,GISS-E2-R) in 1850s. Higher variance value would indicate a more spread out status of various models. It is worth noticing that lower respiratory infection relative risk has a much higher variance level than other disease endpoints, which means that there would be more uncertainty coming from LRI relative risk output from model difference. 70
Figure 48 The variance of the prediction of ambient $PM_{2.5}$ concentration derived relative risk for cardiopulmonary disease, lung cancer and lower respiratory infection between various models (MIROC-CHEM,NCAR-CAM3.5,NCAR-CAM5.1,GISS-E2-R) in 2000s. Higher variance value would indicate a more spread out status of various models. 71
Figure 49 Grid averaged COPD relative risk value for GISS-E2-R from 1850s to 2010s. Grid average is a depiction of how the relative risk level has developed globally since preindustrial times. There is a general increasing trend since pre-industrial times. 73
Figure 52 Global relative risk for lung cancer from January to June of the three year average data from 1850 to 1852 with the ambient $PM_{2.5}$ concentration output from GISS-E2-R model based on the integrated risk function developed for GBD(Burnett et al., 2014b) for each figure, vertical axes indicate latitude and horizontal axes indicate longitude. The map plot indicate the monthly level of relative risk over a global terrain by applying the concentration-risk function from IER model for LNC disease endpoint. .. 105
Figure 53 Global relative risk for lung cancer from July to December of the three year average data from 1850 to 1852 with the ambient $PM_{2.5}$ concentration output from GISS-E2-R model based on the integrated risk function developed for GBD(Burnett et al., 2014b) for each figure, vertical axes indicate latitude and horizontal axes indicate longitude. The map plot indicate the monthly level of relative risk over a global terrain by applying the concentration-risk function from IER model for LNC disease endpoint. .. 106
Figure 50 Global relative risk for lower respiratory infection disease from January to June of the three year average data from 1850 to 1852 with the ambient $PM_{2.5}$

concentration output from GISS-E2-R model based on the integrated risk function developed for GBD(Burnett et al., 2014b) for each figure, vertical axes indicate latitude and horizontal axes indicate longitude. The map plot indicate the monthly level of relative risk over a global terrain by applying the concentration-risk function from IER model for LRI disease endpoint. 107
Figure 51 Global relative risk for cardiopulmonary disease from July to December of the three year average data from 1850 to 1852 with the ambient $PM_{2.5}$ concentration output from GISS-E2-R model based on the integrated risk function developed for GBD(Burnett et al., 2014b) for each figure, vertical axes indicate latitude and horizontal axes indicate longitude. The map plot indicate the monthly level of relative risk over a global terrain by applying the concentration-risk function from IER model for LRI disease endpoint. 108
Figure 54 Global relative risk for cardiopulmonary disease from January to June of the three year average data from 1860 to 1862 with the ambient $PM_{2.5}$ concentration output from GISS-E2-R model based on the integrated risk function developed for GBD(Burnett et al., 2014b) for each figure, vertical axes indicate latitude and horizontal axes indicate longitude. The map plot indicate the monthly level of relative risk over a global terrain by applying the concentration-risk function from IER model for COPD disease endpoint. 109
Figure 55 Global relative risk for cardiopulmonary disease from July to December of the three year average data from 1860 to 1862 with the ambient $PM_{2.5}$ concentration output from GISS-E2-R model based on the integrated risk function developed for GBD(Burnett et al., 2014b) for each figure, vertical axes indicate latitude and horizontal axes indicate longitude. The map plot indicate the monthly level of relative risk over a global terrain by applying the concentration-risk function from IER model for COPD disease endpoint. 110
Figure 56 Global relative risk for lung cancer from January to June of the three year average data from 1860 to 1862 with the ambient $PM_{2.5}$ concentration output from GISS-E2-R model based on the integrated risk function developed for GBD(Burnett et al., 2014b) for each figure, vertical axes indicate latitude and horizontal axes indicate longitude. The map plot indicate the monthly level of relative risk over a global terrain by applying the concentration-risk function from IER model for LNC disease endpoint. .. 111
Figure 57 Global relative risk for lung cancer from July to December of the three year average data from 1860 to 1862 with the ambient $PM_{2.5}$ concentration output from GISS-E2-R model based on the integrated risk function developed for GBD(Burnett et al., 2014b) for each figure, vertical axes indicate latitude and horizontal axes indicate longitude. The map plot indicate the monthly level of relative risk over a global terrain by applying the concentration-risk function from IER model for LNC disease endpoint. .. 112
Figure 58 Global relative risk for lower respiratory infection disease from January to June of the three year average data from 1860 to 1862 with the ambient $PM_{2.5}$ concentration output from GISS-E2-R model based on the integrated risk function developed for GBD(Burnett et al., 2014b) for each figure, vertical axes indicate latitude and horizontal axes indicate longitude. The map plot indicate the monthly level of

relative risk over a global terrain by applying the concentration-risk function from IER model for LRI disease endpoint..... 113
Figure 59 Global relative risk for lower respiratory infection disease from July to December of the three year average data from 1860 to 1862 with the ambient $PM_{2.5}$ concentration output from GISS-E2-R model based on the integrated risk function developed for GBD(Burnett et al., 2014b) for each figure, vertical axes indicate latitude and horizontal axes indicate longitude. The map plot indicate the monthly level of relative risk over a global terrain by applying the concentration-risk function from IER model for LRI disease endpoint..... 114
Figure 60 Global relative risk for cardiopulmonary disease from January to June of the three year average data from 2000 to 2002 with the ambient $PM_{2.5}$ concentration output from GISS-E2-R model based on the integrated risk function developed for GBD(Burnett et al., 2014b) for each figure, vertical axes indicate latitude and horizontal axes indicate longitude. The map plot indicate the monthly level of relative risk over a global terrain by applying the concentration-risk function from IER model for COPD disease endpoint. 115
Figure 61 Global relative risk for cardiopulmonary disease from July to December of the three year average data from 2000 to 2002 with the ambient $PM_{2.5}$ concentration output from GISS-E2-R model based on the integrated risk function developed for GBD(Burnett et al., 2014b) for each figure, vertical axes indicate latitude and horizontal axes indicate longitude. The map plot indicate the monthly level of relative risk over a global terrain by applying the concentration-risk function from IER model for COPD disease endpoint. 116
Figure 62 Global relative risk for lung cancer from January to June of the three year average data from 2000 to 2002 with the ambient $PM_{2.5}$ concentration output from GISS-E2-R model based on the integrated risk function developed for GBD(Burnett et al., 2014b) for each figure, vertical axes indicate latitude and horizontal axes indicate longitude. The map plot indicate the monthly level of relative risk over a global terrain by applying the concentration-risk function from IER model for LNC disease endpoint. .. 117
Figure 63 Global relative risk for lung cancer from July to December of the three year average data from 2000 to 2002 with the ambient $PM_{2.5}$ concentration output from GISS-E2-R model based on the integrated risk function developed for GBD(Burnett et al., 2014b) for each figure, vertical axes indicate latitude and horizontal axes indicate longitude. The map plot indicate the monthly level of relative risk over a global terrain by applying the concentration-risk function from IER model for LNC disease endpoint. .. 118
Figure 64 Global relative risk for lower respiratory infection from January to June of the three year average data from 2000 to 2002 with the ambient $PM_{2.5}$ concentration output from GISS-E2-R model based on the integrated risk function developed for GBD(Burnett et al., 2014b) for each figure, vertical axes indicate latitude and horizontal axes indicate longitude. The map plot indicate the monthly level of relative risk over a global terrain by applying the concentration-risk function from IER model for LRI disease endpoint. 119

Figure 65 Global relative risk for lower respiratory infection from July to December of the three year average data from 2000 to 2002 with the ambient $PM_{2.5}$ concentration output from GISS-E2-R model based on the integrated risk function developed for GBD(Burnett et al., 2014b) for each figure, vertical axes indicate latitude and horizontal axes indicate longitude. The map plot indicate the monthly level of relative risk over a global terrain by applying the concentration-risk function from IER model for LRI disease endpoint. 120
Figure 66 Global relative risk for cardiopulmonary disease from January to June of the three year average data from 2030 to 2032 with the ambient $PM_{2.5}$ concentration output from GISS-E2-R model based on the integrated risk function developed for GBD(Burnett et al., 2014b) for each figure, vertical axes indicate latitude and horizontal axes indicate longitude. The map plot indicate the monthly level of relative risk over a global terrain by applying the concentration-risk function from IER model for COPD disease endpoint. 121
Figure 67 Global relative risk for cardiopulmonary disease from July to December of the three year average data from 2030 to 2032 with the ambient $PM_{2.5}$ concentration output from GISS-E2-R model based on the integrated risk function developed for GBD(Burnett et al., 2014b) for each figure, vertical axes indicate latitude and horizontal axes indicate longitude. The map plot indicate the monthly level of relative risk over a global terrain by applying the concentration-risk function from IER model for COPD disease endpoint. 122
Figure 68 Global relative risk for lung cancer from January to June of the three year average data from 2030 to 2032 with the ambient $PM_{2.5}$ concentration output from GISS-E2-R model based on the integrated risk function developed for GBD(Burnett et al., 2014b) for each figure, vertical axes indicate latitude and horizontal axes indicate longitude. The map plot indicate the monthly level of relative risk over a global terrain by applying the concentration-risk function from IER model for LNC disease endpoint. .. 123
Figure 69 Global relative risk for lung cancer from July to December of the three year average data from 2030 to 2032 with the ambient $PM_{2.5}$ concentration output from GISS-E2-R model based on the integrated risk function developed for GBD(Burnett et al., 2014b) for each figure, vertical axes indicate latitude and horizontal axes indicate longitude. The map plot indicate the monthly level of relative risk over a global terrain by applying the concentration-risk function from IER model for LNC disease endpoint. .. 124
Figure 70 Global relative risk for lower respiratory infection from January to June of the three year average data from 2030 to 2032 with the ambient $PM_{2.5}$ concentration output from GISS-E2-R model based on the integrated risk function developed for GBD(Burnett et al., 2014b) for each figure, vertical axes indicate latitude and horizontal axes indicate longitude. The map plot indicate the monthly level of relative risk over a global terrain by applying the concentration-risk function from IER model for LRI disease endpoint. 125
Figure 71 Global relative risk for lower respiratory infection from July to December of the three year average data from 2030 to 2032 with the ambient $PM_{2.5}$ concentration output from GISS-E2-R model based on the integrated risk function developed for

GBD(Burnett et al., 2014b) for each figure, vertical axes indicate latitude and horizontal axes indicate longitude. The map plot indicate the monthly level of relative risk over a global terrain by applying the concentration-risk function from IER model for LRI disease endpoint. 126
Figure 72 Global relative risk for lung cancer from January to June of the three year average data from 2050 to 2052 with the ambient $PM_{2.5}$ concentration output from GISS-E2-R model based on the integrated risk function developed for GBD(Burnett et al., 2014b) for each figure, vertical axes indicate latitude and horizontal axes indicate longitude. The map plot indicate the monthly level of relative risk over a global terrain by applying the concentration-risk function from IER model for LNC disease endpoint. .. 127
Figure 73 Global relative risk for lung cancer from July to December of the three year average data from 2050 to 2052 with the ambient $PM_{2.5}$ concentration output from GISS-E2-R model based on the integrated risk function developed for GBD(Burnett et al., 2014b) for each figure, vertical axes indicate latitude and horizontal axes indicate longitude. The map plot indicate the monthly level of relative risk over a global terrain by applying the concentration-risk function from IER model for LNC disease endpoint. .. 128
Figure 74 Global relative risk for lower respiratory infection from January to June of the three year average data from 2050 to 2052 with the ambient $PM_{2.5}$ concentration output from GISS-E2-R model based on the integrated risk function developed for GBD(Burnett et al., 2014b) for each figure, vertical axes indicate latitude and horizontal axes indicate longitude. The map plot indicate the monthly level of relative risk over a global terrain by applying the concentration-risk function from IER model for LRI disease endpoint. 129
Figure 75 Global relative risk for lower respiratory infection from July to December of the three year average data from 2050 to 2052 with the ambient $PM_{2.5}$ concentration output from GISS-E2-R model based on the integrated risk function developed for GBD(Burnett et al., 2014b) for each figure, vertical axes indicate latitude and horizontal axes indicate longitude. The map plot indicate the monthly level of relative risk over a global terrain by applying the concentration-risk function from IER model for LRI disease endpoint. 130

CHAPTER ONE
INTRODUCTION AND GENERAL INFORMATION

1.1 $PM_{2.5}$ POLLUTION DEFINITION

$PM_{2.5}$ is defined as air pollutants with a diameter of 2.5 micrometers or less. The small sizes makes $PM_{2.5}$ penetrable and able to invade even the smallest airways of respiratory systems so as to cause related health impact among human beings.

The ground level $PM_{2.5}$ concentration has increased since preindustrial times along with the severity of $PM_{2.5}$ pollution in the current era due to the anthological emissions associated with population growth and excessive emission from human activities.

1.3 $PM_{2.5}$ AND ITS RELATED HEALTH IMPACT

In recent years, $PM_{2.5}$ has been found to be associated with a large variety of health problems including premature mortality. EPA standards suggest that $PM_{2.5}$ should be controlled under 12 $\mu g/m^3$ annually and 35 $\mu g/m^3$ daily to avoid adverse health impact. However, adverse health impact has been found to be associated with fine particulate pollution even with pollution level lower than the EPA suggestion level. (Shi et al., 2015) $PM_{2.5}$ has been found to be linked to 3.3 million annual premature mortality over a global range in 2010. (Lelieveld et. al., 2015)

In our study, the global burden of disease (GBD) assessment is applied to address the premature mortality derived from global $PM_{2.5}$ model data and the adverse health impact is assumed to be only associated with the mass concentration of $PM_{2.5}$ as source effect is not considered. Such assumptions can be seen as plausible for GBD studies as in Burnett's study, the mass concentration is the main factor taken into consideration. To further address such problems, the black carbon (BC) data might be regarded as an additional indicator of health impact to adjust the toxicity of fine particles according to Janssen's study. (Janssen et al., 2011)

Primarily short term health impact is vastly examined and discussed from case studies or cohort studies. Linkage between $PM_{2.5}$ exposure and acute diseases is verified in

many studies. For example, Ischemic heart disease (IHD) was found to be associated with short-term exposure to fine particulates. (Pope et al., 2006) BenMAP-CE is a tool developed and promoted by US-EPA to calculate the air pollution related acute health impact over the terrain of US and China by selected C-R functions from various references.

Compared with PM_{10}(particles with diameter smaller than 10 micrometer) or TSP(total suspend particle), $PM_{2.5}$ is a good indicator of health impact since the fine particles are more penetrable to lung cells and enter bloodstreams compared with coarser particles. In a cohort study in Shanghai, particles with diameter ranging from 2.5 to 10 μm, health impact is attenuated and less precise while $PM_{2.5}$ is statistically significant in adverse health impact. (Kan et al., 2007)

1.4CLIMATE CHANGE AND EMISSION RELATED $PM_{2.5}$ CAUSED HEALTH IMPACT

The severity of $PM_{2.5}$ in current years has been recognized and emphasized by multiple studies and with interests in addressing the future $PM_{2.5}$ induced adverse health impact, especially premature mortality, to examine how far climate change alone would bring us regarding this problem.

The Atmospheric Chemistry and Climate Model Intercomparison Project (ACCMIP) utilizes the new observation added to atmospheric chemistry to optimize the simulations of tropospheric ozone and aerosols. The modeled data from ACCMIP is used to calculate the $PM_{2.5}$ mass concentration derived relative risk and premature mortality from pre-industrial time to the future era.

1.41ACCMIP MODELS

GFDL-AM3 is utilized to examine the $PM_{2.5}$ concentration related health impact from 1850 to 2000 in Fang's study and it is found that the $PM_{2.5}$ concentration change during industrial period is mainly caused by changes in direct emission. (Fang et. al., 2013) GISS-E2-R is utilized to analyze the future $PM_{2.5}$ variation compared with baseline including pre-industrial time and present day in the Beijing-Tianjin-Hebei (Jing-Jin-Ji)

area with four different emission scenarios. (Jie et. al., 2016) Among ACCMIP models, NCAR-CAM5.1 and GISS-E2-R-TOMAS have the most extensive description of aerosols compared with other models that can be used in this study. GISS-E2-R includes the data from 1850 to 2100 for each year, so it is the most continuous data from the model in ACCMIP. This advantage helps to assist in the studies of Jing-jin-ji area concentration projection.

The number of aerosol particle as well as the mass of each component are represented by internally-mixed log-normal modes in NCAR- CAM5.1. While aerosol is represented by 108 size-resolved aerosol tracers plus three bulk aerosol-phase tracers in 12-size bins ranging from 10nm to 10μm in dry diameter in GISS-E2-R. The LMDzORINCA model simulates the distribution of aerosols by superposition of log-normal modes. All other models use the bulk approach to calculate $PM_{2.5}$. (Lamarque et al., 2013)

1.42 Chronic health impact

Long-term exposure has also been proved to cause health impact when short-term health impact is excluded from a case study in the Schwartz's study. (Schwartz, 2000) While most available health impact studies use short-term functions, it should be worth noticing that air pollution exposure can take effect after days. A following-up cohort study suggests the association between chronic exposure and mortality rates for six cities over a 35 year range.(Lepeule et. al., 2012) Chronic health impact is not researched enough in previous studies compared with acute health impact. However, chronic health impact has been associated with decreasing lung function in young adults. (Tager et al., 2005) So it would be important to assess chronic health impact as well to add to the existing references.

1.5 GLOBAL BURDEN OF DISEASE STUDIES

Global burden of disease (GBD) was first launched by World Bank and World Health Organization in 1991 to close the gap between global challenges and lack of source information. The GBD study provides a systemic approach to appraise information for each condition in a critical way. (Murray et. al., 2013) Projection of future GBD is

projected from 1990 to 2020 in Murray's study as to help with decision making. (Murray et. al., 1997) GBD provides the information of the morbidity or mortality over a global range derived from air pollution so as to assess the impact over a global range. GBD results can also provide insight into specific regional problems by providing the spatial distribution of risk or mortality. Population distribution is considered as well as air pollution concentration in GBD assessment of outdoor premature mortality.(Brauer et al., 2012) In conclusion, GDB studies can be helpful in decision making and there is still a lack of comprehensive air pollution derived premature mortality over a long time range.

CHAPTER TWO
LITERATURE REVIEW

Ambient fine particles ($PM_{2.5}$), defined as particles less than 2.5 microns in aerodynamic diameter, is found to be associated with daily mortality and cardiovascular mortality from a study conducted in Shanghai. The compositions of $PM_{2.5}$ include sulfate, nitrate, organic carbon, elemental carbon, dust and biological materials while PM_{10} is mainly composed of crustal material and primary organic materials. Although PM_{10} is also listed as a critical pollutant, the results of this study actually indicate that there is no significant association between $PM_{10-2.5}$ and mortality. So it is logical and plausible to establish $PM_{2.5}$ as an indicator of particle health impact. (Kan et al., 2007) The starting concentration for the all six cities were less than 18 $\frac{\mu g}{m^3}$ and each increase of 10 in $PM_{2.5}$ is found to be associate with an increase of 14% in all-cause mortality, 26% in cardiovascular mortality and 37% in lung-cancer mortality. As concentration vary from 8 to 15, the relation between chronic exposure to $PM_{2.5}$ and all-cause, cardiovascular or lung-cancer mortality is found to be linear. (Lepeule et. al., 2012) From the meta-analysis results from short-term exposure to fine particulate matter, SO_4^{2-}, NO_3^-, EC and OC are found to be positively associated with the increase in all cause, cardiovascular and respiratory mortality with carbon being most strongly associated. (1.3% per $\mu g/m^3$) (Atkinson et. al., 2014)

Anthological activities have influenced air pollution and related health impact since preindustrial times. This paper intends to look into the air pollution changes in the field of fine particulate matter, or more specifically $PM_{2.5}$, since preindustrial times that can be attributed to anthological activities. Multiple models from the ACCMIP datasets are used for the results comparison. Silvia's paper looks into the global mortality changes due to ozone and fine particulate matter concentration changes attributed from both emission variation and climate change since preindustrial times. Concentration is modeled by an ensemble of chemistry-climate models and Concentration response functions(CRFs) are selected from American Chemical Society(ACS) studies to calculate the global burden of disease distribution of air pollution related premature

death. The results indicate that there are 470,000 premature respiratory resulted from ozone and 2.1 million $PM_{2.5}$ related cardiorespiratory disease (93%) and lung cancer (7%) mortality. It indicates that climate change might have little influence on global mortality. Silvia's study estimated the mortality at a higher accuracy using 1,850 air pollution modelling results instead of counterfactual low concentrations. But the CRFs might cause additional deviation or uncertainty compared with integrated risk functions when it comes to GBD calculation as the CRFs were originally used for America terrain. There is large variation among different models. $PM_{2.5}$ related mortality is widespread in heavily populated regions including East Asia, India, Southeast Asia, Europe and Former Soviet Union. One model (HadGEM2) estimates -283,000 deaths from $PM_{2.5}$ decreases from climate change while the whole 5 models estimate 2,200 climate change related mortality. The multi-model median mortality is 61,000 annual deaths and would rise to 74,000 if HadGEM2 is excluded from the calculation. (Silva et al., 2013)

In Cohen's study (Cohen et al., 2006), mortality from PM exposure was studied for all fourteen WHO regions with economic, meteorological and demographic data from 304 cities in the year of 2000. Years lost is utilized to calculate the burden of disease from mortality from cardiopulmonary diseases and lung cancer in adults, together with acute respiratory infection of school children as the estimation is made based upon US cohort study derived risk coefficients. It is assumed in the study that there is a linear association between death risk and $PM_{2.5}$ mass concentration ranging from 7.5 to 50μg/m^3. Uncertainty might come from such assumption regarding both the response curve shape and counterfactual level. For COPD, LC and ARI there are 3%, 5%, 1% mortality contribution over a global horizon and those three diseases contribute up to 0.8 million premature death and 6.4 million years lost overall. The developing Asia takes up two thirds of the global burden of outdoor air pollution. Cohen's study includes only urban area and excludes ozone impacts, thus might underestimating the $PM_{2.5}$ health effect.

In Anenberg's paper (Anenberg et. al., 2010), long-term relative risk functions for ozone and $PM_{2.5}$ from epidemiology literature are utilized to simulate concentration instead of

using measurement data. Measurement data may not include rural areas and assumptions may be required for background air pollution. The results indicate that 3.5 ± 0.9 million cardiopulmonary and $220{,}000 \pm 80{,}000$ lung cancer mortalities (30 ± 7.6 million years of life lost) might be attributed to anthropogenic $PM_{2.5}$ annually. Difference in methodology lead to 50% difference in $PM_{2.5}$ mortality estimation compared with previous measurement derived results and that might be another reason why we should expand the simulation studies. Observations show that there is an increase of background concentration in remote regions since preindustrial times. A global atmospheric chemical transport model is used to estimate mortality even for regions with sparse air quality measurements. Anthropogenic air pollution is defined as the changes in pollution concentration between preindustrial and present levels. The health impact functions assume that there is a log-linear relationship between relative risk (RR) and concentration. The RR function for $PM_{2.5}$ is from Krewski's study(Krewski et al., 2009) with reanalysis of ACS studies. MOZART-2 is used to simulate pollutant concentration with a resolution of $2.8° \times 2.8°$. $PM_{2.5}$ is defined as SO_4+NO_3+BC+1.4*OC with the assumption of unchanged concentration of dust, sea salt and secondary organic aerosols.

According to Pope's study (Pope et al., 2011), for lung-cancer mortality there is a nearly linear association reaching RRs>40. When $PM_{2.5}$ concentration is low, cardiovascular disease accounts for higher proportion of mortality while lung cancer is more important when concentration is high. In Apte's study (Apte et. al., 2015), 10 km global data is used for pollutant concentration and IER functions developed for global burden of disease 2010 is utilized to estimate the attributable mortality effect from regional and global air quality improvement. In relatively clean regions, modest improvement would have large effect. While being in more polluted areas, major improvements would be required to substantially reduce $PM_{2.5}$ derived mortality. Five diseases including IHD, stroke, COPD, LC, ALRI account for 20.1 million deaths in 2010.

In Wu's paper (Wu et al., 2016), GISS-E2-R model was utilized for the relative change in PM2.5 concentration from preindustrial time to future era. The results indicate that for Jing-Jin-Ji area, which is located in China, will experience $PM_{2.5}$ peak in 2020-2040. J.

Lelieveld's study (Lelieveld et. al., 2015) illustrates that the premature deaths derived from $PM_{2.5}$ pollution is predominant in Asia, especially India and China. There is also an increasing trend of mortality as it would double by 2050 based on a business-as-usual emission scenario. In Lelieveld's paper, a secondary analysis is conducted under the assumption that carbonaceous species are five times more toxic than crustal species, nitrate and sulfate. For the reliability of SSP datasets, the analysis from Jiang's research (Jiang, 2014) actually indicates that the interactions implied by the demographic assumptions in the SSPs fit the description from the literature results. Some inconsistency issues might come from inconsistent definitions of regions and limitations in the understanding of future interaction pattern changes through various socioeconomic development stages.

IER model assumed that the toxicity of $PM_{2.5}$ is only related to the mass exposure rather than composition. Such assumption might be a little bit too general as the composition of fine particle may vary greatly depending on different emission sources. In the IER model, it is assumed that RRs are functions of $PM_{2.5}$ mass concentration and are independent of component distribution. (Burnett et al., 2014a) PM toxicity might vary on account of composition. For example, carbonaceous specie has been shown to be more toxic and is assumed to be five times more toxic than inorganic components in Lelieveld's paper. (Lelieveld et. al., 2015)

In Janssen's paper (Janssen et al., 2011) that was based on the meta-analysis of 34 papers on time-series studies, the toxicity of black carbon particle was compared with $PM_{2.5}$. The adverse mortality effect of black carbon particle is larger than $PM_{2.5}$ alone. $1\mu g/m^3$ increase in $PM_{2.5}$ is associated with 0.19% increase in all-cause mortality and 0.29% increase in cardiovascular mortality. For EC, there is 1.45% increase in all-cause mortality and 1.77% increase in cardiovascular mortality. From long-term exposure cohort studies, RR for EC is 7-16 times higher than that of $PM_{2.5}$. There is 40%-70% EC in $PM_{2.5}$ of roadside source.

COPD is among the leading cause for global YLDs whether in 1990 and 2013. There is an increase of 96.4% of heart failure from 1990 to 2013 and one third of that is caused by ischaemic heart disease. (Bill et. al., 2015) It is estimated that 89% of the worldwide

population has been exposed to $PM_{2.5}$ contamination level that exceeds WHO air quality guidelines with annual average level 10 $\mu g/m^3$ while 32% of the global population are exposed to concentration exceeding 35 $\mu g/m^3$. It is estimated that 800,000 deaths and 6.4 million lost years are attributed to fine particulate matter exposure in 2000. In Brauer's study (Brauer et al., 2012), TM5 and satellite remote sensing data were averaged to indicate the concentration level over a global range. SAT approach, which measures the concentration level according to satellite observation of AOD, provides data even for regions without proper ground-level measurement data.

One long-term Cohort study (Cao et al., 2011) in China indicate that there is significant association between air pollution and mortality from cardiopulmonary disease and lung cancer through proportional hazards regression model. 14 WHO regions in 2000 were investigated for economic, meteorological, demographic and PM data to estimate the burden of disease. $PM_{2.5}$ concentration was achieved by PM_{10} concentration and available spatial distribution of $PM_{2.5}/PM_{10}$ ratio. It is assumed that there is linear correlation between $PM_{2.5}$ concentration and risk within 7.5 and 50 $\mu g/m^3$. $PM_{2.5}$ pollution is estimated to be responsible for 3% of adult cardiopulmonary mortality, 5% of trachea, bronchus, lung cancer mortality and 1% of acute respiratory disease derived mortality among children in the GBD analysis. Developing countries contribute majorly to the global burden of disease while Asia specifically contributes two-thirds of the GBD. (Cohen et al., 2006)

Asides from the probability of health impact from persistent exposure to high concentration of PM, it is also found that low concentration of PM may still pose as health risk regarding non-accidental and cardiovascular mortality. From the cohort study of Canadians, mortality is found to be associated with long-term $PM_{2.5}$ exposure even at mean concentration of 8.7 $\mu g/m^3$ from the output of standard Cox models.(Crouse et al., 2012) SeaWiFS and MIRS are combined with GEOS-Chem to derive the first global satellite $PM_{2.5}$ estimate at a grid size of 10km*10km. There has been 0.55 $\frac{\mu g}{m^3}/year$ (2.1%/year) increase from 1998 to 2012 regarding global population weighted $PM_{2.5}$ concentration. (Donkelaar et. al., 2014)

CHAPTER THREE
METHODOLOGY

3.1 PARTICULATE CONCENTRATION

The Atmospheric Chemistry and Climate Model Intercomparison Project (ACCMIP) includes a series of time slice experiments that are conducted to reveal the long-term changes in atmospheric composition and radiative forcing from preindustrial times to recent years and predict the effects further into the future. The time scale ranges from 1850 to 2100. Among all the four RCP scenarios, RCP 6.0 includes short lived precursor emissions that are different from the others while RCP 2.6 and RCP 8.5 provide the extremes in 2100 climate change or methane levels. The $PM_{2.5}$ data are included in the following models: GISS-E2-R, GFDL-AM3, CICERO-OsloCTM2, NCAR-CAM3.5, NCAR-CAM5.1, MIROC-CHEM, HadGEM2.(Lamarque et al., 2013)

$PM_{2.5}$ mass calculation for models without direct $PM_{2.5}$ output is calculated using:
$PM_{2.5}=BC + OA + SO_4 + SOA + NO_3 + NH_4 + 0.25*SS + 0.1*Dust$

Gridded $PM_{2.5}$ or components data are collected from different models and various sceneries as input. To facilitate the usage of population data and make different model comparable, model regrid was applied to original data converting the different gridded concentration data to the same grid (0.5°*0.5°).

3.2 POPULATION DATASETS

Population data for 1980-2100 was collected from the Center for global environmental research to calculate mortality.

3.2.1 SSPs scenarios

In the SSP1 scenario, the future is in a sustainable pathway with education and health investment. The population would be low and the human well-being is being heavily emphasized. SSP2 scenario assumes medium fertility with medium mortality, medium migration and medium education level while SSP3 refers to a world that population

growth is mainly in developing countries. SSP4 considers the future world of high inequalities. SSP5 indicates a world that emphasizes technological progress and economic growth. (KC et. al., 2014)

3.2.2 The advantage of SSPs

For climate change related research, the Shared Socio-economic Pathways (SSPs) has also been used as demographic data input. For example, in Lutz's research, the variation in population size and structure were studied regarding the contribution towards greenhouse gas emission and capacity of adapting to climate change. IPCC-SRES (Intergovernmental Panel on Climate Change—Special Report on Emissions Scenarios) scenarios only include trajectories for total population size, SSPs address the predicted trajectories for all age, sex and education details for all countries. (Lutz et. al., 2015) When measuring the total mortality from IHD, the mortality distribution is closely associated with age. So more detailed prediction would be required to achieve the results.

3.3 $PM_{2.5}$ DERIVED RRS AND MORTALITY BASED UPON IER MODEL

3.3.1 RRs value

The IER functions developed by Burnett are used for assessing the global burden of disease is as below.

For the calculation of relative risk value:

For $z < z_{cf}$,

$RR_{IER}(z)=1$

When exposure level is lower than the threshold, there would be no additional health risk since RR=1 means the risk is exactly the baseline.

For $z \geq z_{cf}$,

$RR_{IER}(z)=1+\alpha\{1-\exp[-\gamma(z-z_{cf})^{\delta}]\}$

For exposure larger than threshold value, relative risk is larger than 1 and the increase is determined by the difference between exposure level and threshold level, disease endpoint parameters (α, γ, δ).

Z-exposure to $PM_{2.5}$ ($unit: \mu g/m^3$)

$z_{cf} - counterfactual\ concentration\ below\ which\ there\ is\ no\ additional\ risk$

The unknown parameter sets (α, γ, δ) are estimated by nonlinear regression methods and there are different parameter values for various locations or diseases. The advantage of IER model compared with traditional concentration-response (CR) functions is that this model can be applied to global range analysis without causing too much uncertainty associated with the limitation of endpoints.(Burnett et al., 2014a) The lookup table from Apte's study (Apte et. al., 2015) was utilized to calculate the RRs for this study. The three main chronic diseases related to $PM_{2.5}$ concentration variation are COPD (chronic obstructive pulmonary disease), LNC (lung cancer), LRI (lower respiratory infection). It indicates that IER model is superior in predicting RR compared with seven other forms of models in previous references. RR values were calculated with the IER model data of 1000 endpoints from apte's research to generate the relative risk values for COPD, LRI, LNC, IHD that are associated with $PM_{2.5}$ mass concentration variation from a time range of 1850 to 2100.

3.3.2 Mortality value

The mortality rate in each grid is calculated as below:

$$M_{i,j} = P_i \times \hat{I}_{j,k} \times (RR_j(C_i) - 1)$$

$$\hat{I}_{j,k} = \frac{I_{j,k}}{\overline{RR}_{j,k}}$$

$P_i - population\ of\ grid\ cell\ i$

$I_{j,k} - reported\ regional\ average\ annual\ disease\ incidence\ mortality\ rate\ for$

$endpoint\ j\ in\ region\ k$

$C_i - annualaverage\ PM2.5\ concentration\ in\ cell\ i$

$RR_j(C_i) - relative\ risk\ for\ endpoint\ j\ at\ concentration\ C_i$

Population normalized RR value:

$$\overline{RR}_{j,k} = \frac{\sum_{i=1}^{N} P_i \times RR_j\ (C_i)}{\sum_{i=1}^{N} P_i}$$

Population normalization is useful in adjusting exposure level. For example, there is grid A and grid B with the same risk value derived from concentration and the population is 100 in grid A while the population is 0 in grid B. The exposure in grid B would not add to the normalized value since no population means no exposure while grid A would add to the normalized value by the extent limited by population in grid A. This example illustrates that normalization is an effective way to measure human related exposure. Spatial distribution of $PM_{2.5}$ concentration would be only relevant to the measurement when the population is not blank. Non-populated areas including oceans can be excluded from contributing to the exposure calculation while highly-populated areas would further add to calculation.

The change in mortality: $\Delta M_{i,j}$=$P_i \times \hat{I}_{j,k} \times (RR_j(C_i^*) - RR_j(C_i))$

Since there might be multiple risk factors for point estimates, it is not accurate to describe the reduction in attributable mortality as “lives saved”. It can be regarded as the reduction of mortality statistically under certain scenario with given data and parameters. The result is statistically significant but may not be associated with one or two human being as speaking. The change in mortality between baseline situation and hypothetical situation would be an insight into policy making.

The simplified mortality change function from Lelieveld’s paper (Lelieveld et al., 2015)($\Delta Mort = y_0$[(RR-1)/RR]Pop) is applied to the calculation.

3.4 INTEGRATION AND COMPARISON

3.4.1 The world regions and related integrated data

UN divides the world into 10 regions in the UN Millenium Development Goals (MDG) regions according to development extent. The MDG regions include developed countries (DC), caucasus and central Asia (CIS), Northern Africa (NA), Latin America and the Carribbean (LAC), Eastern Asia (EA), Southern Asia (SA), South-eastern Asia (SEA), Western Asia (WA) and Oceania (O).[1] The development extent of regions would be an important consideration since both population and anthological emission could be related to the development extent. Figure 1 is the UN division map.

3.4.2 The reason for using three year average data

For long-term climate change and pollution changes, one year data would be not sufficient enough to represent a decade. So for common long-term climate change or pollution variation studies, the way to represent decade data is to use multi-year average.

3.4.3 Time series

1850 is used to describe the air pollution related health impact in the past at the end of industrial evolution. 2000 is used to represent the current years. 2030 would be a good indicator for the sustainability achievements for the future. It is predicted by UN that at the time of 2050, 70% of world population to be crammed into poor, overcrowded, polluted urban areas so the mortality variation based upon air pollution and population would be a major problem in the future.[2] The year around 2050 should a good indicator of future scenarios.

3.4.4 Comparison

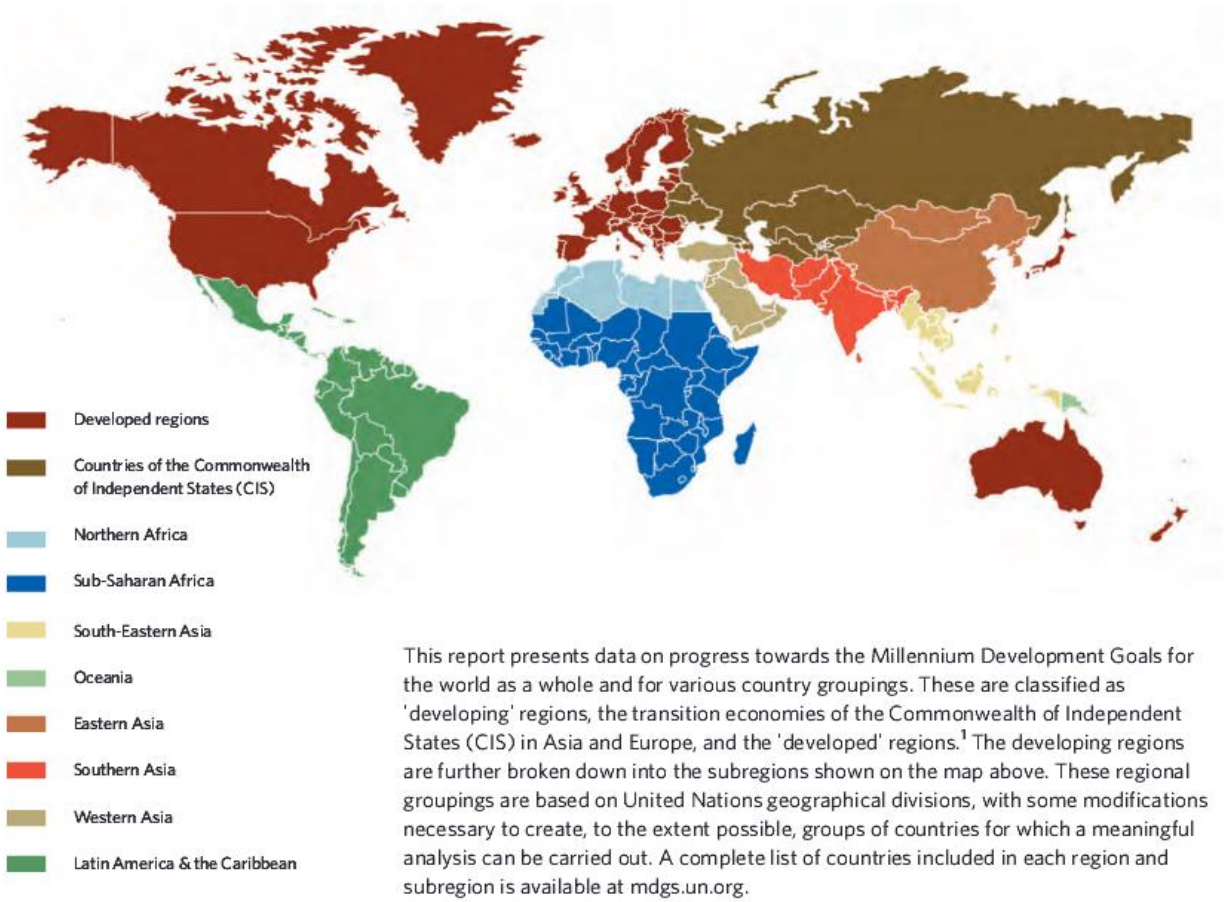
The output RRs and mortality are compared within different sceneries and models. Comparisons are also made between our study and other studies found in the literature.

---

[1] http://mdgs.un.org/unsd/mdg/Host.aspx?Content=Data/RegionalGroupings.htm

[2] https://aftermathnews.wordpress.com/2010/03/24/un-by-2050-70-of-world-population-to-be-crammed-into-poor-overcrowded-polluted-urban-corridors-comprising-a-tiny-fraction-of-habitable-land/

Regional Groupings



This report presents data on progress towards the Millennium Development Goals for the world as a whole and for various country groupings. These are classified as 'developing' regions, the transition economies of the Commonwealth of Independent States (CIS) in Asia and Europe, and the 'developed' regions.[1] The developing regions are further broken down into the subregions shown on the map above. These regional groupings are based on United Nations geographical divisions, with some modifications necessary to create, to the extent possible, groups of countries for which a meaningful analysis can be carried out. A complete list of countries included in each region and subregion is available at mdgs.un.org.

[1] Since there is no established convention for the designation of 'developed' and 'developing' countries or areas in the United Nations system, this distinction is made for the purposes of statistical analysis only.

Figure 1 UN regions[3]

[3] http://nuclearsuntan.blogspot.com/2011/11/un-divides-world-into-10-regional.html

3.5 UNCERTAINTY MEASUREMENT

3.5.1 Uncertainty in concentration data

The variation in RRs and $\Delta mortality$ between various climate models and different sceneries are calculated for each spatial grid and each MDG region. For various radiative forcing scenarios, best scenario (RCP 2.6) with +2.6W/m^2 increased forcing is theoretical quite different from the worst scenario (RCP 8.5) with +8.5W/m^2. What effect would various scenarios cast upon the projection, the association between radiation forcing and near surface fine particle concentration and the possible future coming from worst scenario are taken into consideration when analyzing the problem. RCP 2.6 and RCP 8.5 provide extremes in 2100 climate change and methane levels. RCP 6.0 is significantly different than the others since it contains very different short-lived precursor emissions. (Lamarque et al., 2013)

Furthermore, various models depict the distribution differently due to the mechanism. Natural emission alone can cause the significant variation among models. NCAR-CAM5.1 and GISS-E2-R describe aerosols in an extensive way. Representation of non-methane hydrocarbon chemistry varies among different models, which is responsible for different model performance. Aerosol in NCAR-CAM5.1 is represented by three internally-mixed log- normal modes (Aitken, accumulation, and coarse) while aerosol in GISS-E2-R is represented by 108 size-resolved aerosol tracers plus three bulk aerosol-phase tracers. LMDzORINCA model uses a modal approach to simulate the distribution of aerosols. All other models use the bulk approach. Models except GISS-E2-R includes limited heterogeneous reactions. Half of all ACCMIP models include the indirect effect of aerosols. Since different models work differently, there is no way of assuming any model has the best prediction results. Some models do predict with higher sensitivity for certain regions. In atmospheric or climate change related modelling studies, multi-ensemble is used to increase projection accuracy.

In Fowler's study (Toggweiler et.al., 2001), multi-model ensemble is used to assess the precipitation extremes in UK. Ensemble generally increase the skill, reliability and consistency of predictions compared with single model so that it would be useful in lowering projection errors. In climate models, the equally weighted average of several

models is usually found to agree better than any single models. In IPCC reports, unweighted multi-model means is usually used to present best guess projection instead of one model. (Tebaldi et. al., 2007) Since it is complicated to determine the weight for each model, unweighted mean would be used in this study to output the ensemble results.

3.5.2 Uncertainty in population data

The variation of mortality caused by various sceneries of population (SSP1, SSP2, SSP3) is calculated for each grid and UN region. Since SSP1 represents the sustainable population pathway, SSP2 indicates intermediate challenges while SSP3 is the scenario of fragmentation, the projection of mortality and population normalized relative risk or $PM_{2.5}$ concentration exposure can be varied due to the various assumptions of future population distribution and total number.

CHAPTER FOUR
RESULTS

4.1 SEASONAL DISTRIBUTION OF RR_S FROM GISS-E2-R MODEL OUTPUT

For relative risk values, the value 1 is regarded as baseline which means there is no additional health risk and the larger risk value indicates elevated risk. For example, in regions with risk of 2, the exposure health impact is twice of that of baseline or background. So, if the population distribution does not change, the premature mortality caused by certain disease from time A should be twice of the mortality value from time B for the same region. Risk is an extent to which exposure might influence the population living in certain region, so population is a major factor in determining how influential it is of health relative risk. Population normalization and mortality is calculated to make such linkage.

In some cases, a value slightly less than 1 was calculated due to the data processing. In these cases, it does not mean the risk is actually reduced since there is no way of having a risk value less than the background. Risk values less than 1 should be treated as 1 but such values does mean than the near surface concentration is so low compared with health impact function that no additional risk should be considered.

Figure 2-3, 50-51, 52-53 depict the monthly relative risk for COPD, LNC, LRI respectively in 1850s from the data collected and averaged from GISS-E2-R model outputted $PM_{2.5}$ concentration.

Figures 54 - 59 depict the monthly relative risk for COPD, LNC, LRI respectively in 1860s from the data collected and averaged from GISS-E2-R model outputted $PM_{2.5}$ concentration.

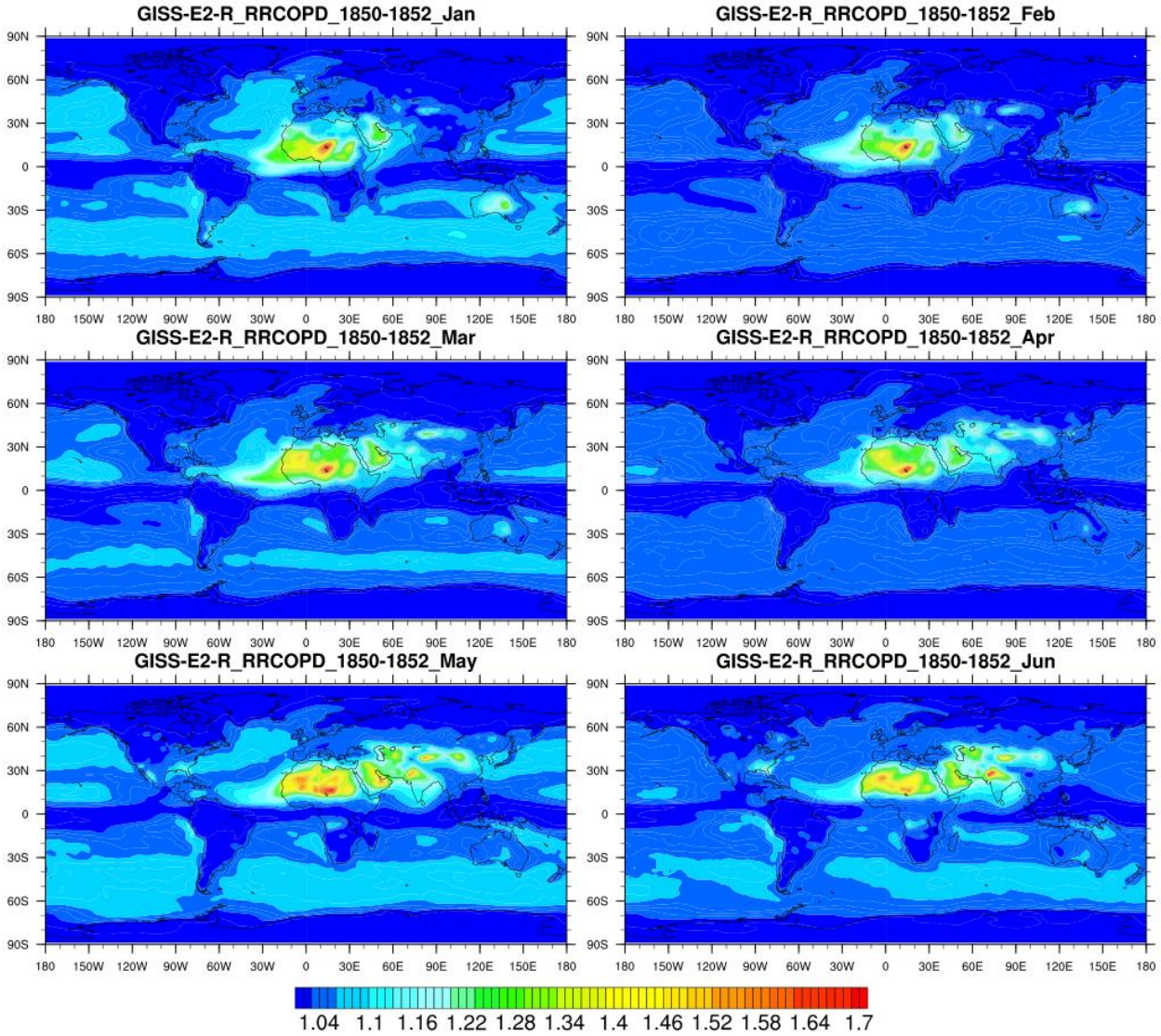


Figure 2 Global relative risk for cardiopulmonary disease from January to June of the three year average data from 1850 to 1852 with the ambient $PM_{2.5}$ concentration output from GISS-E2-R model based on the integrated risk function developed for GBD(Burnett et al., 2014b) for each figure, vertical axes indicate latitude and horizontal axes indicate longitude. The map plot indicate the monthly level of relative risk over a global terrain by applying the concentration-risk function from IER model for COPD disease endpoint.

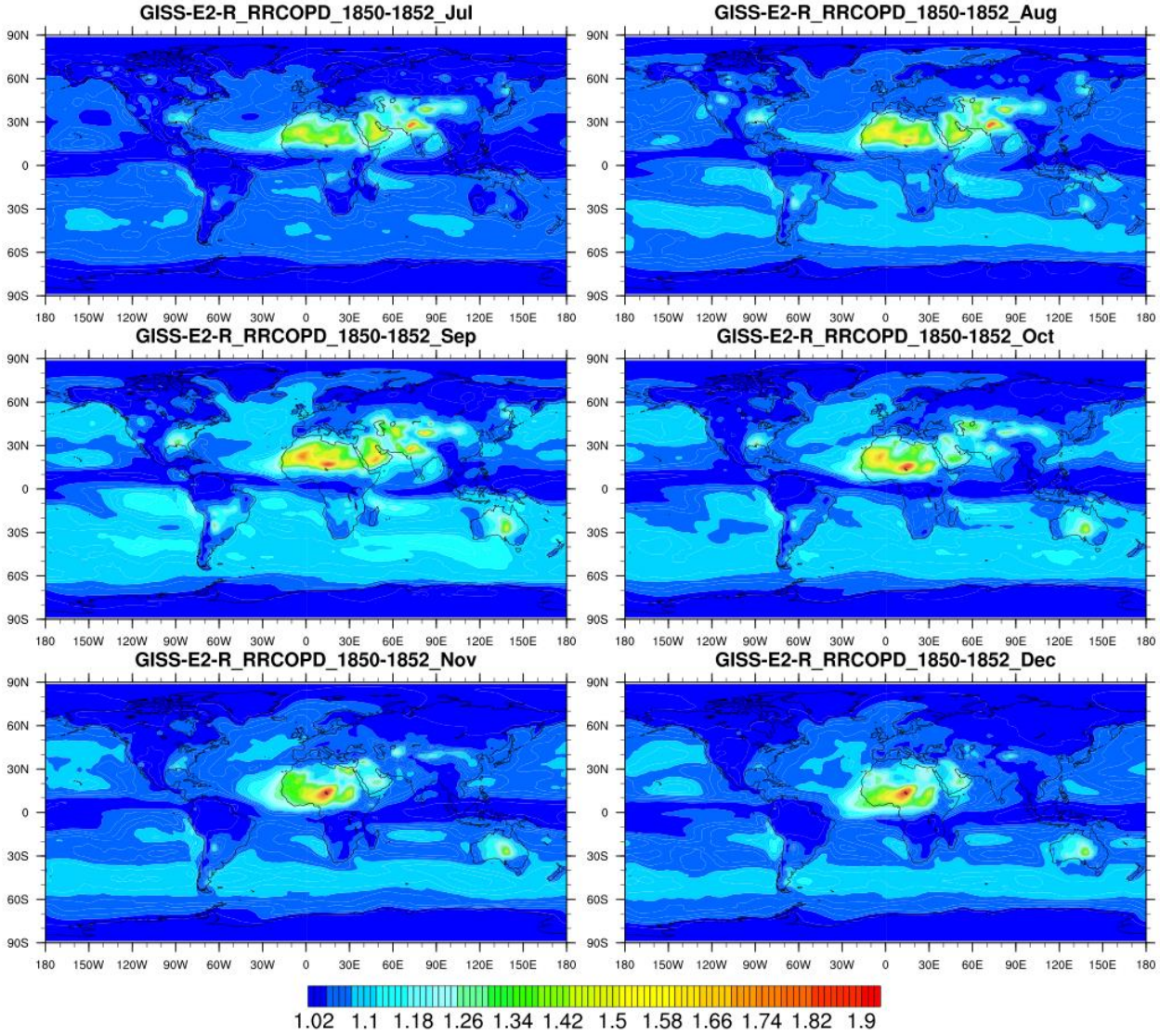


Figure 3 Global relative risk for cardiopulmonary disease from July to December of the three year average data from 1850 to 1852 with the ambient $PM_{2.5}$ concentration output from GISS-E2-R model based on the integrated risk function developed for GBD(Burnett et al., 2014b) for each figure, vertical axes indicate latitude and horizontal axes indicate longitude. The map plot indicate the monthly level of relative risk over a global terrain by applying the concentration-risk function from IER model for COPD disease endpoint.

From the spatial distribution of relative risk for cardiopulmonary disease (RRCOPD) over the global terrain in pre-industrial times, it is observed that there is a widely distributed elevated RR value in September compared with previous month. The peak value start to spread from northern Africa to Western Asia and southern Asia since May. The risk peak in Western and Southern Asia start to decrease since October. Overall there is only a slight elevation of relative risk of COPD disease due to $PM_{2.5}$ surface concentration while the highest peak exist in Africa regions. The RR value for the whole globe ranges from 1.02 to 1.7, which indicates that health risk is not elevated for the preindustrial times. The relative risk of LNC ranges from to 2.05 with relatively lower concentration levels in February and July. LRI disease risk is more varied compared with COPD and LNC. There is a slight elevation in RR value for COPD in 1860s compared with 1850s with an increase from 1.7 to 2.24.

LNC risk value is majorly elevated as the peak value has increased from 2.05 in 1850 to 3.05 in 1860. The elevation indicates a major increase in fine particulate induced lower respiratory infection health risk in the pre-industrial times. The relative risk is overall low in August. Such output means that for maximum exposure regions the risk for lung cancer due to air pollution has increased from twice the baseline to three times the baseline.

Figure 60-61, 62-63, 64-65 describe the disease risk for COPD, LNC, LRI respectively in 2000s. Figure 66-67, 68-69, 70-71 depict the relative risk for COPD, LNC, LRI respectively in 2030s. Figure 4-5, 72-73, 74-75 depict the relative risk for COPD, LNC, LRI respectively in 2050s.

The risk value is much elevated in eastern Asia in April and May, then it start to decrease in June and increase to a higher level again in August, September and October. The reason for such seasonal variation might be partially due to seasonal change in Asia dust storm.

The RCP2.6 scenario actually assumes the best emission situation as the emission of all three major greenhouse gas species (CO_2, CH_4, N_2O) are projected to keep decreasing since 2000s. The comparison between 1850s and 2050s (under RCP2.6

scenario) shows that there is not much difference between the seasonal distribution and overall risk elevation levels of preindustrial times and future era.

It shows a widespread elevation in RR values all over the globe in April since 1900s. There is a lower level of RR distribution in May, Jun, July for future times compared with current years from the comparison of 1900s-2000s and 2030s-2050s.

4.2 ANNUAL PLOT OF GISS-E2-R MODEL OUTPUT

Figure 6-9 describe the annual relative risk of COPD endpoint plot from 1850s to 2090s from GISS-E2-R with RCP2.6 as the future emission scenario.

The annual plot of COPD relative risk distribution from 1850 to 2090 shows that there are lower levels of COPD relative risk for the time of 1860s, 1910s, 1970s while there is a relatively high level in 1850s. COPD relative risk value varies from 1.02 to 1.58. The elevated value starts emerge in southern Asia since 1980s and emerge in south-eastern Asia since 2000s. The elevated level is projected to disappear since 2050s.

The spatial distribution of LRI (figure 5) is very consistent all through the time period. There starts to be an elevated risk value in southern Asia since 1980s and it is projected to last till 2060s. Aerosol loading has increased substantially in South and East Asia since 1979 with high level of $PM_{2.5}$ distributed in eastern, southeastern, northern and northwestern China, northern India and part of Southeast Asia. Aerosol optical depth satellite results indicate the general positive trend in $PM_{2.5}$ concentration projection over China for the past few decades. The emission in eastern Asia, especially China, can vary hugely according to the government policy. Dust storm also has an impact upon the $PM_{2.5}$ variation. (EANET, 2015)

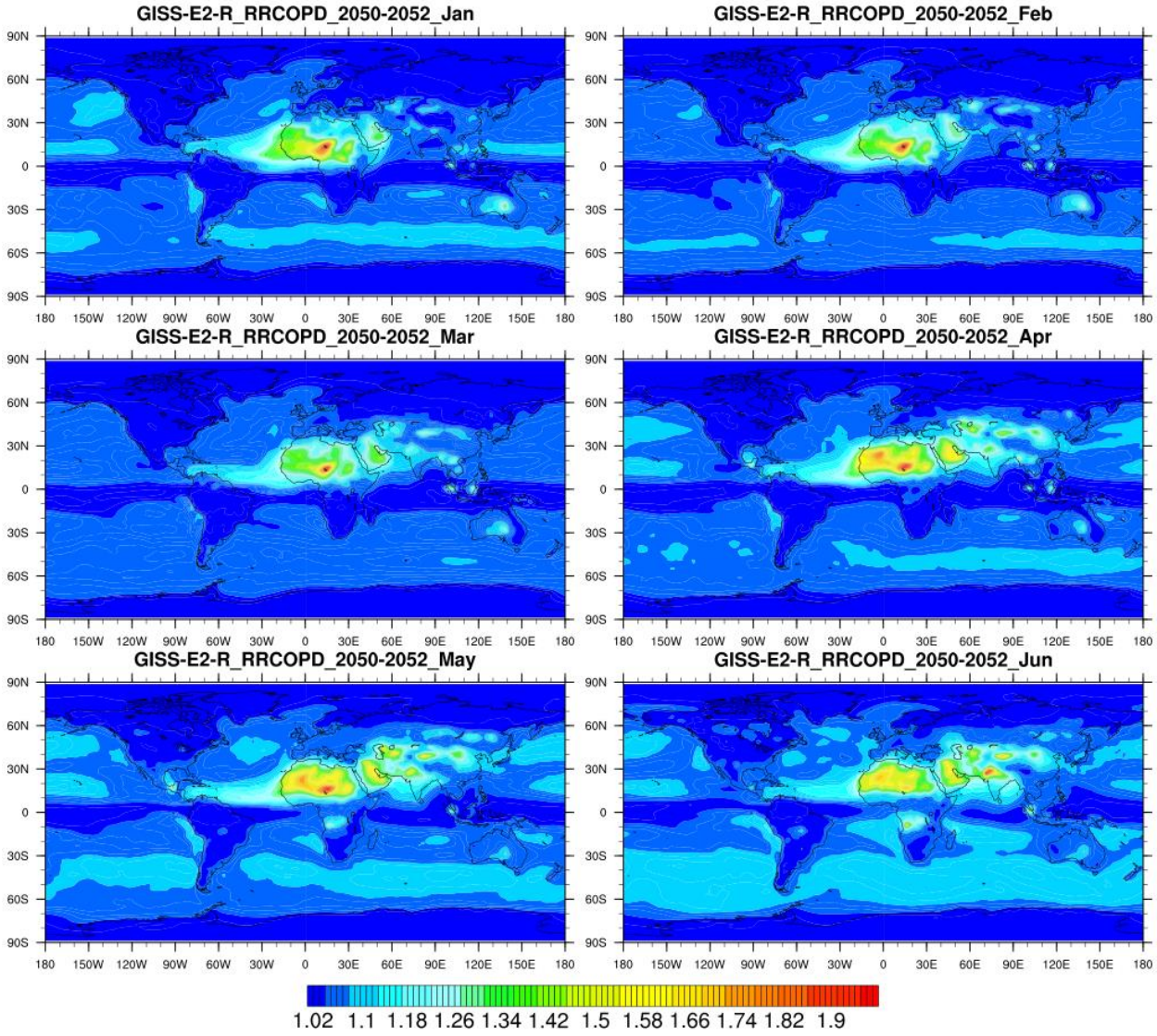


Figure 4 Global relative risk for cardiopulmonary disease from January to June of the three year average data from 2050 to 2052 with the ambient $PM_{2.5}$ concentration output from GISS-E2-R model based on the integrated risk function developed for GBD(Burnett et al., 2014b) for each figure, vertical axes indicate latitude and horizontal axes indicate longitude. The map plot indicate the monthly level of relative risk over a global terrain by applying the concentration-risk function from IER model for COPD disease endpoint.

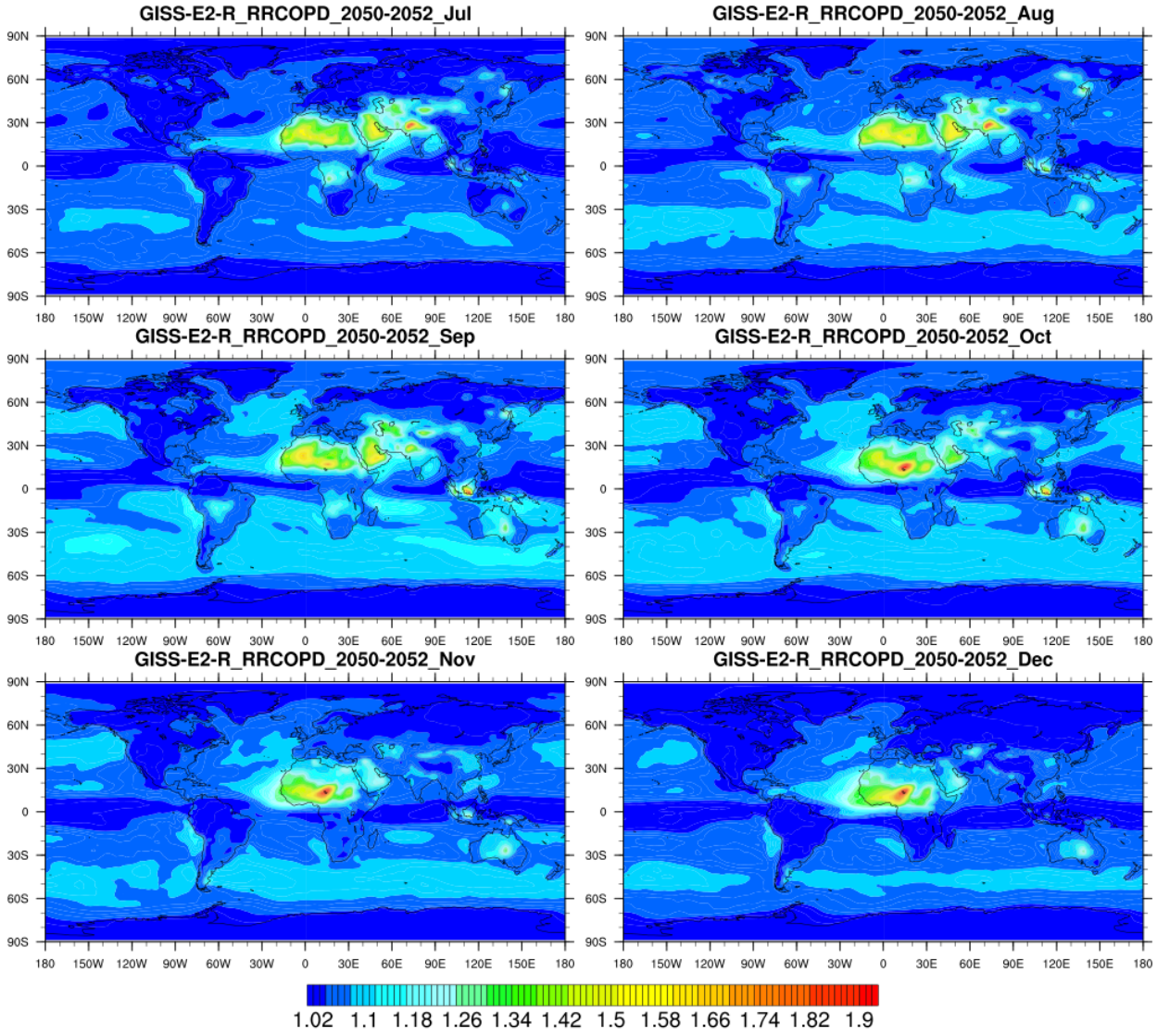


Figure 5 Global relative risk for cardiopulmonary disease from July to December of the three year average data from 2050 to 2052 with the ambient $PM_{2.5}$ concentration output from GISS-E2-R model based on the integrated risk function developed for GBD(Burnett et al., 2014b) for each figure, vertical axes indicate latitude and horizontal axes indicate longitude. The map plot indicate the monthly level of relative risk over a global terrain by applying the concentration-risk function from IER model for COPD disease endpoint.

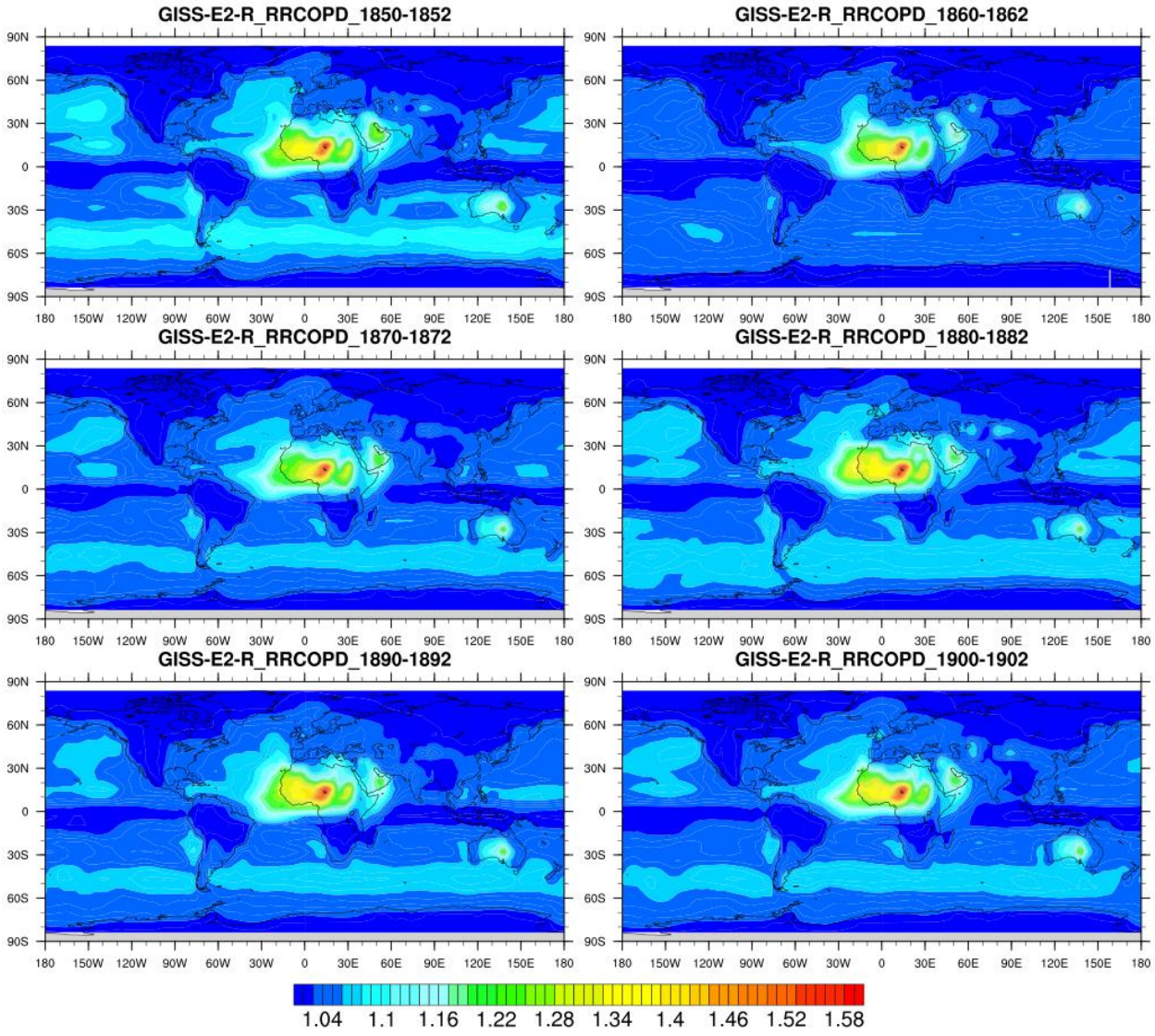


Figure 6 Global relative risk for cardiopulmonary disease for 6 time periods from 1850s to 1900s with the ambient $PM_{2.5}$ concentration output from GISS-E2-R model based on the integrated risk function developed for GBD(Burnett et al., 2014b) *for each figure, vertical axes indicate latitude and horizontal axes indicate longitude. The map plot indicate the level of relative risk over a global terrain by applying the concentration-risk function from IER model for COPD disease endpoint. Note that the Saharan dust regions might present an elevated relative risk all through 6 decades and there is no other obvious increase of risk in other regions.*

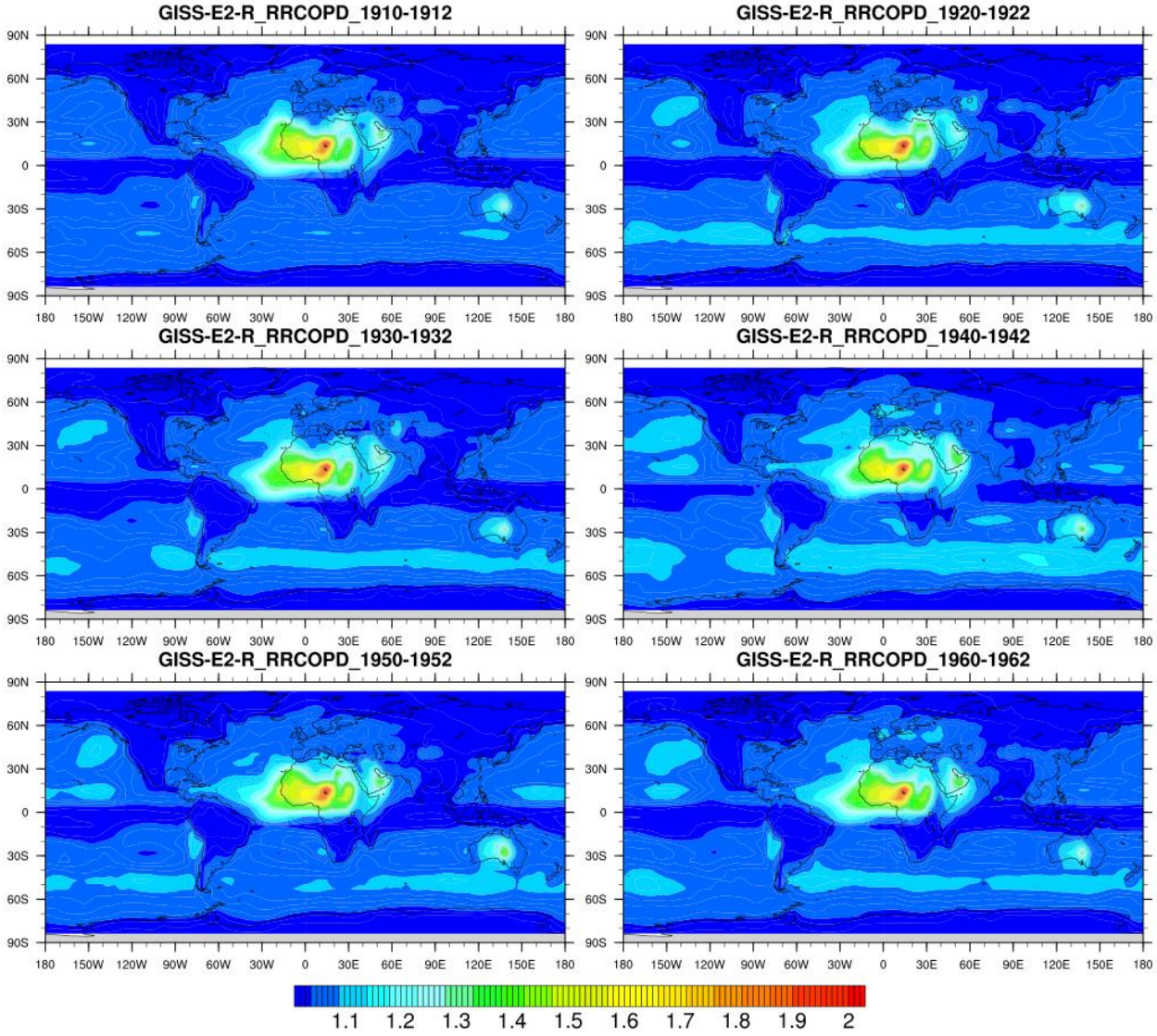


Figure 7 Global relative risk for cardiopulmonary disease for 6 time periods from 1910s to 1960s with the ambient $PM_{2.5}$ concentration output from GISS-E2-R model based on the integrated risk function developed for GBD(Burnett et al., 2014b) *for each figure, vertical axes indicate latitude and horizontal axes indicate longitude. The map plot indicate the level of relative risk over a global terrain by applying the concentration-risk function from IER model for COPD disease endpoint. Note that the peak value might be higher than previous decades.*

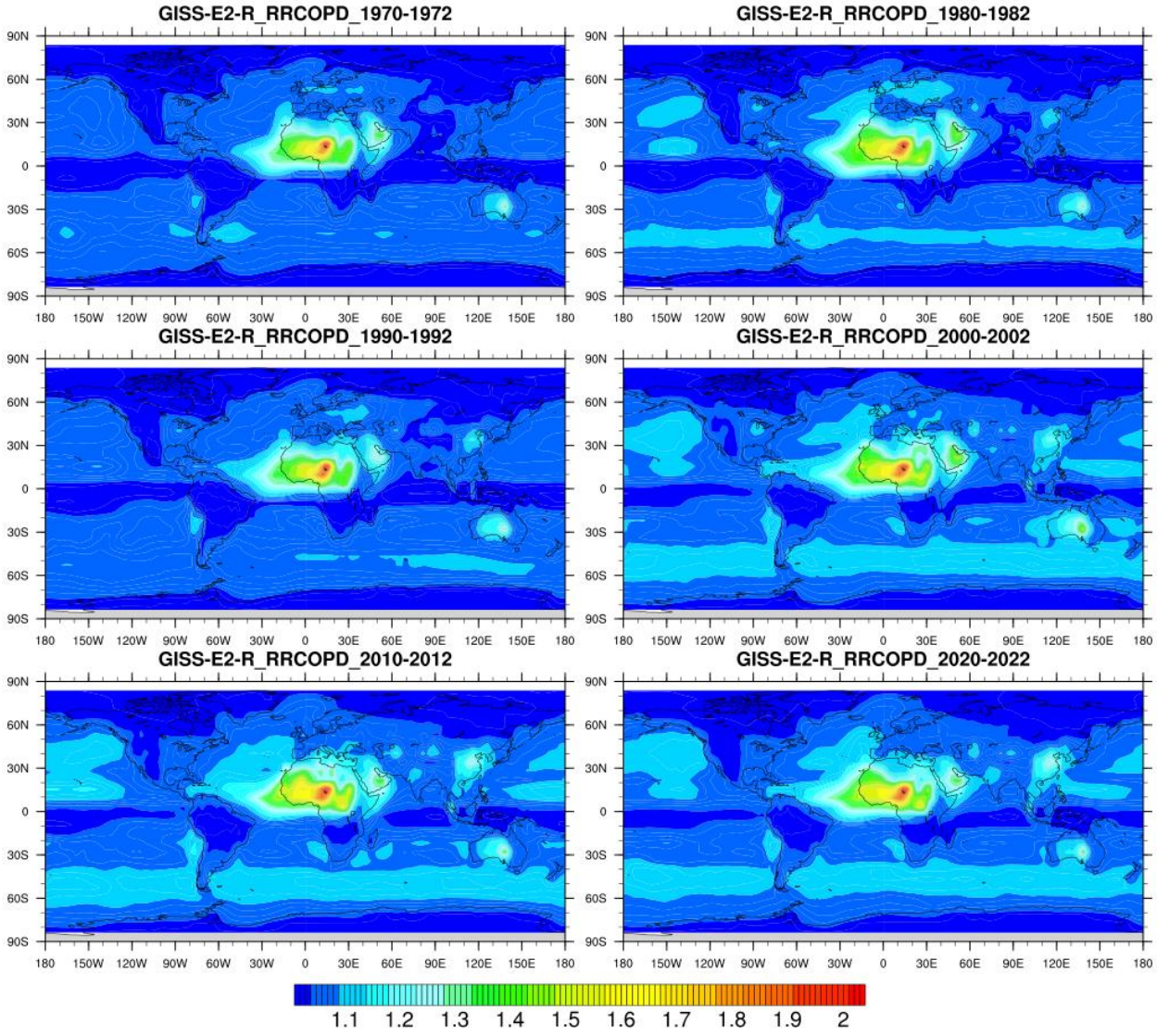


Figure 8 Global relative risk for cardiopulmonary disease for 6 time periods from 1970s to 2020s with the ambient $PM_{2.5}$ concentration output from GISS-E2-R model based on the integrated risk function developed for GBD(Burnett et al., 2014b) *for each figure, vertical axes indicate latitude and horizontal axes indicate longitude. The map plot indicate the level of relative risk over a global terrain by applying the concentration-risk function from IER model for COPD disease endpoint. Note that eastern Asia and other parts of Asia are associated with risk elevation since 2000s.*

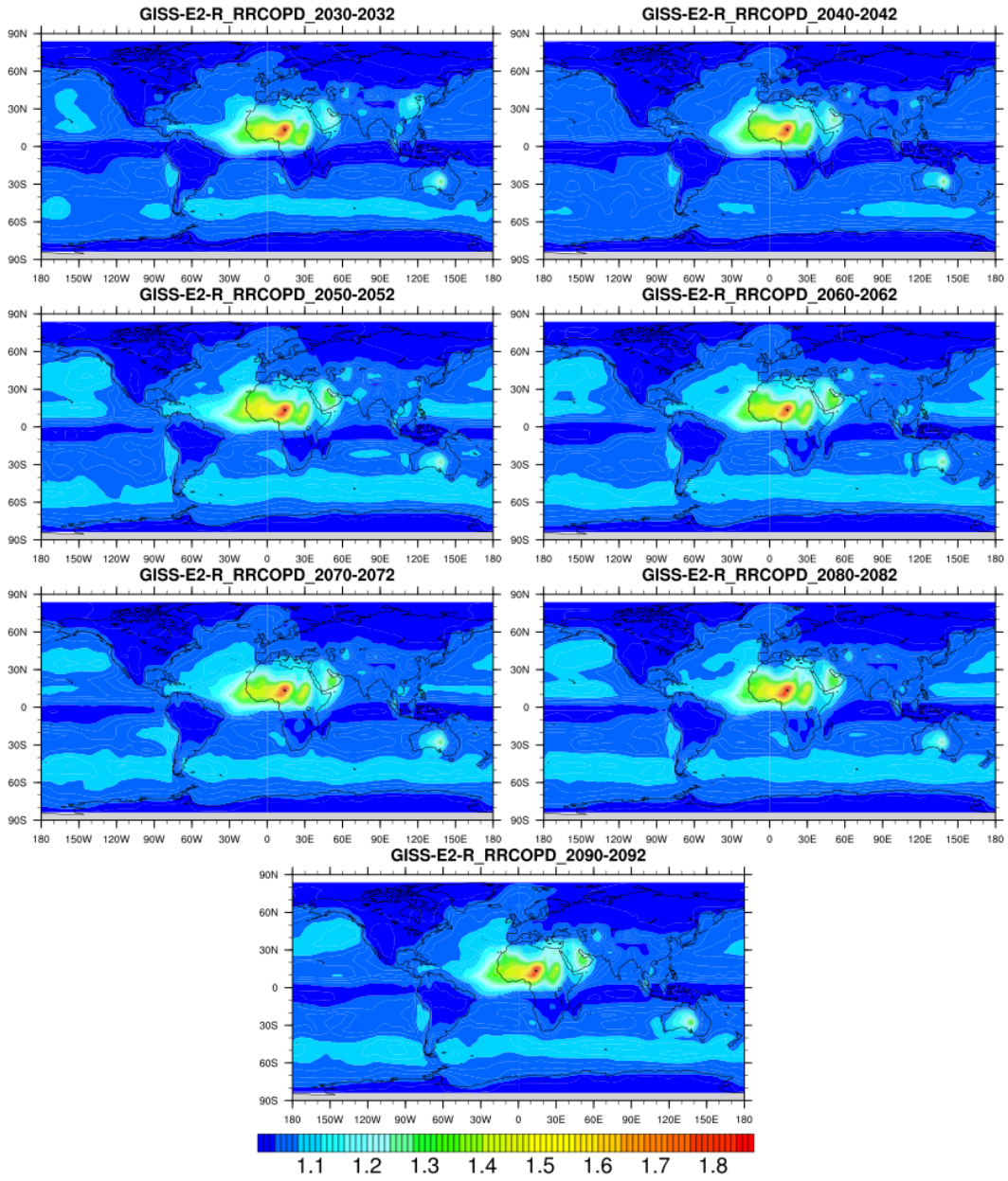


Figure 9 Global relative risk for cardiopulmonary disease for 7 time periods from 2030s to 2090s with the ambient $PM_{2.5}$ concentration output from GISS-E2-R model based on the integrated risk function developed for GBD(Burnett et al., 2014b) *for each figure, vertical axes indicate latitude and horizontal axes indicate longitude. The map plot indicate the level of relative risk over a global terrain by applying the concentration-risk function from IER model for COPD disease endpoint. Note that the elevation in Asia start to decrease since 2040s with peak value in Saharan and Australia consistent all through the time period.*

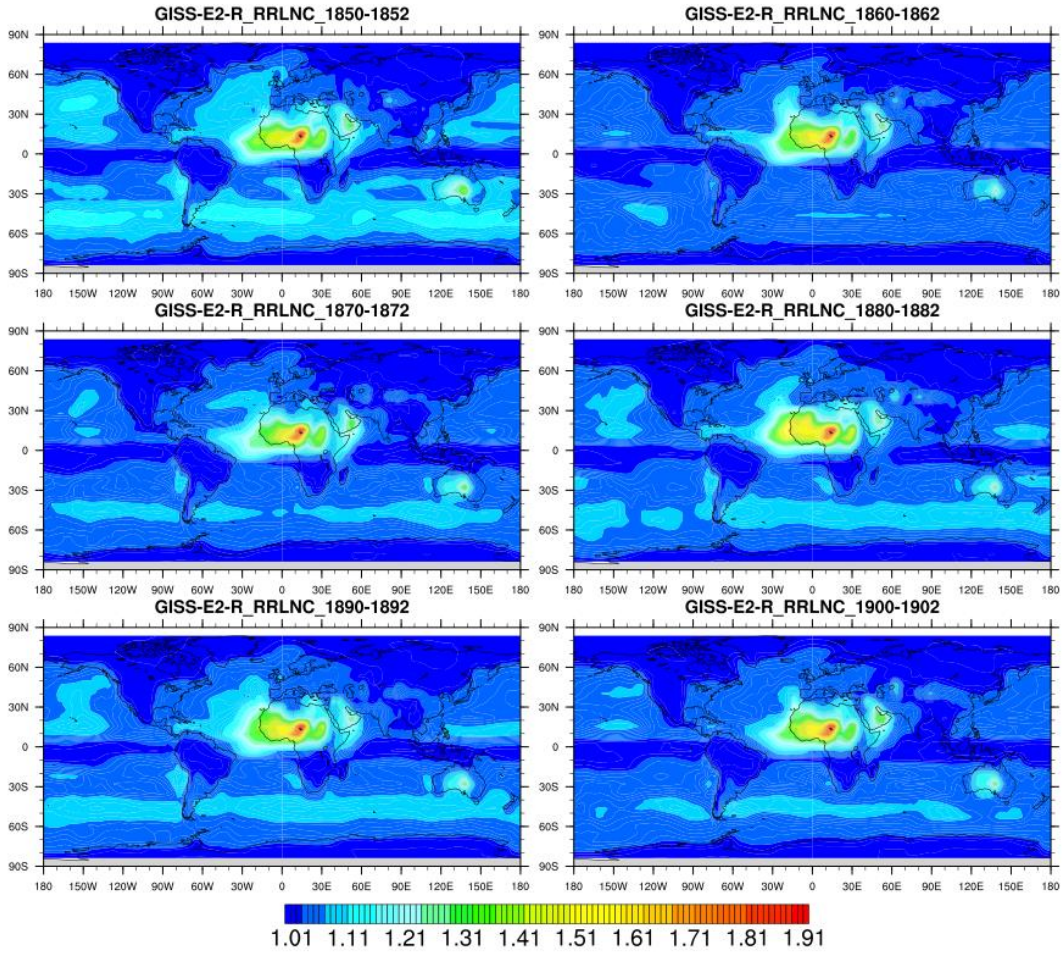


Figure 10 Global relative risk for lung cancer for 6 time periods from 1850s to 1900s with the ambient $PM_{2.5}$ concentration output from GISS-E2-R model based on the integrated risk function developed for GBD(Burnett et al., 2014b) *for each figure, vertical axes indicate latitude and horizontal axes indicate longitude. The map plot indicate the level of relative risk over a global terrain by applying the concentration-risk function from IER model for LNC disease endpoint.*

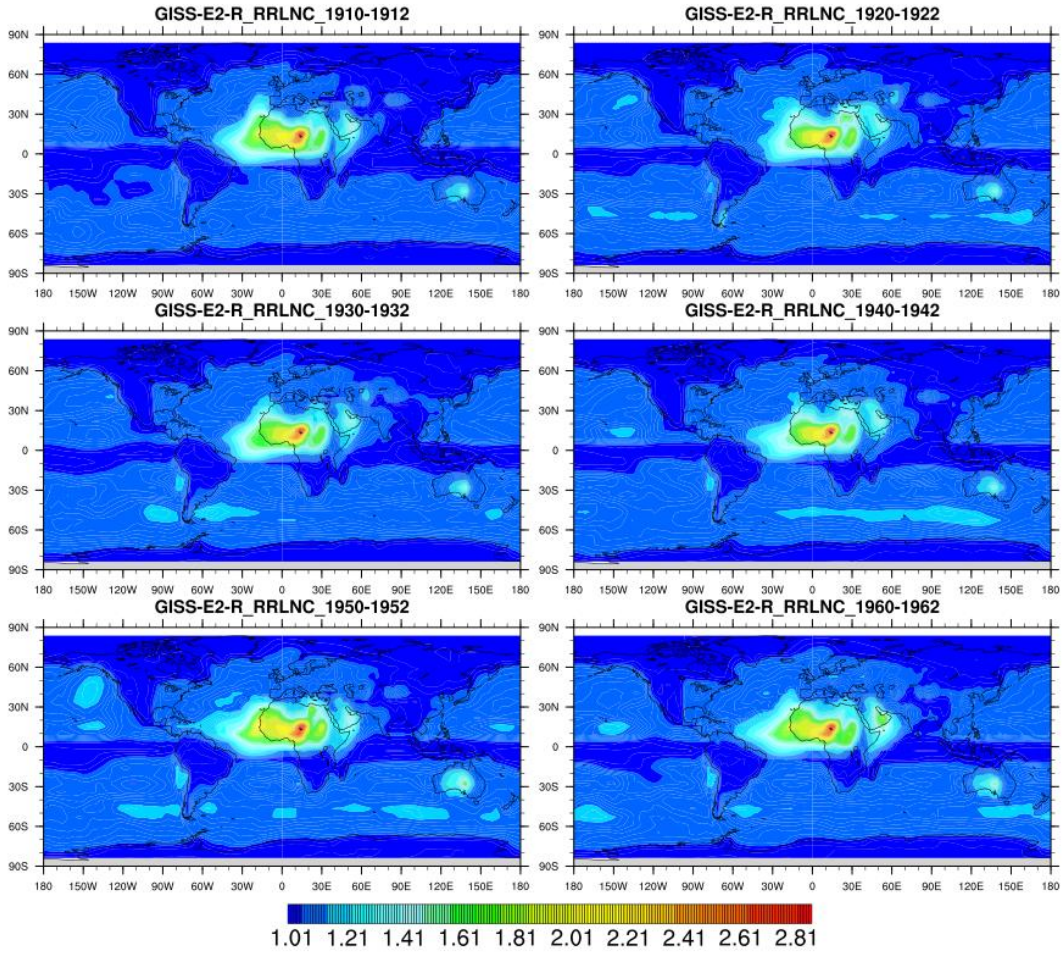


Figure 11 Global relative risk for lung cancer for 6 time periods from 1910s to 1960s with the ambient $PM_{2.5}$ concentration output from GISS-E2-R model based on the integrated risk function developed for GBD(Burnett et al., 2014b) *for each figure, vertical axes indicate latitude and horizontal axes indicate longitude. The map plot indicate the level of relative risk over a global terrain by applying the concentration-risk function from IER model for LNC disease endpoint.*

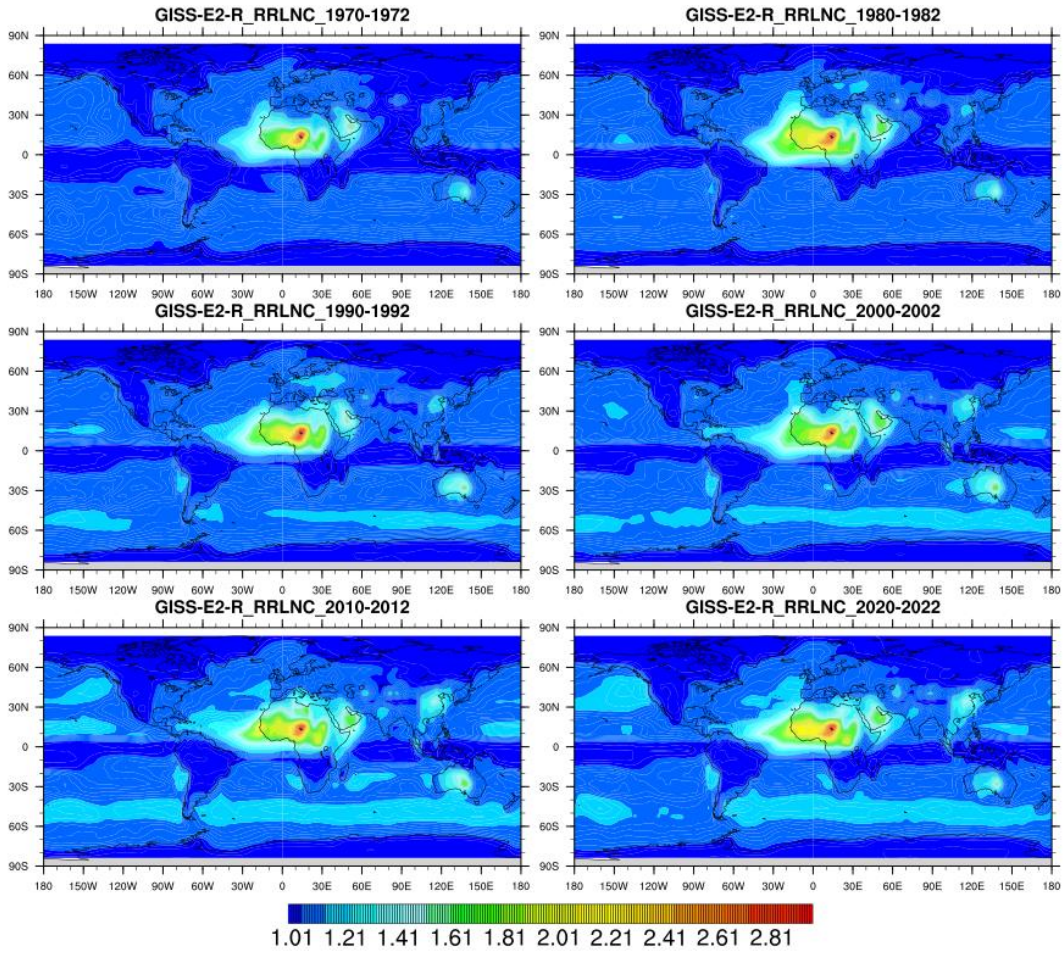


Figure 12 Global relative risk for lung cancer for 6 time periods from 1970s to 2020s with the ambient $PM_{2.5}$ concentration output from GISS-E2-R model based on the integrated risk function developed for GBD(Burnett et al., 2014b) *for each figure, vertical axes indicate latitude and horizontal axes indicate longitude. The map plot indicate the level of relative risk over a global terrain by applying the concentration-risk function from IER model for LNC disease endpoint.*

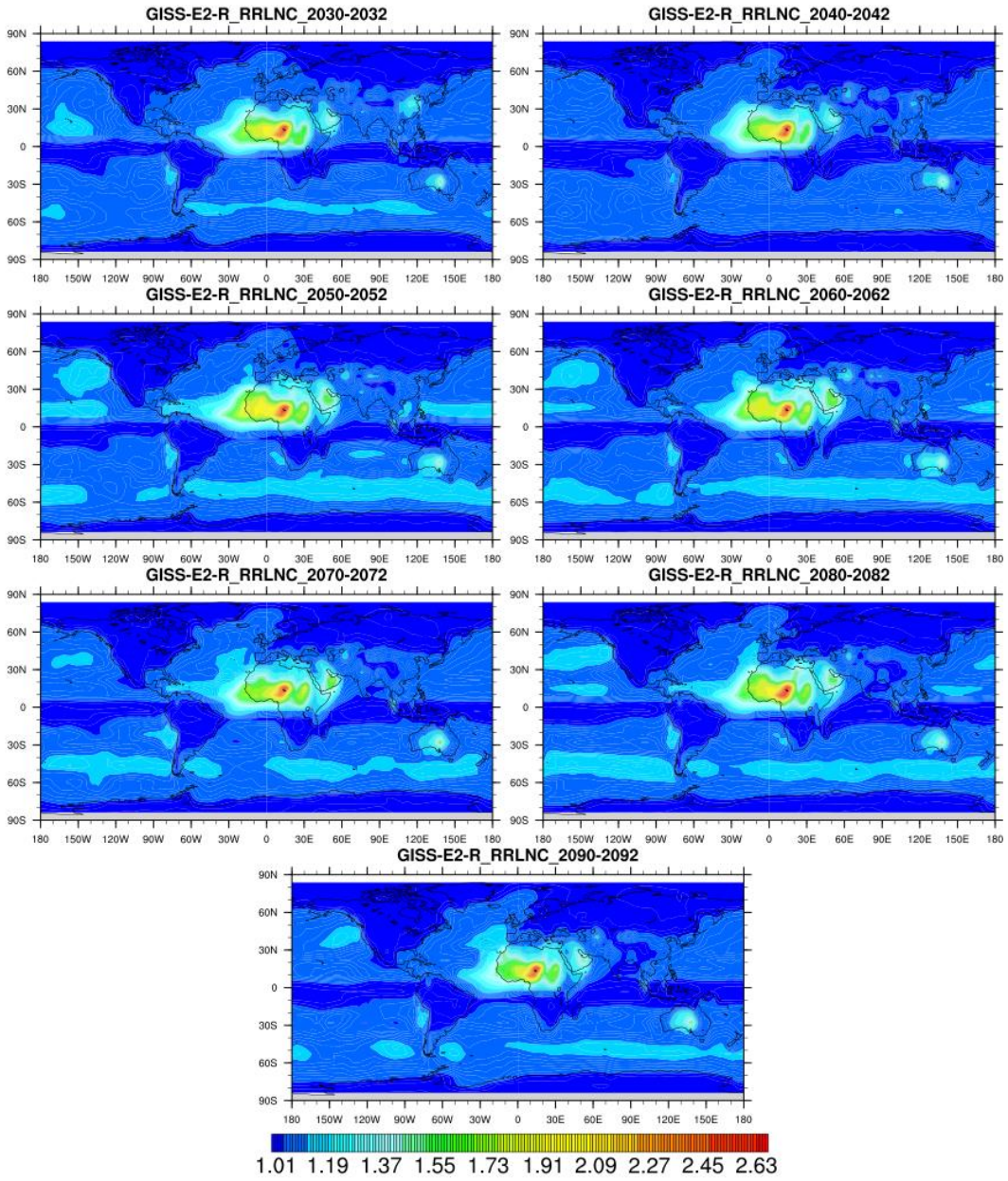


Figure 13 Global relative risk for lung cancer for 7 time periods from 2030s to 2090s with the ambient $PM_{2.5}$ concentration output from GISS-E2-R model based on the integrated risk function developed for GBD(Burnett et al., 2014b) *for each figure, vertical axes indicate latitude and horizontal axes indicate longitude. The map plot indicate the level of relative risk over a global terrain by applying the concentration-risk function from IER model for LNC disease endpoint.*

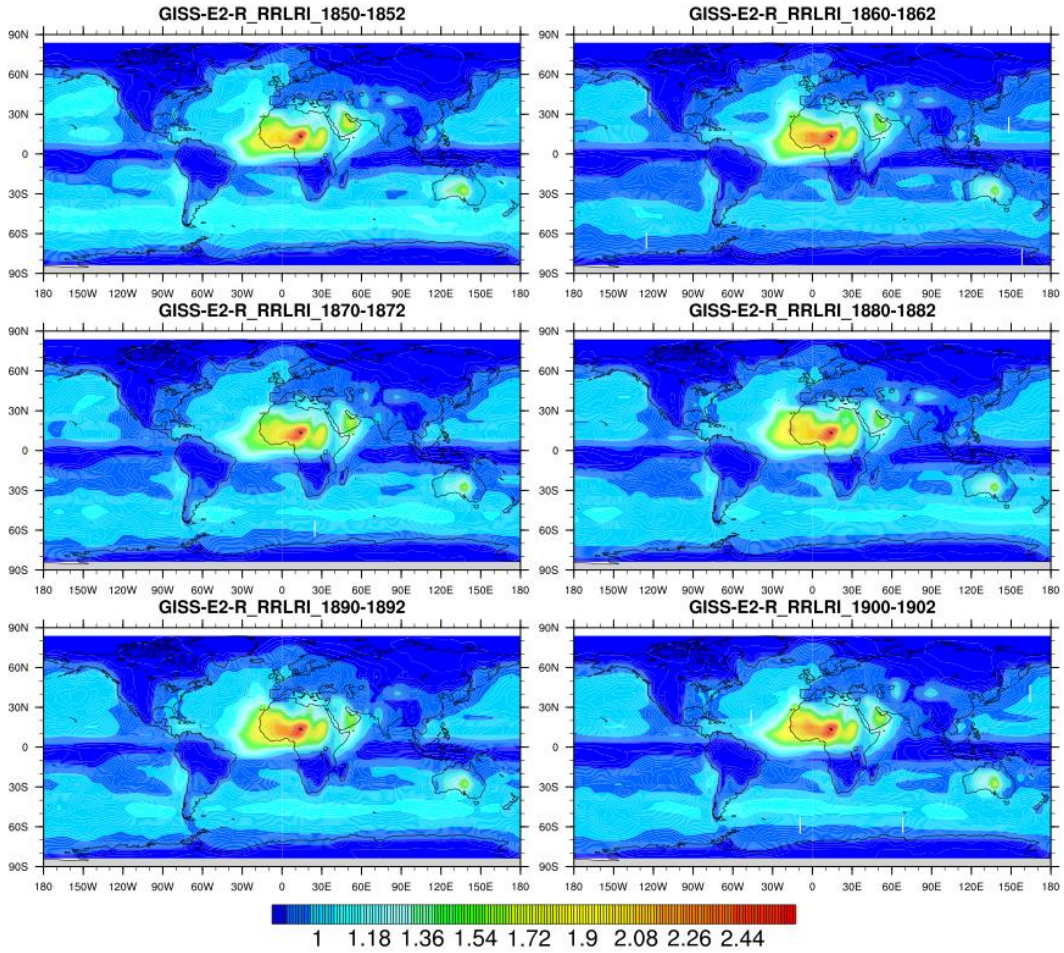


Figure 14 Global relative risk for lower respiratory infection for 6 time periods from 1850s to 1900s with the ambient $PM_{2.5}$ concentration output from GISS-E2-R model based on the integrated risk function developed for GBD(Burnett et al., 2014b) *for each figure, vertical axes indicate latitude and horizontal axes indicate longitude. The map plot indicate the level of relative risk over a global terrain by applying the concentration-risk function from IER model for LRI disease endpoint.*

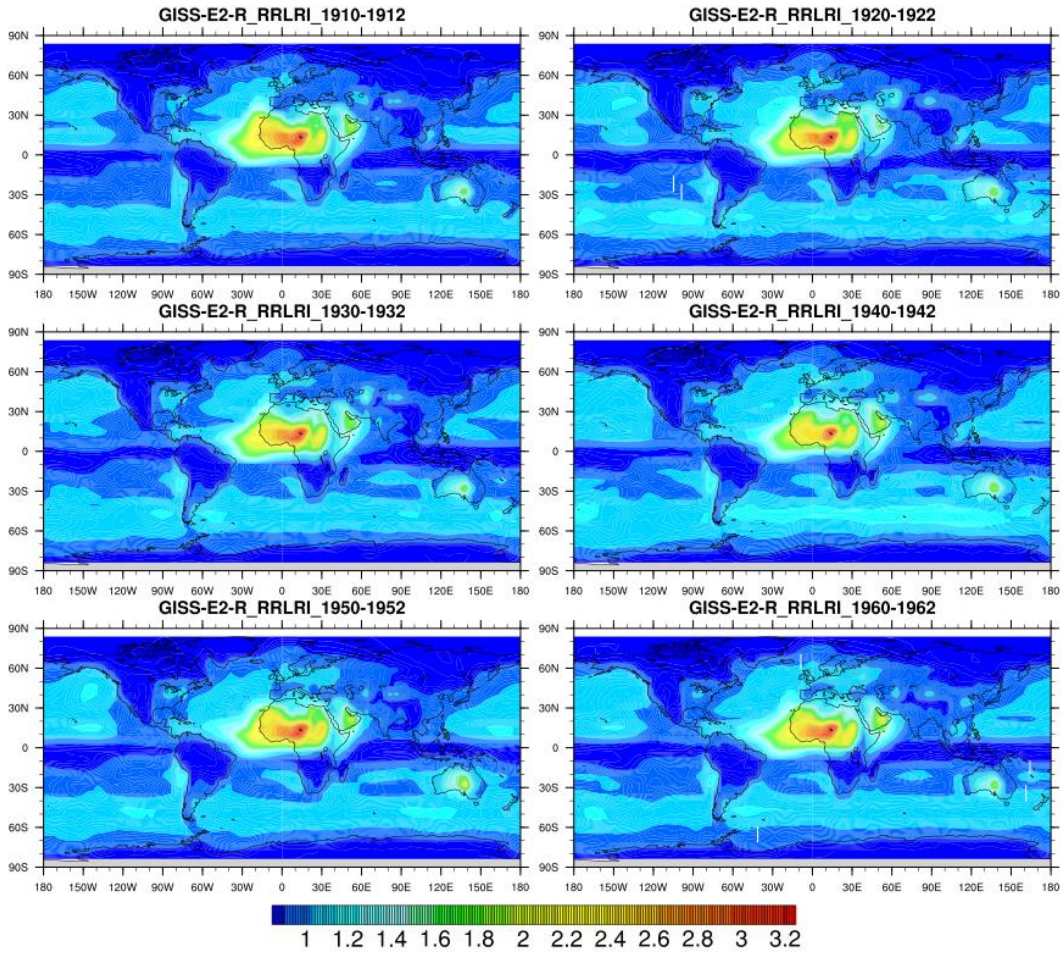


Figure 15 Global relative risk for lower respiratory infection for 6 time periods from 1910s to 1960s with the ambient $PM_{2.5}$ concentration output from GISS-E2-R model based on the integrated risk function developed for GBD(Burnett et al., 2014b) *for each figure, vertical axes indicate latitude and horizontal axes indicate longitude. The map plot indicate the level of relative risk over a global terrain by applying the concentration-risk function from IER model for LRI disease endpoint.*

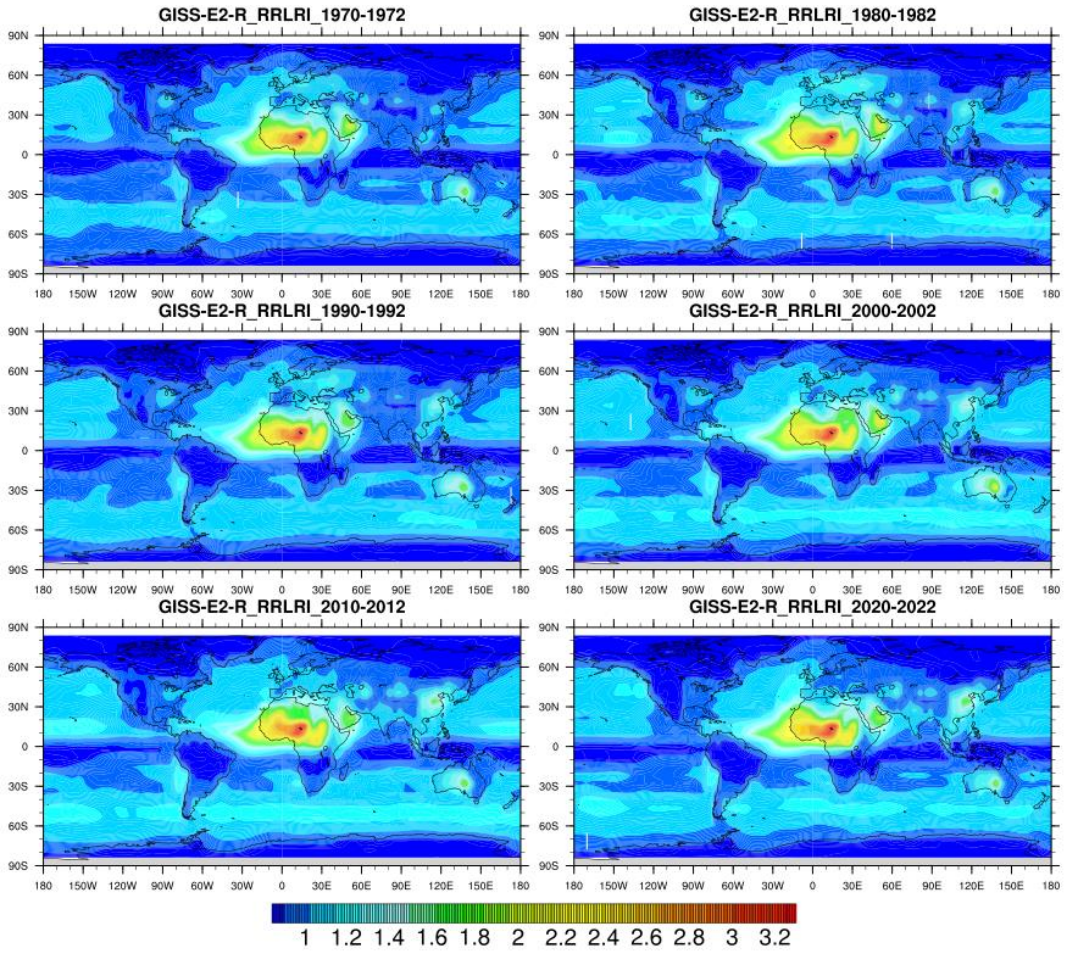


Figure 16 Global relative risk for lower respiratory infection for 6 time periods from 1970s to 2020s with the ambient $PM_{2.5}$ concentration output from GISS-E2-R model based on the integrated risk function developed for GBD(Burnett et al., 2014b) *for each figure, vertical axes indicate latitude and horizontal axes indicate longitude. The map plot indicate the level of relative risk over a global terrain by applying the concentration-risk function from IER model for LRI disease endpoint.*

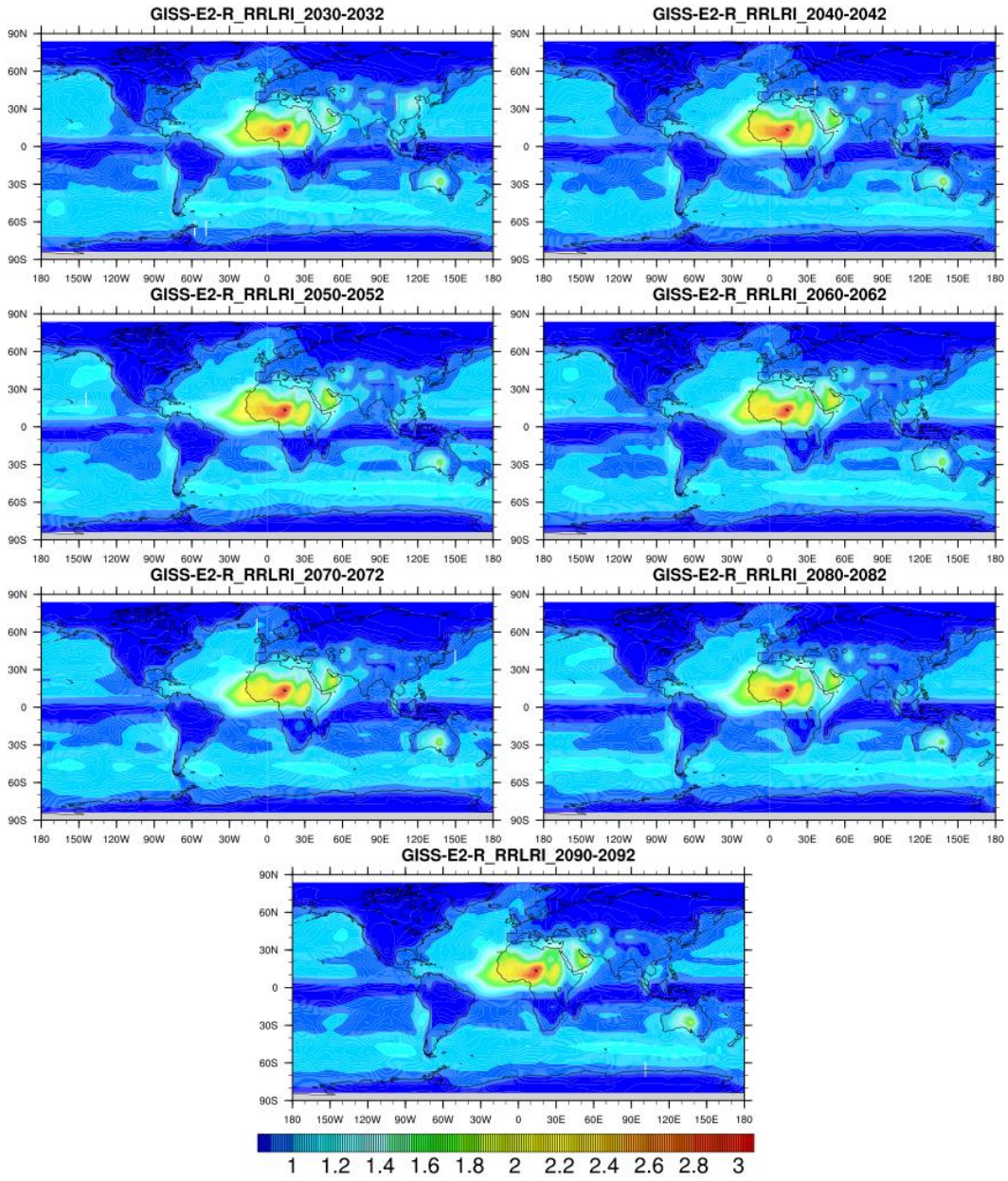


Figure 17 Global relative risk for lower respiratory infection for 7 time periods from 2030s to 2090s with the ambient $PM_{2.5}$ concentration output from GISS-E2-R model based on the integrated risk function developed for GBD(Burnett et al., 2014b) *for each figure, vertical axes indicate latitude and horizontal axes indicate longitude. The map plot indicate the level of relative risk over a global terrain by applying the concentration-risk function from IER model for LRI disease endpoint.*

The annual spatial distribution of LNC risk shows the relatively low level all through the time periods with a relatively high risk level in 1850s. The risk peak in northern Africa regions is persistent all through all seasons and years due to the possible impact from massive Saharan dust storms. With the transport of Saharan dust, some regions of Europe might display positive effect of dust storm fine particle related health impact of cardiac, respiratory mortality but the effect might still be not statistically significant. (Karanasiou et al., 2012) It is found that Saharan dust can transport to regions including United States, the Caribbean and South America, western Mediterranean, Europe, eastern Mediterranean and the Middle East. The elevation of risk in those regions is partially attributed from the Saharan dust storm.

The Saharan region and its surroundings are responsible for 600 to 900Tg of atmospheric dust annually, accounting for half of the global total dust emission. The impact from Saharan dust would increase the relative risk due to its large amount of presence. The health risk from PM_{10} in Saharan dust is widely documented since daily PM_{10} concentration might rise to a level as high as a daily value of $4024 \mu g/m^3$ in extreme situation. (de Longueville et al., 2013) The elevated risk in the Saharan regions and surroundings in this study might be an indication of such problem. The dust loadings might change substantially due to climate change so it would be interesting to look into the long-term change in the dust storm particulates emission. (Goudie et. al., 2001)

4.3 MIROC-CHEM MODEL OUTPUT

Figure 18 depicts the relative risk output from MIROC-CHEM model under RCP2.6 scenario with a time range from 1850s to 2050s.

Compared with GISS-E2-R model, MIROC-CHEM predicts an elevated relative risk in the region of Chile. The risk level in northern and Sub-Saharan Africa remains high all through the time periods. The risk level in eastern Asia is elevated since 1980s and the level start decreasing from 2030s. There is also an obvious elevation in Europe in 1980s, which is consistent with the output from the GISS-E2-R model.

Lower respiratory infection (Figure 19) relative risk values are generally higher than other two diseases. Lower respiratory infection is more sensitive to exposure of surface $PM_{2.5}$ concentration than cardiopulmonary disease or lung cancer. The reason for that is the reatlive risk value for LRI is higher than COPD and LNC when $PM_{2.5}$ concentration exceeds 20.2 $\mu g/m^3$ from IER RR value table.(Apte et al., 2015)

There is a widespread elevated risk level in the 1930s for lung cancer disease. The elevated values in central Asia in the 1850s are no longer perceived in other eras. The difference between 1850s and 1930s might be attributed to the Gobi desert dust storm. (Figure 20)

4.4 RCP SCENARIO COMPARISON

RCP scenarios describe the trend of greenhouse gas emission in the future with RCP 2.6 being the best scenario with the radiation forcing increase of +2.6W/m^2 by 2100 and the emission is cut by 40% in 100 years with RCP8.5 being the worst scenario with the radiative forcing increase of +8.5W/m^2 as the prediction of GtC increase in an order of 15 to 20 by 2100.

Figure 21 depicts the trend of emission of main greenhouse gases across all RCPs. Emission trends of air pollutants are determined by the change in driving force, the assumed air pollution control policy and the assumed climate policy. All the RCP scenarios assume that air pollution emissions would decrease in the future as a general trend. But generally the best greenhouse gas emission scenario RCP 2.6 is associated with the best scenario in air pollution emission while the worst greenhouse gas emission scenario RCP 8.5 is associated with the worst. Only the general trend is as described as above, but the trend in specific regions or at specific time is still undetermined.

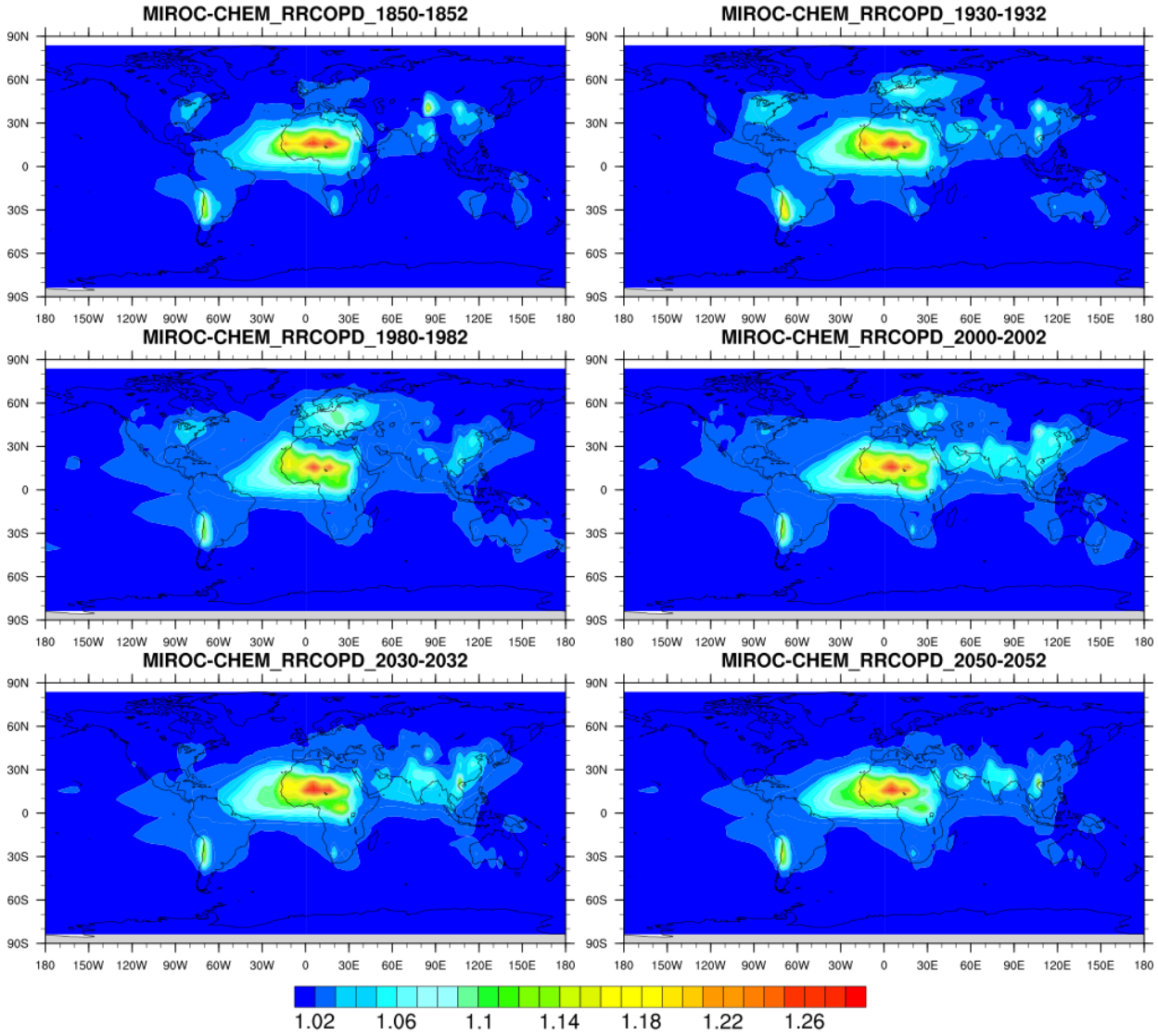


Figure 18 Global relative risk annual plot for cardiopulmonary disease from 1850s to 2050s of the three year average data from the ambient $PM_{2.5}$ concentration output from MIROC-CEHM model based on the integrated risk function developed for GBD(Burnett et al., 2014b) for each figure, vertical axes indicate latitude and horizontal axes indicate longitude. The map plot indicate the monthly level of relative risk over a global terrain by applying the concentration-risk function from IER model for COPD disease endpoint.

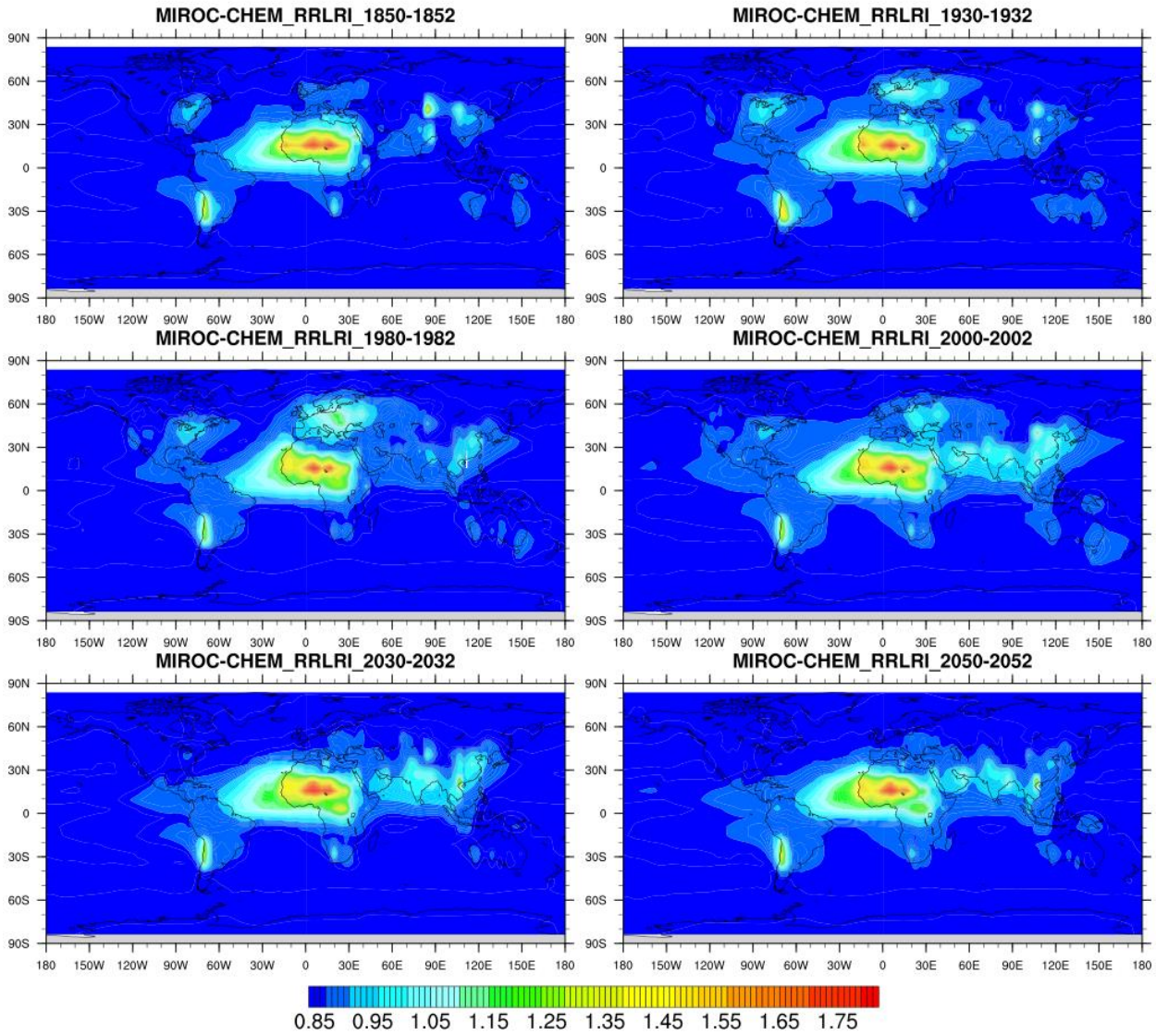


Figure 19 Global relative risk annual plot for lower respiratory infection disease from 1850s to 2050s of the three year average data from the ambient $PM_{2.5}$ concentration output from MIROC-CEHM model based on the integrated risk function developed for GBD(Burnett et al., 2014b) for each figure, vertical axes indicate latitude and horizontal axes indicate longitude. The map plot indicate the monthly level of relative risk over a global terrain by applying the concentration-risk function from IER model for LRI disease endpoint.

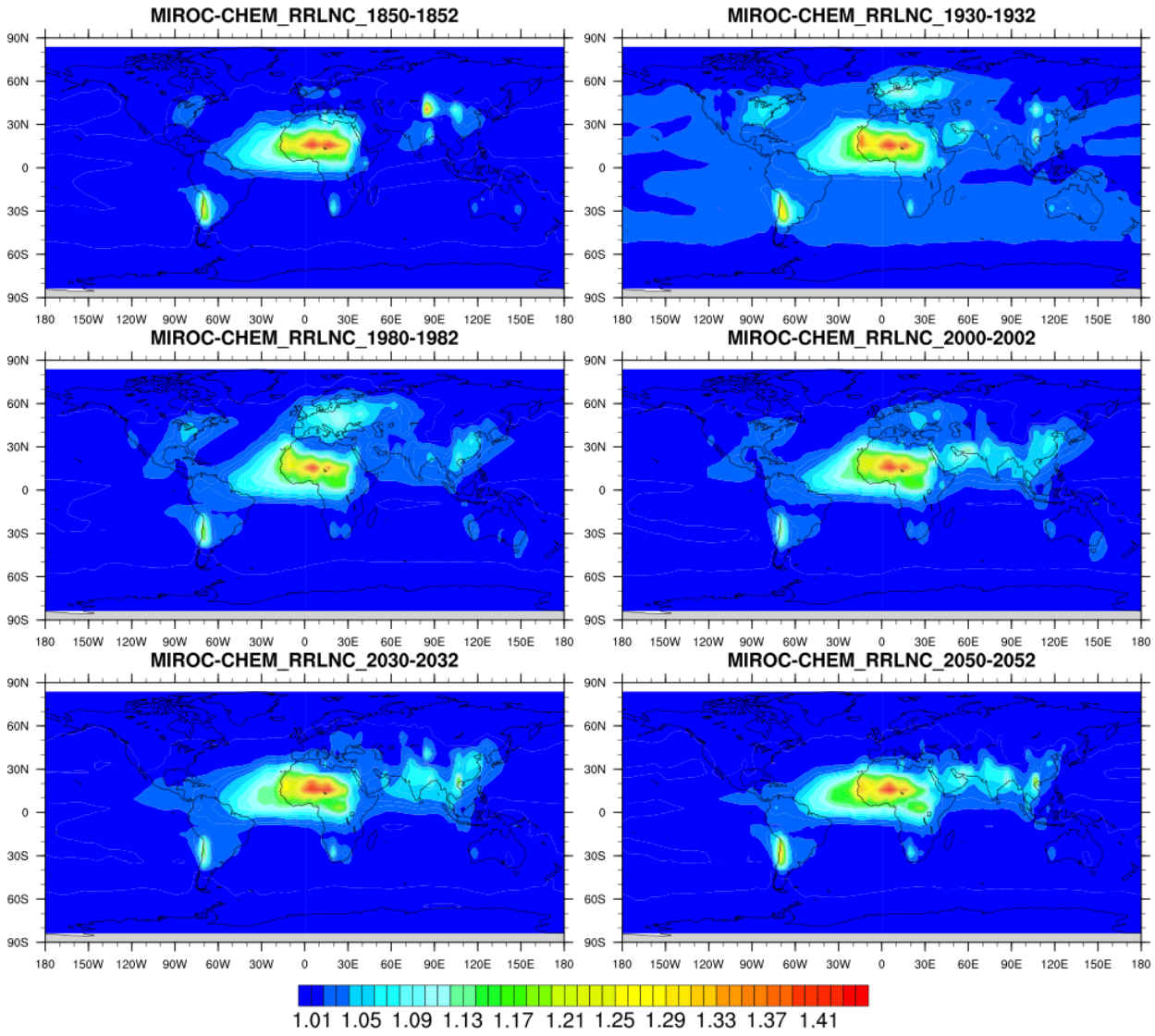


Figure 20 Global relative risk annual plot for lung cancer disease from 1850s to 2050s of the three year average data from the ambient $PM_{2.5}$ concentration output from MIROC-CEHM model based on the integrated risk function developed for GBD(Burnett et al., 2014b) for each figure, vertical axes indicate latitude and horizontal axes indicate longitude. The map plot indicate the monthly level of relative risk over a global terrain by applying the concentration-risk function from IER model for LNC disease endpoint.

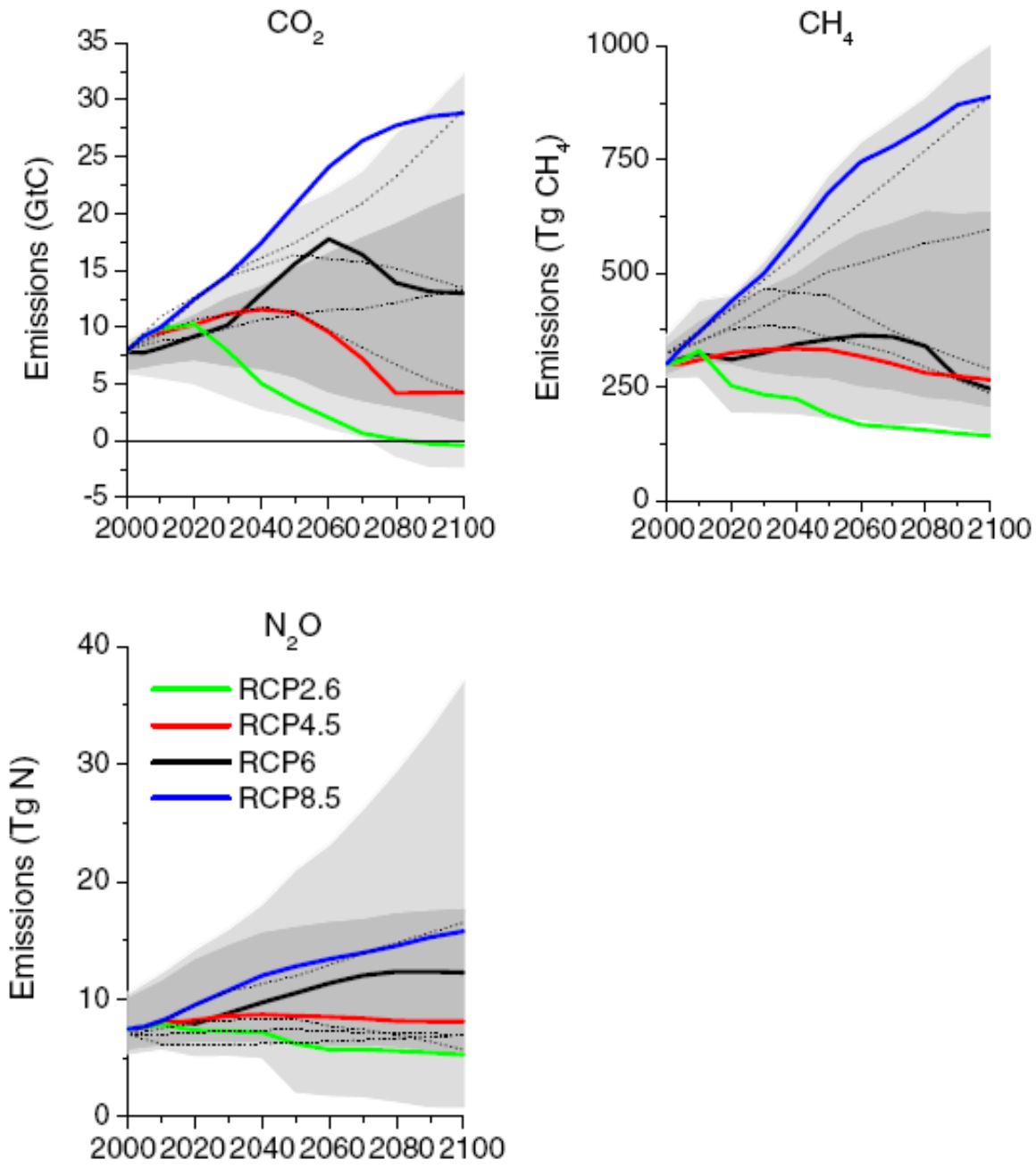


Figure 21 Emissions of main greenhouse gases CO_2, CH_4, N_2O from 2000 to 2100 across all RCPs[4]. The four RCPs, RCP2.6, RCP4.5, RCP6.0, and RCP8.5, refer to a possible range of radiative forcing values in the year 2100 compared with pre-industrial values (+2.6, +4.5, +6.0, and +8.5 W/m^2, respectively) For CO_2 and N_2O, the emission amount increase from 2000 to 2100 from highest to lowest is RCP8.5, RCP6.0, RCP4.5, RCP2.6. For methane emissions, RCP4.5 and RCP 6 share similar trajectory all through the time.

[4] https://www.skepticalscience.com/RCP.php?t=3#trajectories

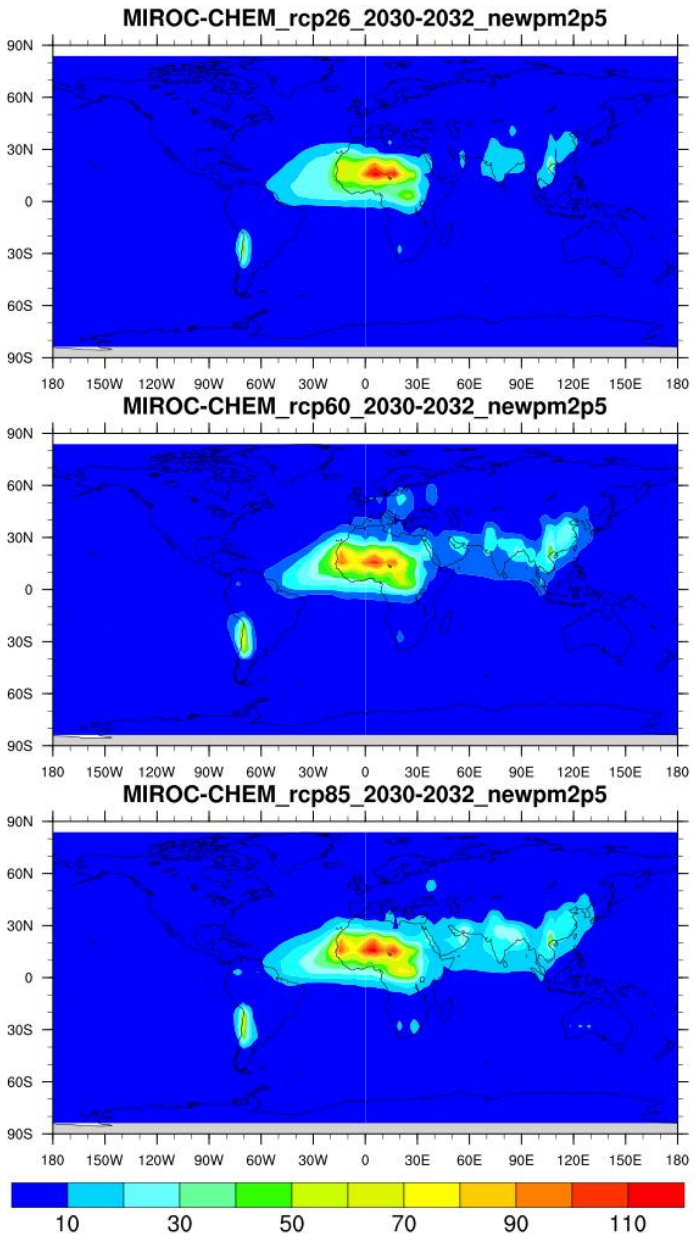


Figure 22 RCP scenarios (RCP2.6, RCP6.0, RCP8.5) comparison for $PM_{2.5}$ surface concentration from MIROC-CHEM model output in 2030s. The ambient $PM_{2.5}$ concentration is the three year average of 2030, 2031, 2032 with unit of $\mu g/m^3$. RCP8.5 depicts the worst scenario, especially in Asia.

Figure 22 describes the $PM_{2.5}$ concentration comparison between RCP2.6, RCP6.0.0 and RCP8.5 scenarios for 2030 projection from MIRCO-CHEM output.
The surface fine particle level is high in RCP8.5 scenario and low in RCP2.6 scenario, especially for the Asian region. The highest radiative forcing (RCP8.5) scenario is associated with the heaviest pollution level in Asia and the Saharan regions. The reason is that dust in dry regions, especially smaller particles, tends to be lofted into the air by wind erosion. So it is possible that dryer and hotter weather patterns in certain regions caused by climate change would increase the intensity or frequency of dust storm activities.

However, the effect of climate change upon dust activities might be complicated and not just limited to air lofting. For example, dust particles both reflect and absorb sunlight and thus reducing the surface temperature. At the same time, the radiative forcing variation would alter the sea-land circulation and affect wind activities. Climate change would also alter monsoon and thus influencing dust storm activities since dust particles cannot travel long distances under very wet conditions and rainfall would cause precipitation of particles. (Miller et. al., 1998)

Overall, all those interactions would contribute to the alteration in dust activities.

The output shows the generally increased severity of dust storm effect in the Saharan regions, which indicates that larger wind erosion might occur with higher radiative forcing.

Figure 23 depicts relative risk of cardiopulmonary disease from MIROC-CHEM model at 2030 from RCP2.6, RCP6.0.0, RCP8.5 scenarios. Figure 24 depicts lower respiratory infection risk while figure 25 depicts lung cancer risk from MIROC-CHEM model at 2030 from RCP2.6, RCP6.0.0, RCP8.5 scenarios respectively.

RCP8.5 has the highest projected level of COPD relative risk in the 2030s. Radiative forcing is the factor influencing the variation.

LRI has very varied relative risk value distribution from various scenarios. RCP6.0.0 has a relatively higher level in Europe region and eastern Asia than other scenarios. (Figure 24)

RCP6.0 has the highest prediction for elevated surface $PM_{2.5}$ concentration level in eastern Asia and Australia.

RCP 6.0 predicts a higher level of RR in eastern Asia, south-eastern Asia as well as western Asia compared with other scenarios in 2030s.

GISS-E2-R has a higher prediction of LRI risk in 2030s than MIROC-CHEM model.

Figure 26 describes the $PM_{2.5}$ concentration comparison between RCP2.6, 6.0 and 8.5 for 2050 projection from MIRCO-CHEM output. RCP6.0 pictures 2050s as more elevated in East Asia while RCP8.5 depicts the high concentration in Saharan regions.

Figure 27, 28, 29 depict the relative risk value comparison between RCP2.6, 6.0 and 8.5 for COPD,LNC,LRI respectively for 2050 projection from MIRCO-CHEM.

The highest risk elevation in Asia is for RCP6.0.0 scenario while the highest risk elevation in northern Africa is for RCP8.5 scenario in 2050s.

For the MIROC-CHEM model output in 2050s, RCP6.0.0 predicts an elevated level in eastern Asia while RCP8.5 predicts a higher level in southern Africa.

So the relative risk for LNC is elevated in eastern and south-eastern Asia for RCP6.0.0 while it is elevated in western and southern Asia for RCP8.5. RCP8.5 also predicts an elevated level in southern Africa.

Figure 30 describes the $PM_{2.5}$ concentration comparison between RCP2.6,4.5, 6.0 and 8.5 for 2050 projection from GISS-E2-R output.

RCP 6.0 is the only scenario that predicts elevated $PM_{2.5}$ in eastern Asia for 2050s.

Figure 31 describes the COPD relative risk comparison between RCP2.6,4.5, 6.0 and 8.5 for 2050 projection from GISS-E2-R output.

RCP 6.0 predicted an elevated risk level in eastern Asia in 2050s.

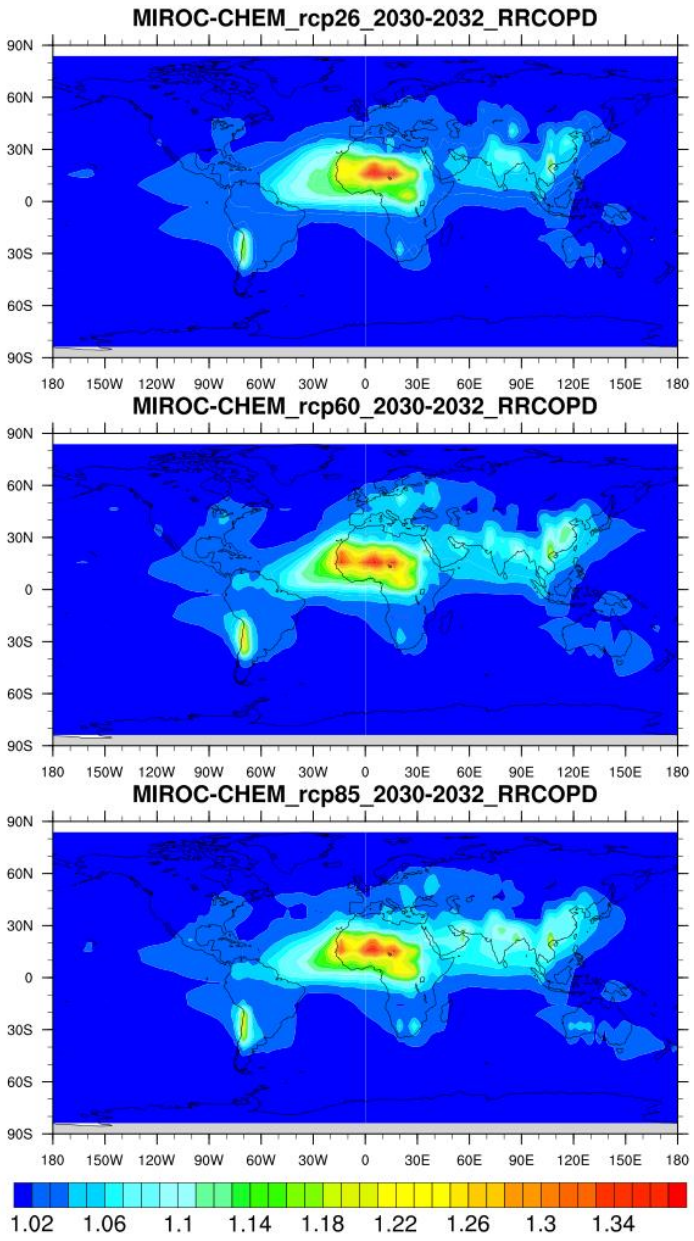


Figure 23 RCP scenarios (RCP2.6, RCP6.0, RCP8.5) comparison for cardiopulmonary disease relative risk from MIROC-CHEM model output in 2030s. The relative risk output is the three year average of 2030, 2031, 2032. RCP8.5 depicts the worst scenario, especially with a widespread elevation in relative risk over Asia.

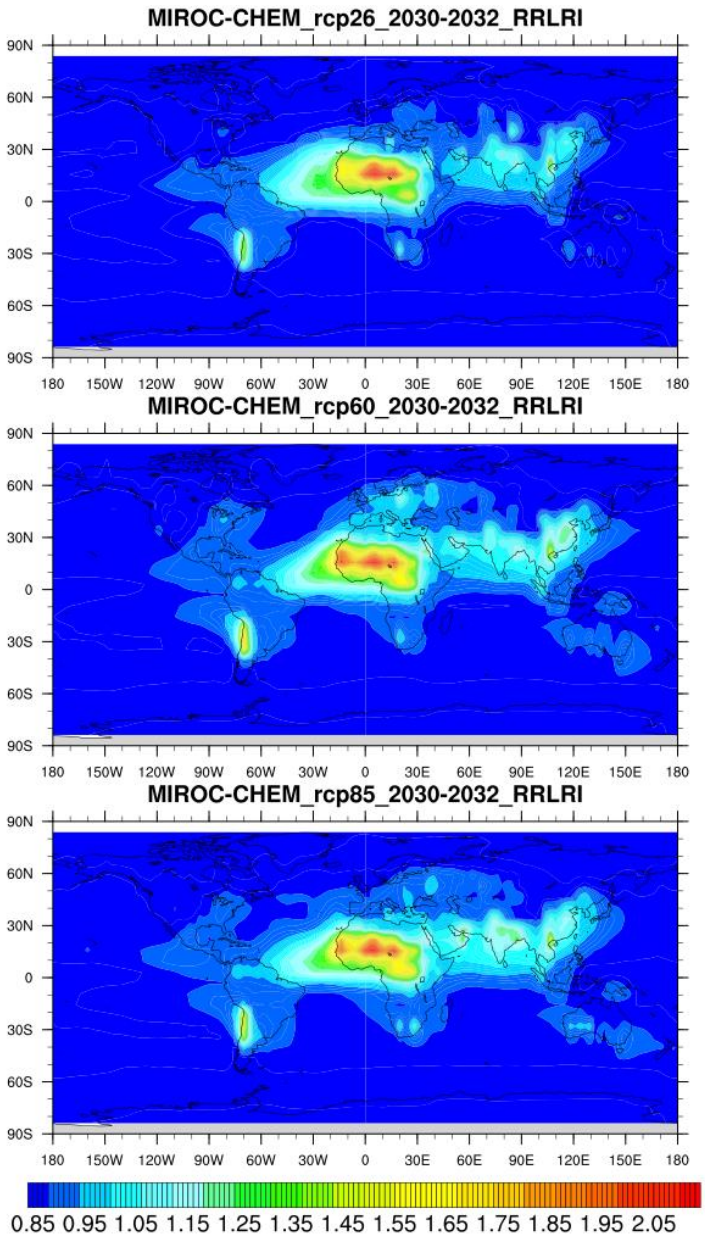


Figure 24 RCP scenarios (RCP2.6, RCP6.0, RCP8.5) comparison for lower respiratory infection disease relative risk from MIROC-CHEM model output in 2030s. The relative risk output is the three year average of 2030, 2031, 2032. RCP8.5 depicts the worst scenario, especially with a widespread elevation in relative risk over Asia.

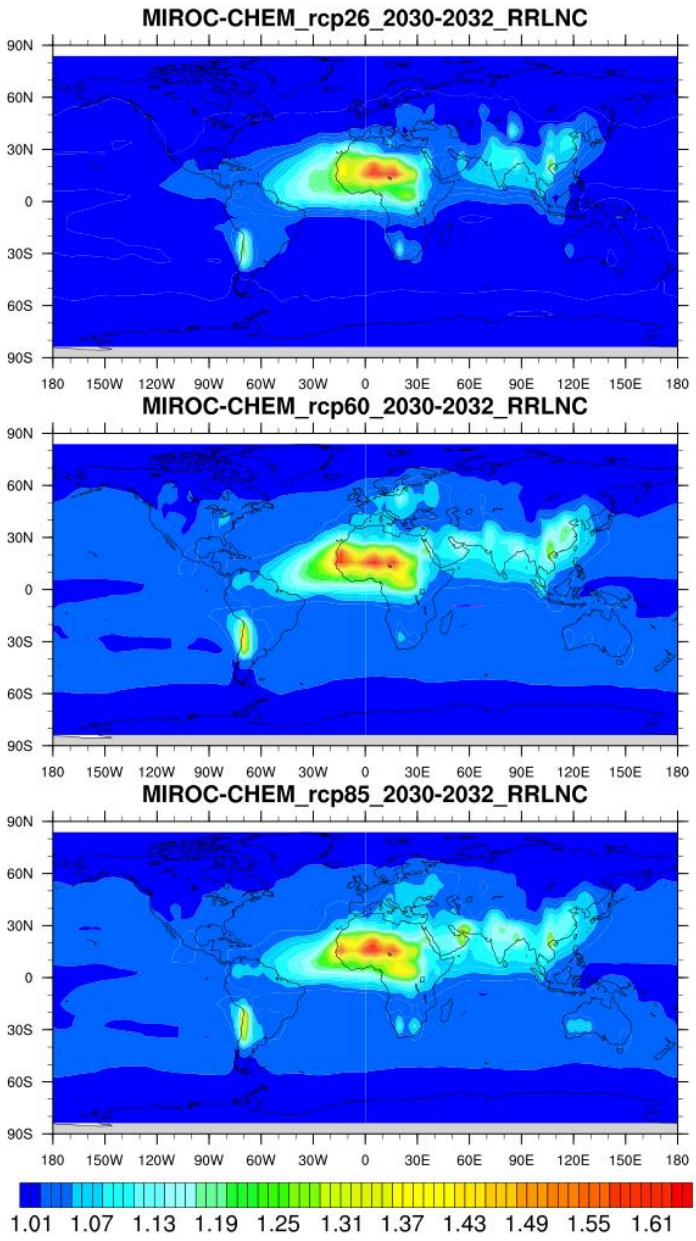


Figure 25 RCP scenarios (RCP2.6, RCP6.0, RCP8.5) comparison for lung cancer relative risk from MIROC-CHEM model output in 2030s. The relative risk output is the three year average of 2030, 2031, 2032. RCP8.5 depicts the worst scenario, especially with a widespread elevation in relative risk over Asia.

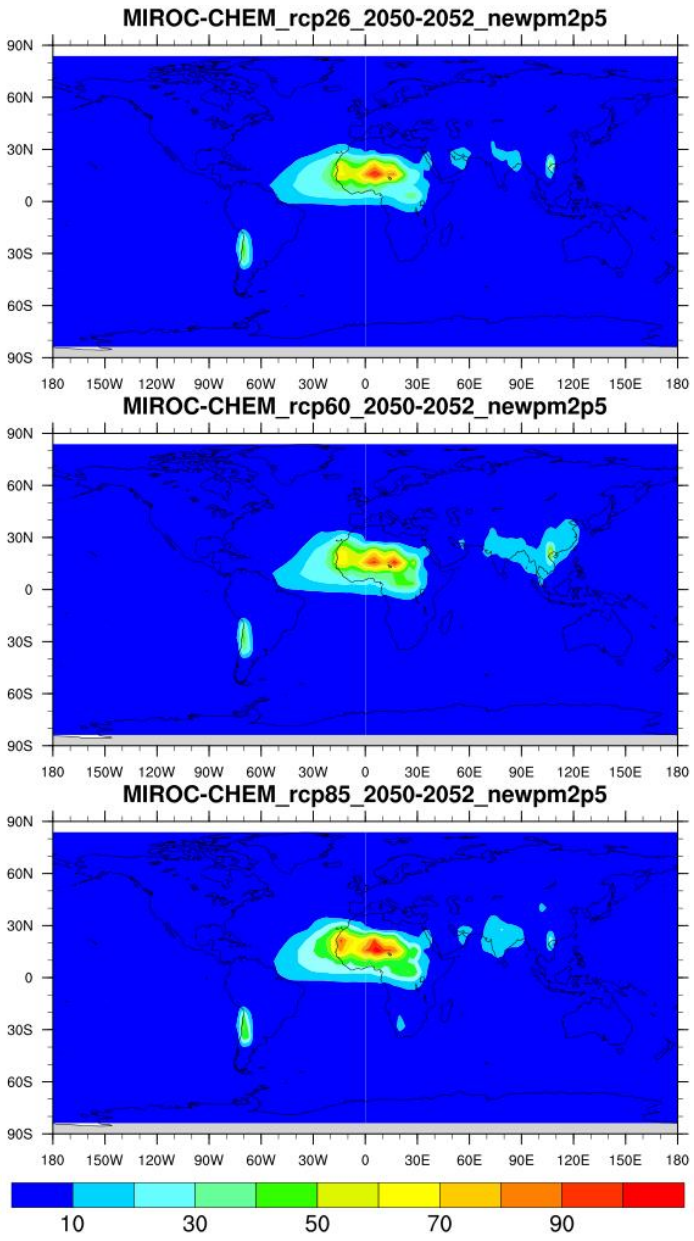


Figure 26 RCP scenarios (RCP2.6, RCP6.0, RCP8.5) comparison for $PM_{2.5}$ surface concentration from MIROC-CHEM model output in 2050s. The ambient $PM_{2.5}$ concentration is the three year average of 2050, 2051, 2052 with unit of $\mu g/m^3$. RCP8.5 depicts the worst scenario, especially in Asia.

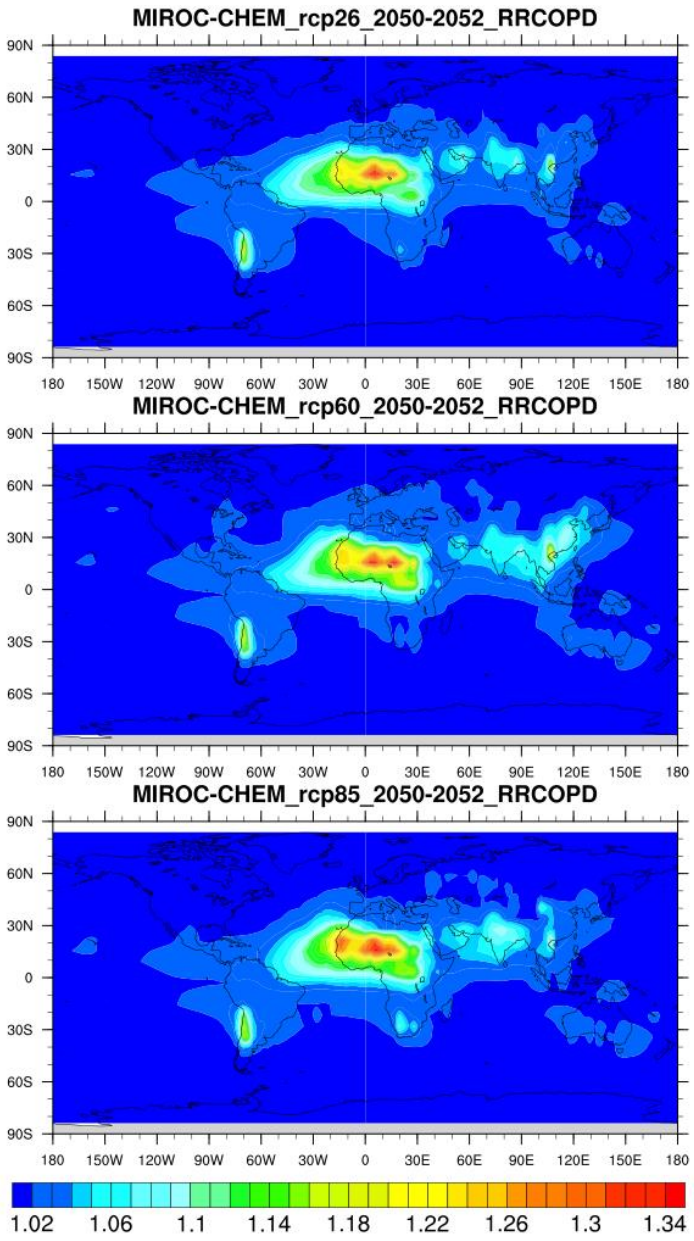


Figure 27 RCP scenarios (RCP2.6, RCP6.0, RCP8.5) comparison for cardiopulmonary disease relative risk from MIROC-CHEM model output in 2050s. The relative risk output is the three year average of 2050, 2051, 2052. RCP8.5 depicts the worst scenario, especially with a widespread elevation in relative risk over Asia.

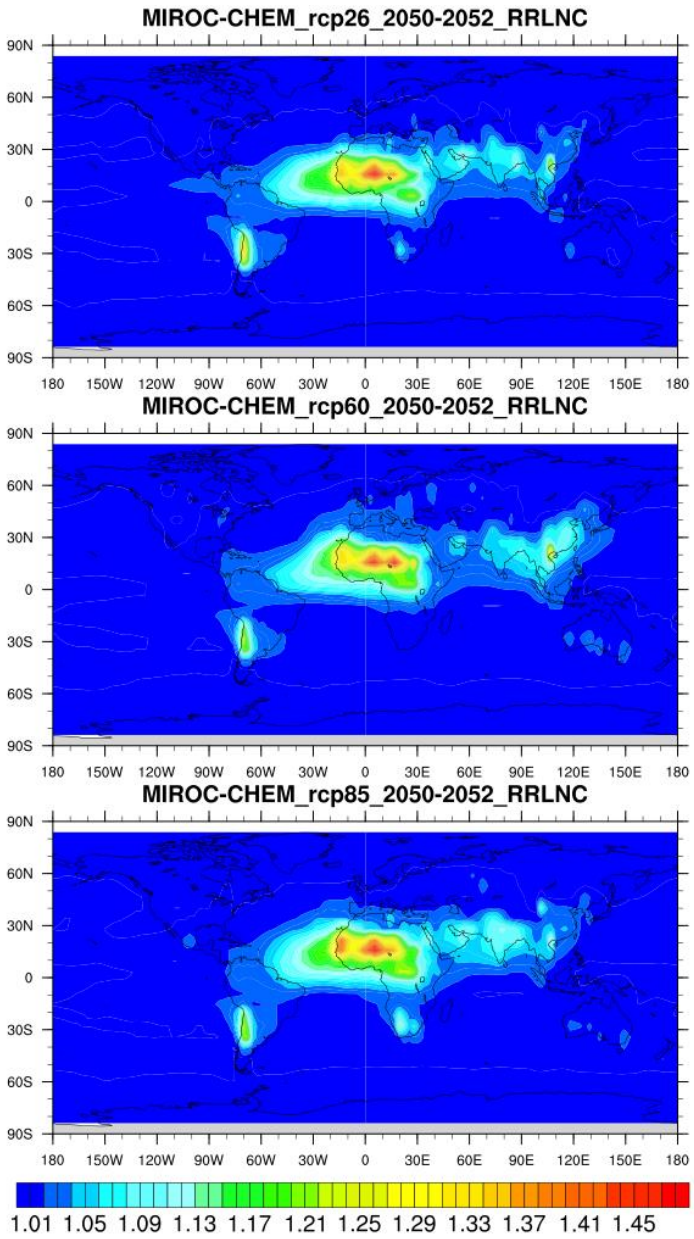


Figure 28 RCP scenarios (RCP2.6, RCP6.0, RCP8.5) comparison for lung cancer relative risk from MIROC-CHEM model output in 2050s. The relative risk output is the three year average of 2050, 2051, 2052. RCP8.5 depicts the worst scenario, especially with a widespread elevation in relative risk over Asia.

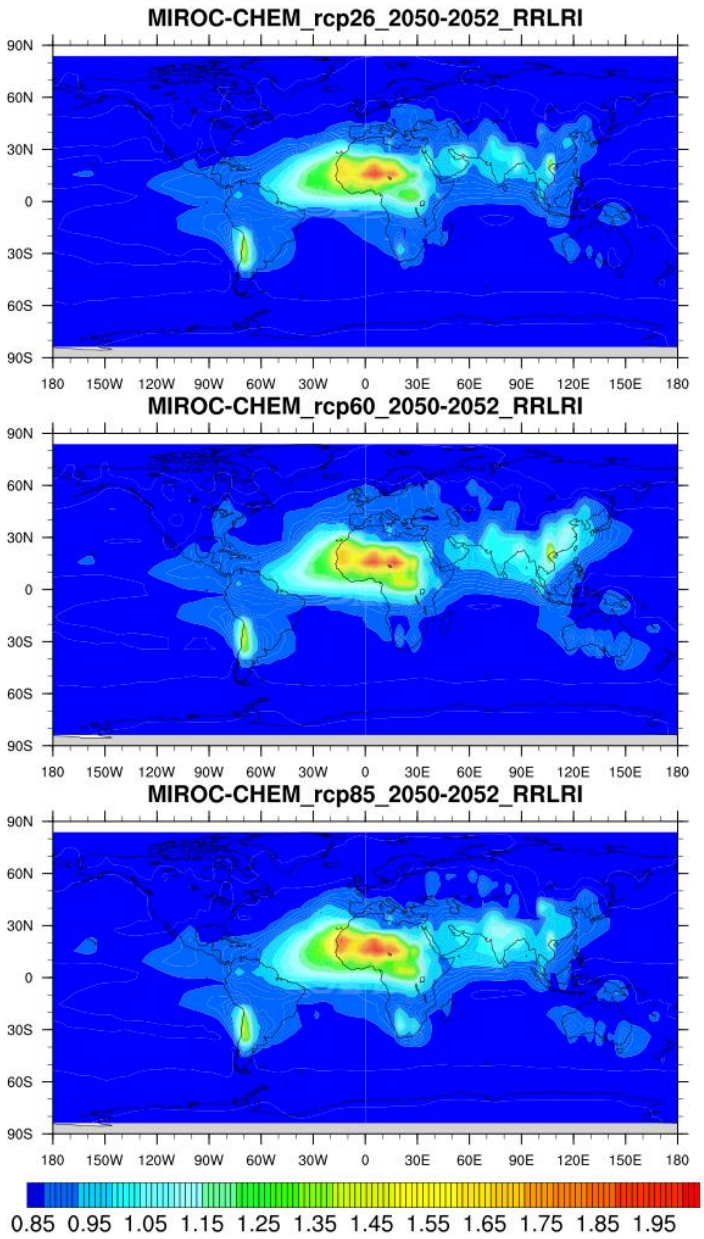


Figure 29 RCP scenarios (RCP2.6, RCP6.0, RCP8.5) comparison for lower respiratory infection relative risk from MIROC-CHEM model output in 2050s. The relative risk output is the three year average of 2050, 2051, 2052. RCP8.5 depicts the worst scenario, especially with a widespread elevation in relative risk over Asia.

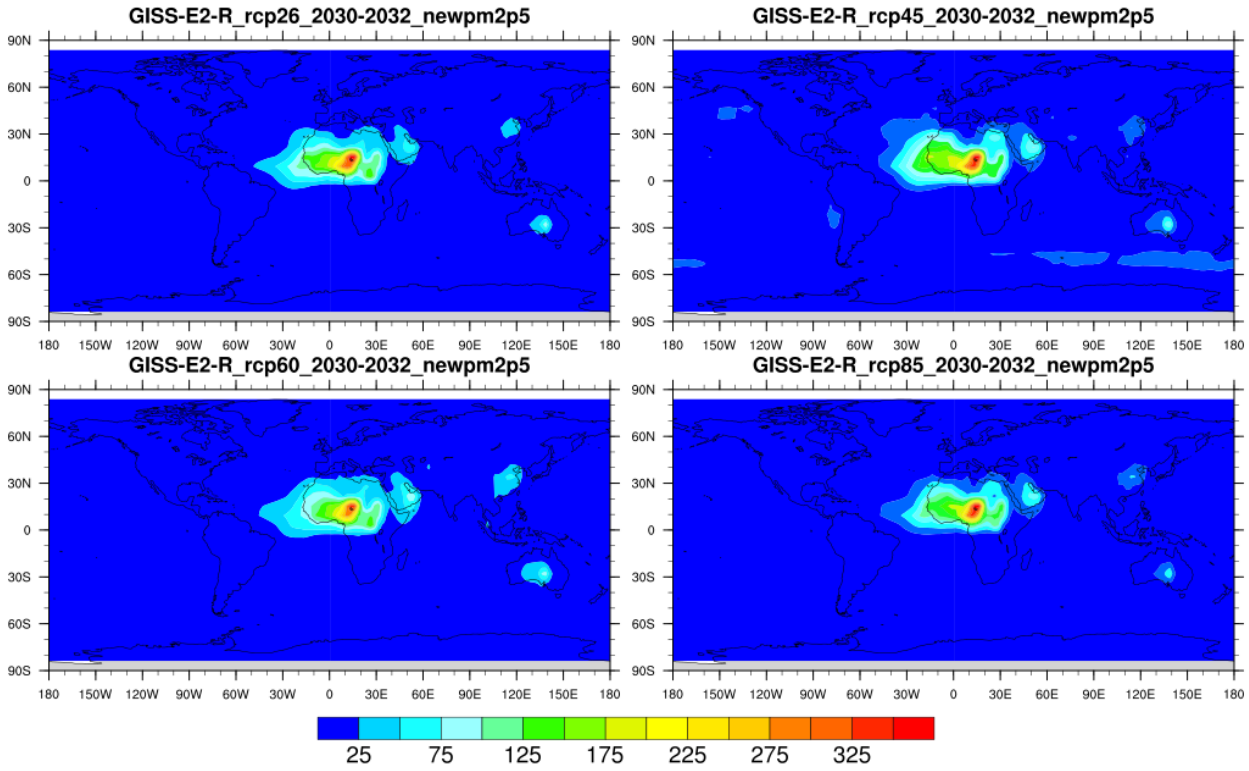


Figure 30 RCP scenarios (RCP2.6, RCP4.5, RCP6.0, RCP8.5) comparison for $PM_{2.5}$ concentration (unit:μg/m^3) from GISS-E2-R model output in 2030s. The relative risk output is the three year average of 2030, 2031, 2032.

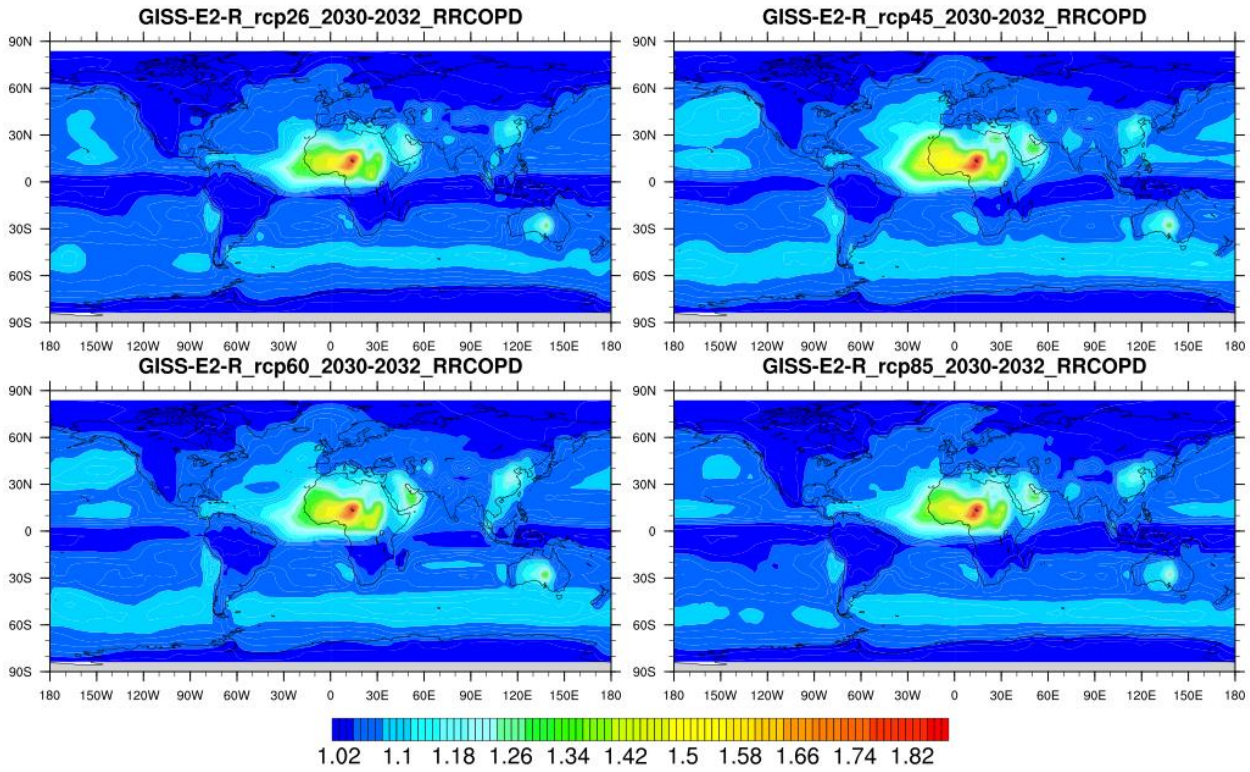


Figure 31 RCP scenarios (RCP2.6, RCP4.5, RCP6.0, RCP8.5) comparison for cardiopulmonary disease relative risk from GISS-E2-R model output in 2030s. The relative risk output is the three year average of 2030, 2031, 2032. RCP6.0 scenario predicts the highest risk level in eastern Asia.

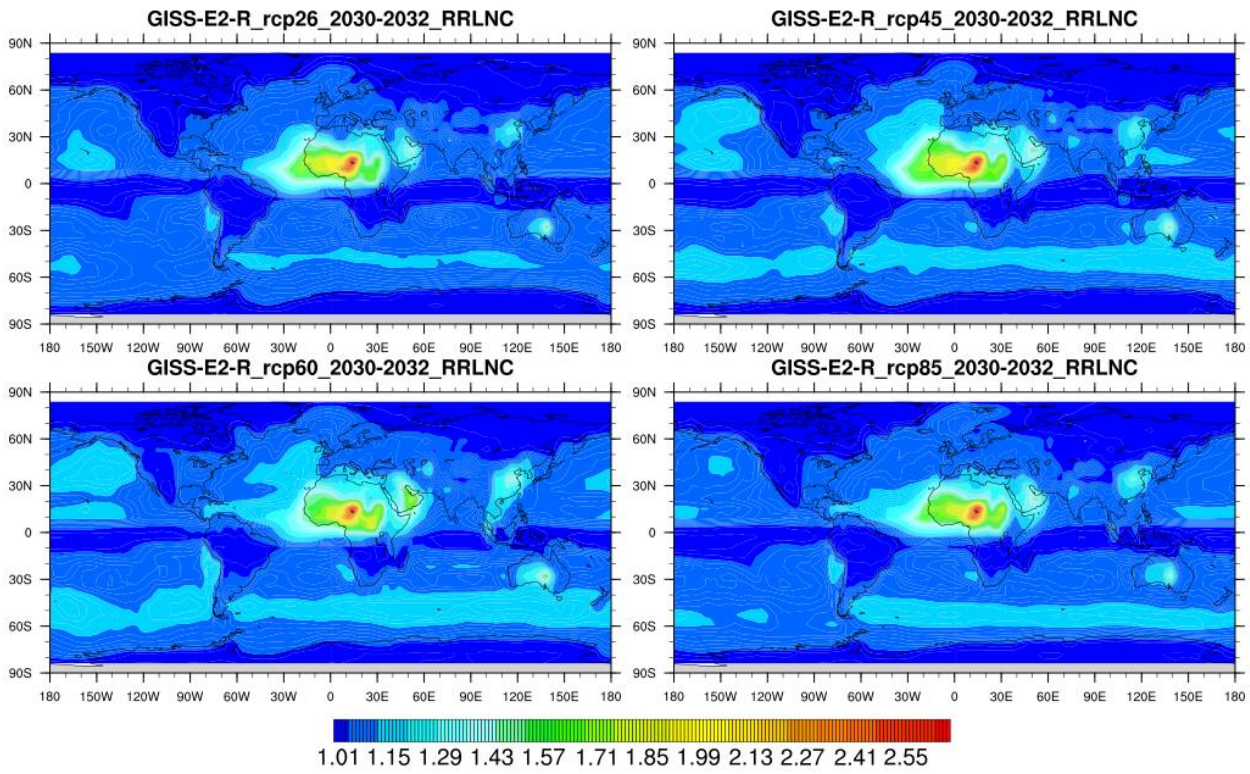


Figure 32 RCP scenarios (RCP2.6, RCP4.5, RCP6.0, RCP8.5) comparison for lung cancer relative risk from GISS-E2-R model output in 2030s. The relative risk output is the three year average of 2030, 2031, 2032. RCP6.0 scenario predicts the highest risk level in eastern Asia.

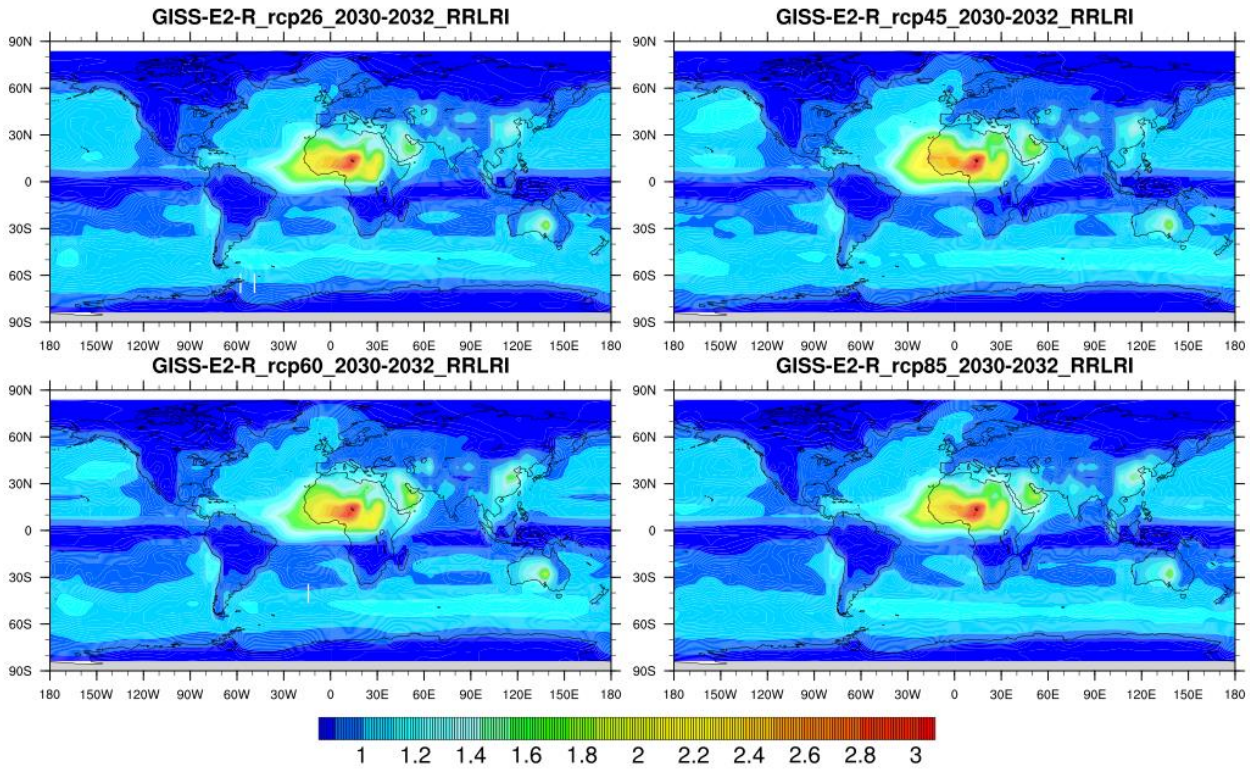


Figure 33 RCP scenarios (RCP2.6, RCP4.5, RCP6.0, RCP8.5) comparison for lower respiratory infection disease relative risk from GISS-E2-R model output in 2030s. The relative risk output is the three year average of 2030, 2031, 2032. RCP6.0 scenario predicts the highest risk level in eastern Asia.

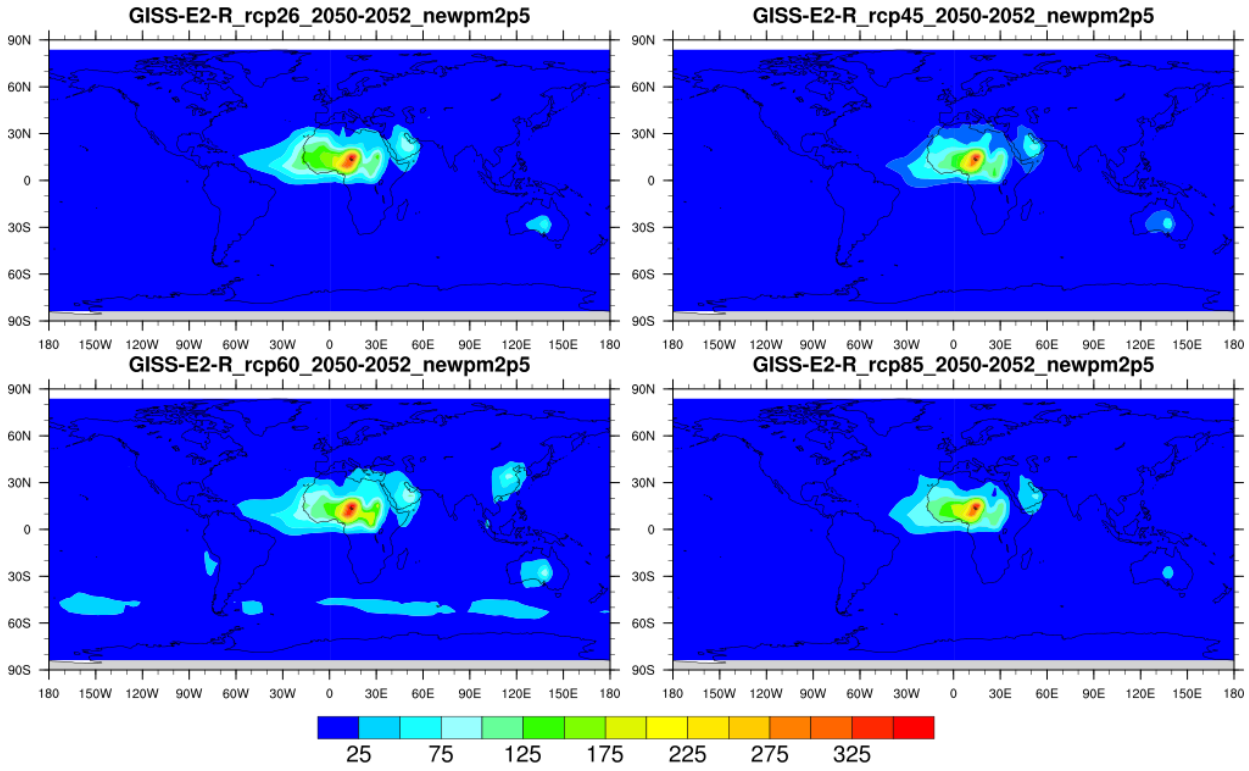


Figure 34 RCP scenarios (RCP2.6, RCP4.5, RCP6.0.0, RCP8.5) comparison for $PM_{2.5}$ concentration (unit: $\mu g/m^3$) from GISS-E2-R model output in 2050s. The relative risk output is the three year average of 2050, 2051, 2052.

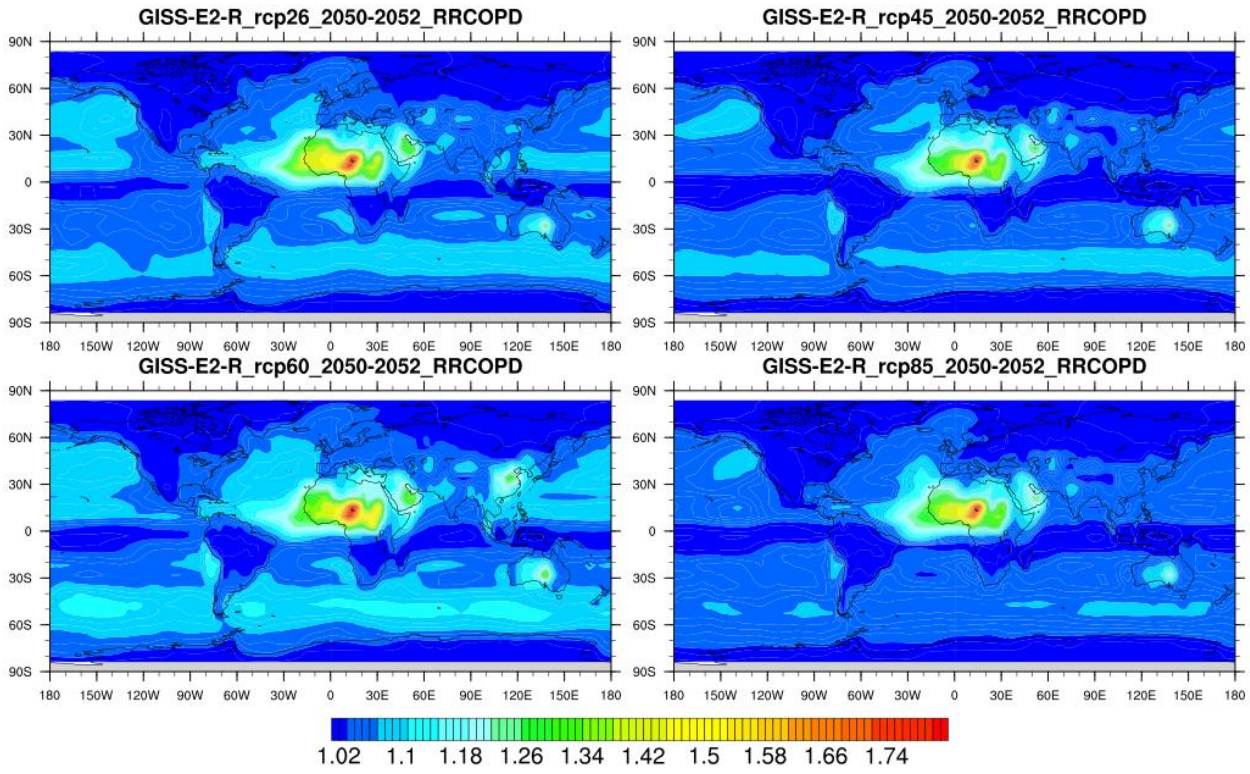


Figure 35 RCP scenarios (RCP2.6, RCP4.5, RCP6.0.0, RCP8.5) comparison for cardiopulmonary disease relative risk from GISS-E2-R model output in 2050s. The relative risk output is the three year average of 2050, 2051, 2052. RCP6.0.0 scenario predicts the highest risk level in eastern Asia.

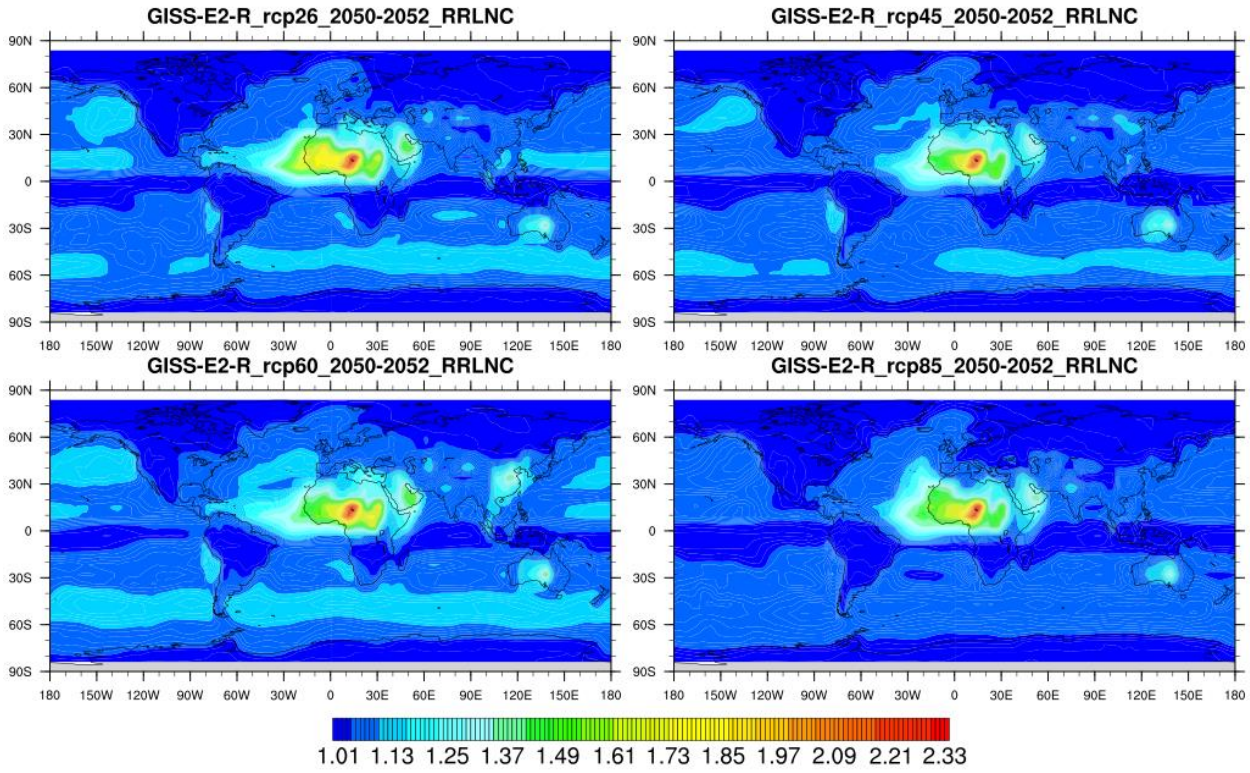


Figure 36 RCP scenarios (RCP2.6, RCP4.5, RCP6.0.0, RCP8.5) comparison for lung cancer disease relative risk from GISS-E2-R model output in 2050s. The relative risk output is the three year average of 2050, 2051, 2052. RCP6.0.0 scenario predicts the highest risk level in eastern Asia.

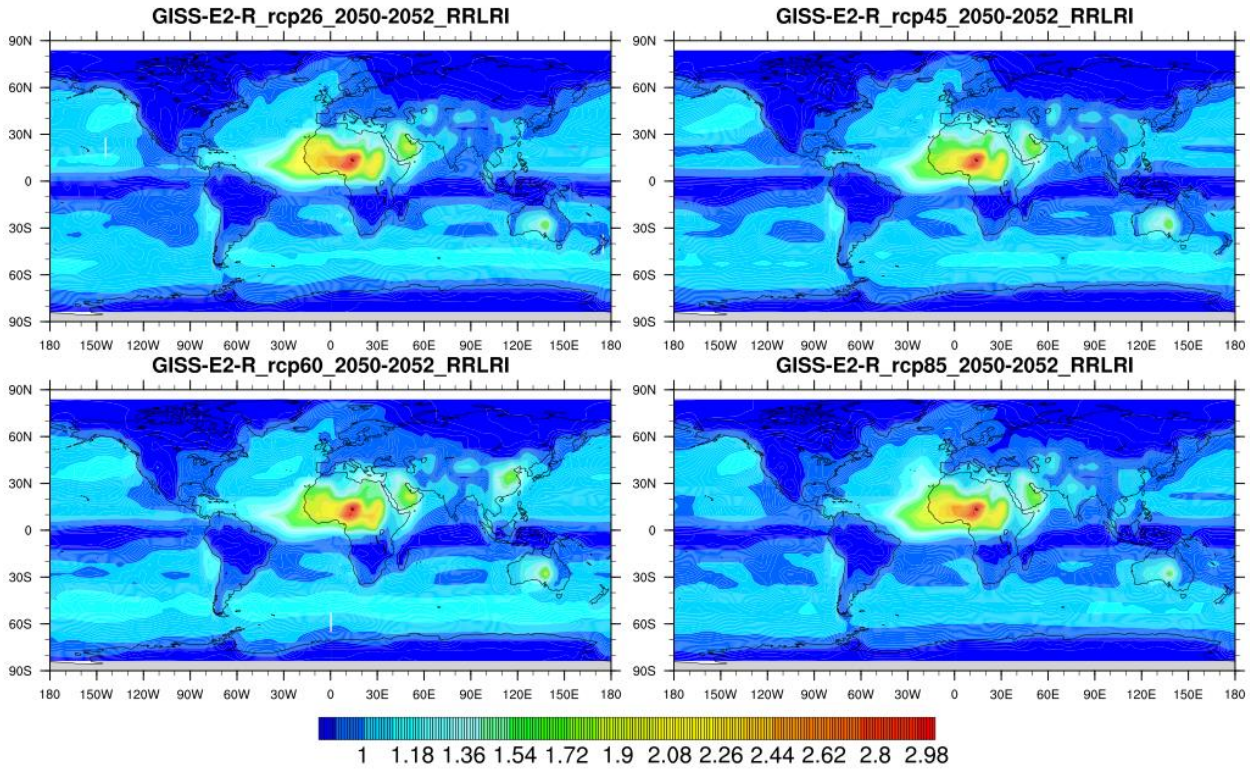


Figure 37 RCP scenarios (RCP2.6, RCP4.5, RCP6.0.0, RCP8.5) comparison for lower respiratory infection relative risk from GISS-E2-R model output in 2050s. The relative risk output is the three year average of 2050, 2051, 2052. RCP6.0.0 scenario predicts the highest risk level in eastern Asia.

4.5 COMPARISON BETWEEN MODELS

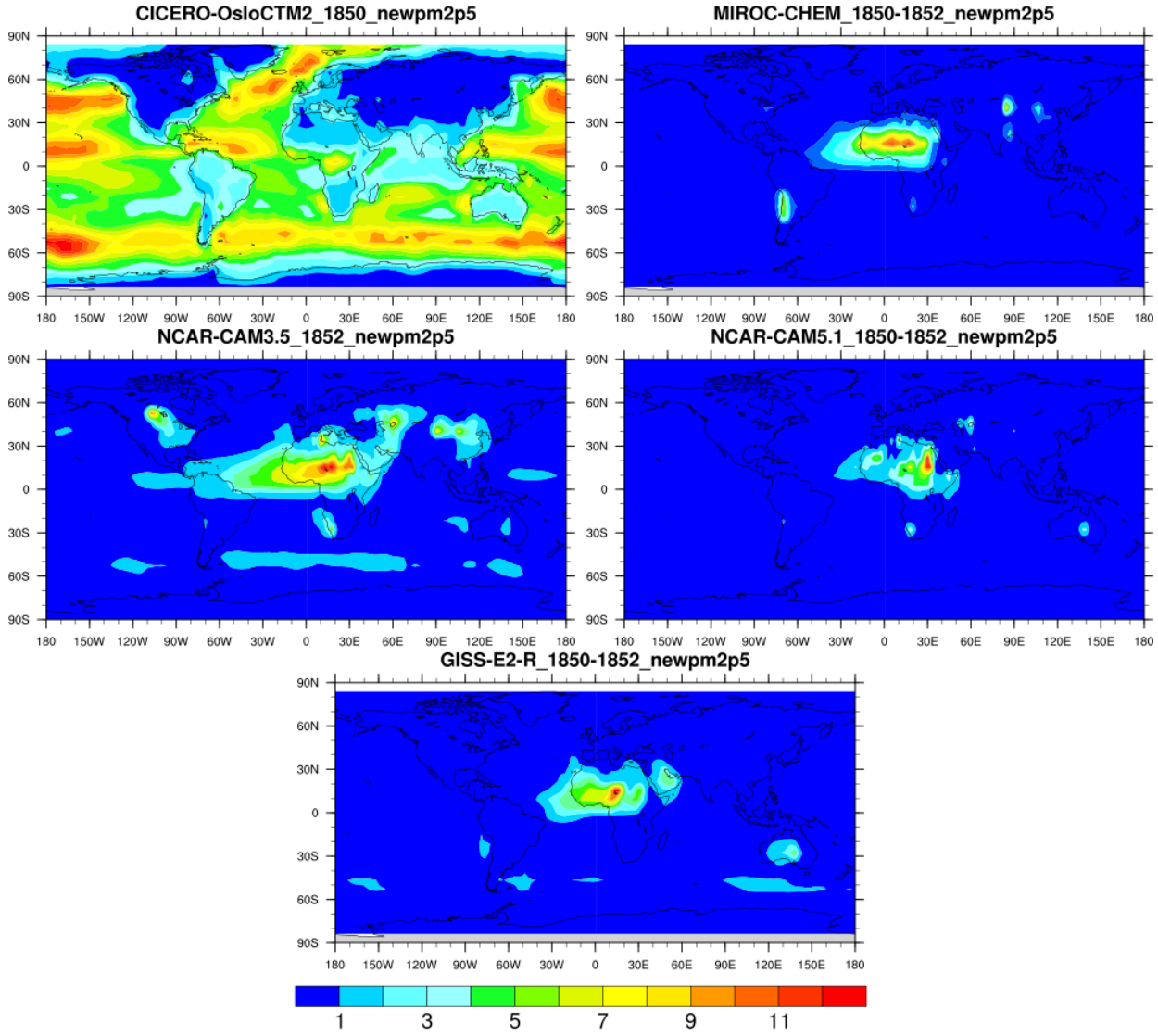


Figure 38 The comparison of ambient $PM_{2.5}$ concentration between various models (CICERO-OsloCTM2, MIROC-CHEM, NCAR-CAM3.5, NCAR-CAM5.1 and GISS-E2-R) in 1850s. CICERO-OsloCTM2 predicts surface concentration in an obvious different way compared with other models while NCAR-CAM3.5 has a generally higher prediction.

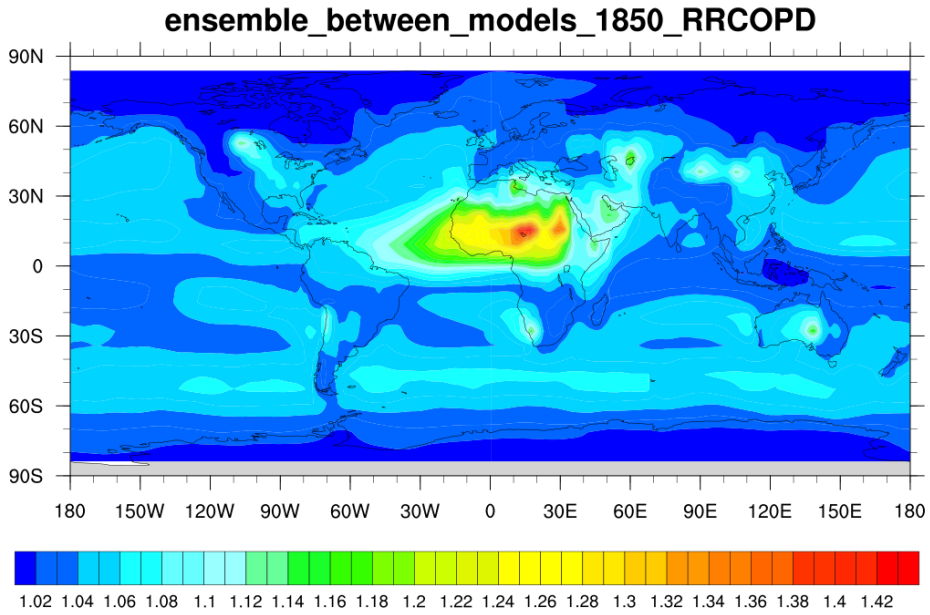


Figure 39 multi-ensemble results for COPD relative risk for 1850s with the unweighted average of cardiopulmonary relative risk from models including MIROC-CHEM, NACR-CAM3.5, NCAR-CAM5.1 and GISS-E2-R.

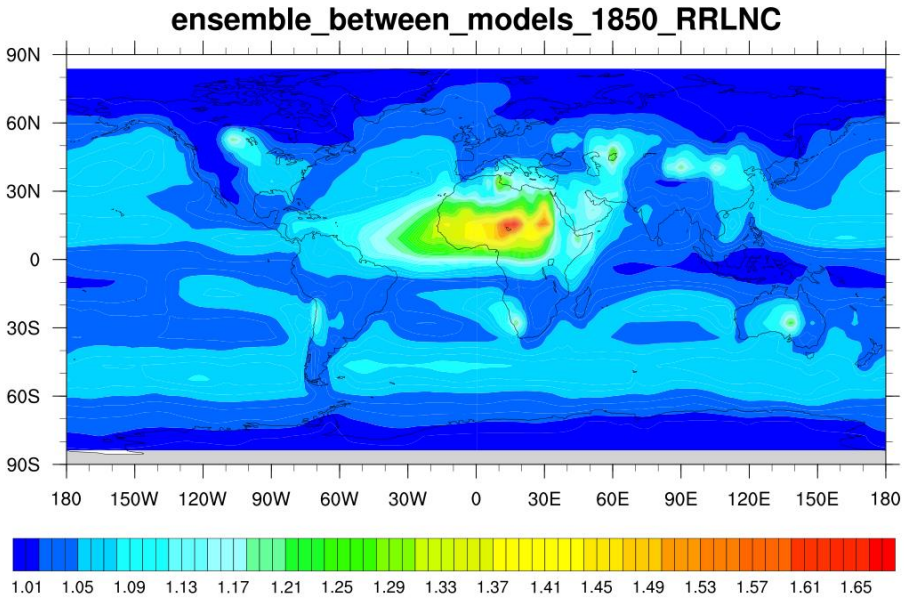


Figure 40 multi-ensemble results for LNC relative risk for 1850s with the unweighted average of lung cancer relative risk from models including MIROC-CHEM, NACR-CAM3.5, NCAR-CAM5.1 and GISS-E2-R.

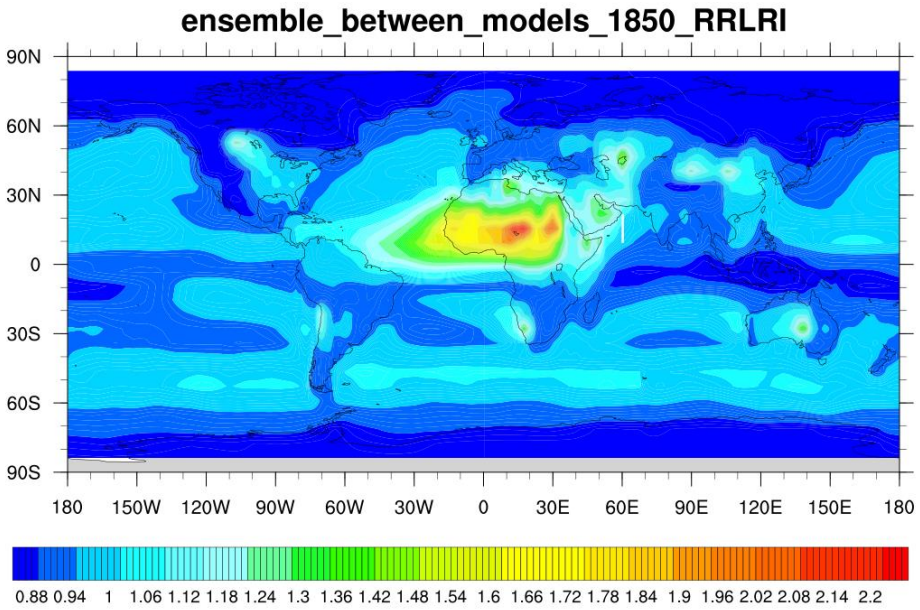


Figure 41 Multi-ensemble results for lower respiratory infection relative risk for 1850s with the unweighted average of lung cancer relative risk from models including MIROC-CHEM, NACR-CAM3.5, NCAR-CAM5.1 and GISS-E2-R.

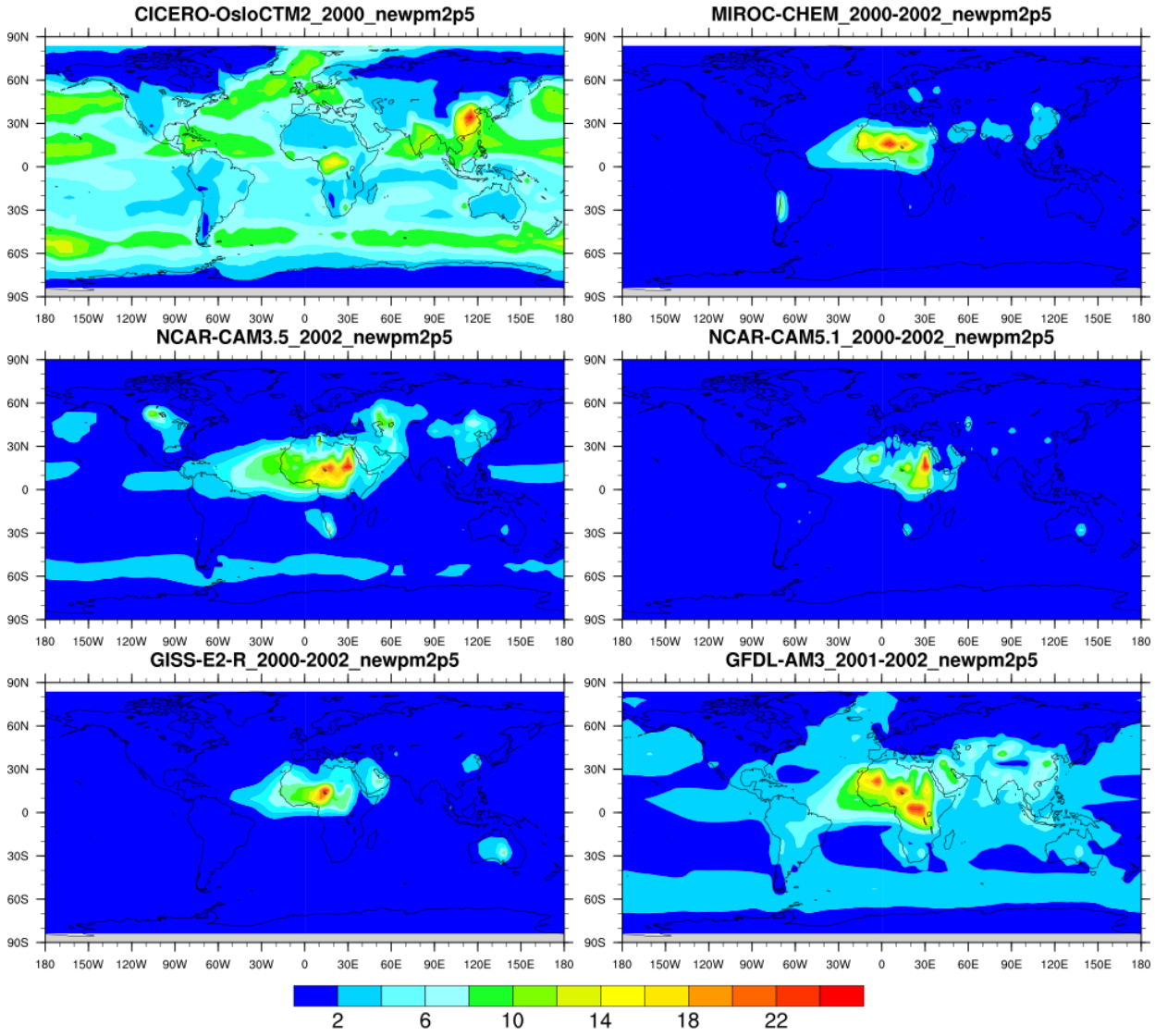


Figure 42 The comparison of ambient $PM_{2.5}$ concentration between various models (CICERO-OsloCTM2, MIROC-CHEM, NCAR-CAM3.5, NCAR-CAM5.1, GISS-E2-R, GFDL-AM3) in 2000s. CICERO-OsloCTM2 predicts surface concentration in an obvious different way compared with other models while GFDL-AM3 has a generally higher prediction.

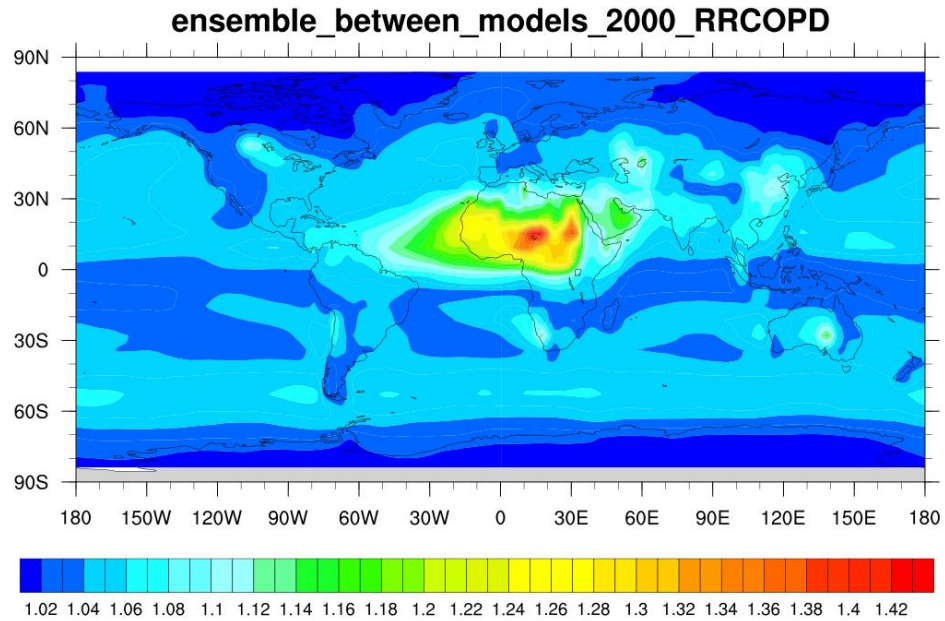


Figure 43 Multi-ensemble results for cardiopulmonary disease relative risk for 2000s with the unweighted average from models including MIROC-CHEM, NACR-CAM3.5, NCAR-CAM5.1, GISS-E2-R and GFDL-AM3.

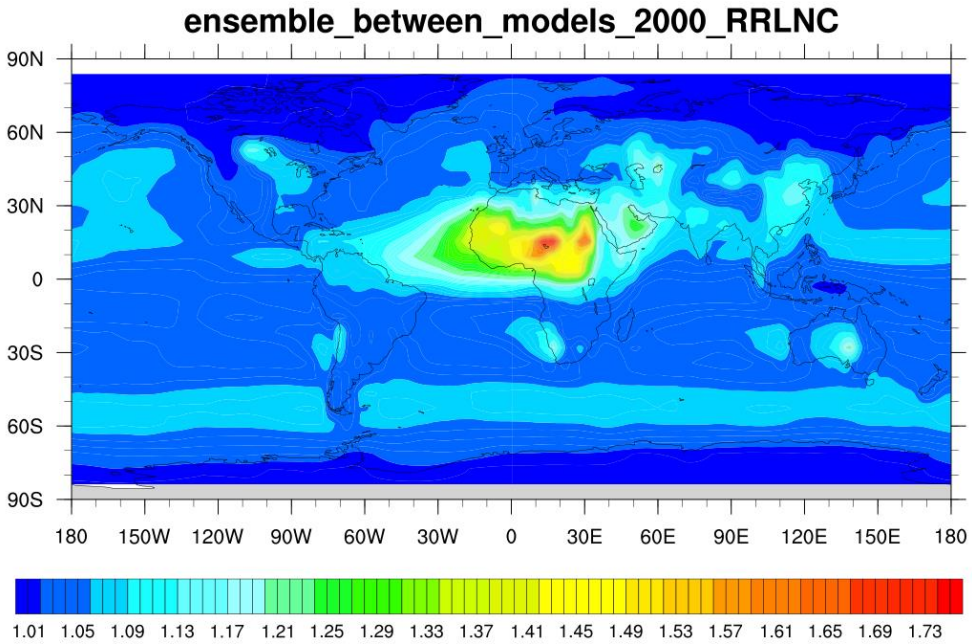


Figure 44 Multi-ensemble results for lung cancer relative risk for 2000s with the unweighted average output from models including MIROC-CHEM, NACR-CAM3.5, NCAR-CAM5.1, GISS-E2-R and GFDL-AM3.

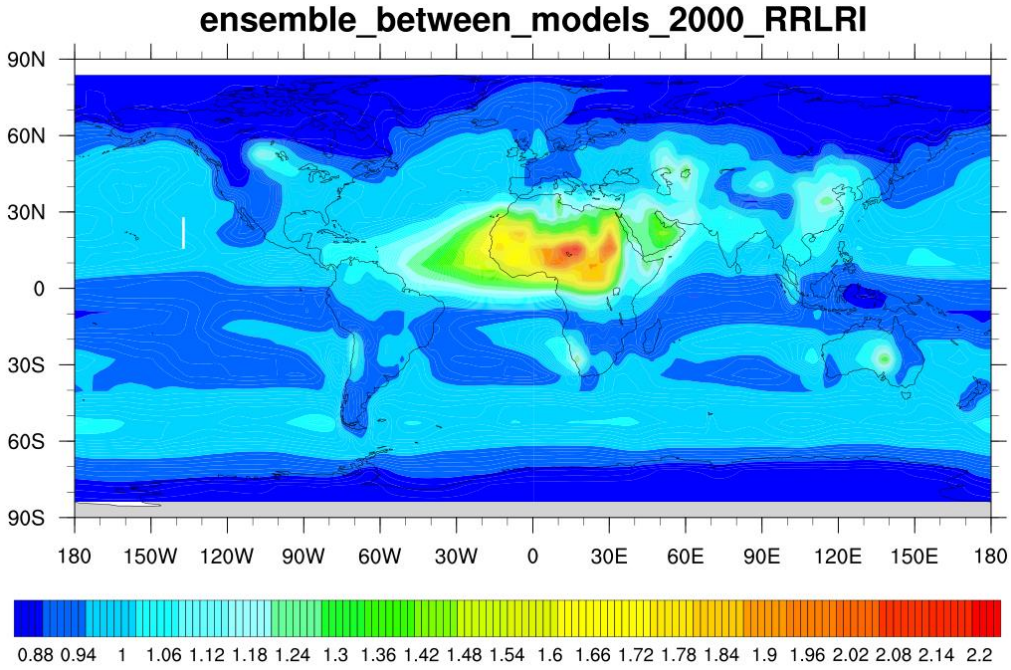


Figure 45 Multi-ensemble results for lower respiratory infection relative risk for 2000s with the unweighted average output from models including MIROC-CHEM, NACR-CAM3.5, NCAR-CAM5.1, GISS-E2-R and GFDL-AM3.

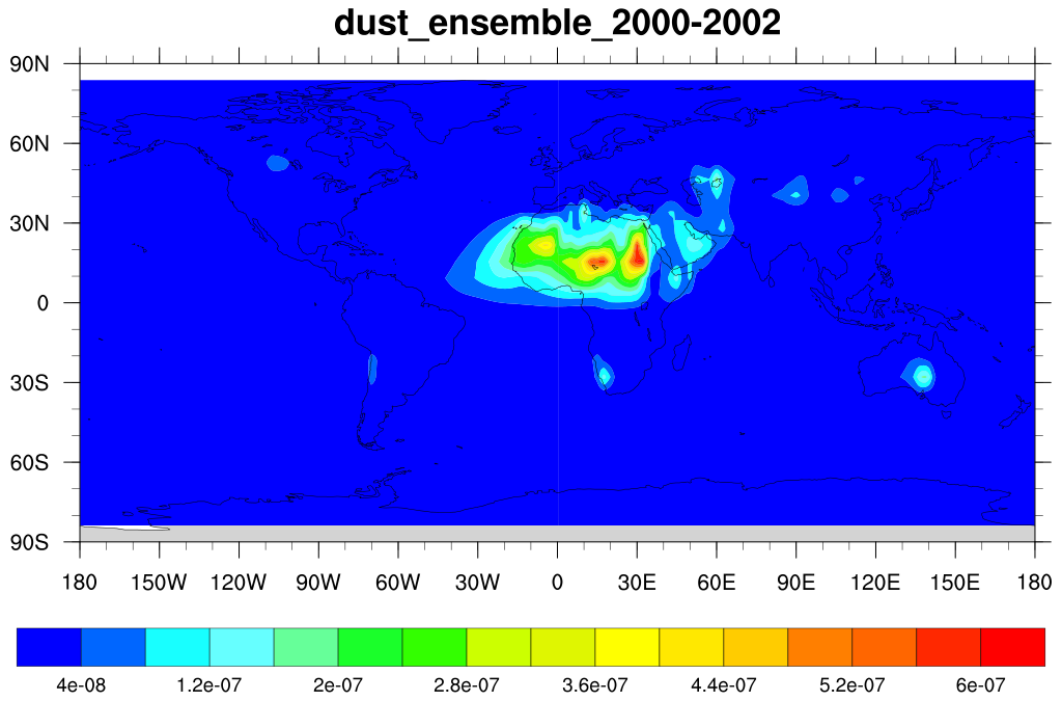


Figure 46 Multi-ensemble results for dust concentration for 2000s with the unweighted average from models including MIROC-CHEM, NACR-CAM3.5, NCAR-CAM5.1, GISS-E2-R and GFDL-AM3.

Figure 38 describes the model comparison for pre-industrial projection of near surface $PM_{2.5}$ concentration from CICERO, MIROC-CHEM, NACR-CAM3.5, NCAR-CAM5.1 and GISS-E2-R.

NCAR-CAM3.5 has a much higher level of $PM_{2.5}$ output for 1850s. CICERO-OsloCTM2 has a very different output compared with other models which can be explained by the lack of continuous data around 1850 and the cumulated deviation of adding up composition components.

Model comparison shows the outliner value for CICERO, so this model would not be used for multi-model ensemble. Models comparison for 1850s shows obvious elevation of relative risk of LRI for NACR-CAM3.5.

Figure 39,40,41 show the ensemble results from MIROC-CHEM, NACR-CAM3.5, NCAR-CAM5.1, GISS-E2-R for relative risk of COPD,LNC,LRI in 1850s. The ensemble results provide the distribution of risk with lower uncertainty from model difference.

Figure 42 describes the model comparison for current year (2000s) projection of near surface $PM_{2.5}$ concentration from GFDL-AM3, CICERO-OsloCTM2, MIROC-CHEM, NACR-CAM3.5, NCAR-CAM5.1 and GISS-E2-R. Compared with 1850s, NCAR-CAM3.5 predicts an elevated level in southern America. GFDL-AM3 predicts a commonly elevated value over the globe and it is shown that the Saharan dust pollution spread to further range than other models. While GISS-E2-R predicts an elevation in central Australia, MIROC-CHEM predicts almost no elevation in this region. For 2000s, CICERO-OsloCTM2 still presents outliner data range compared with others and it would not be used to calculate the unweighted mean value for the multi-ensemble.

Due to the availability of data, only one year's data is used for NCAR-CAM3.5, which might contributes to the uncertainty in unweighted mean results. Multi-model ensemble is conducted for the output from all five models including GFDL-AM3, GISS-E2-R, MIROC-CHEM, NCAR-CAM3.5 and NCAR-CAM5.1 for 2000s.

Figure 43,44,45 show the ensemble results from GFDL-AM3, MIROC-CHEM, NACR-CAM3.5, NCAR-CAM5.1, GISS-E2-R for relative risk of COPD,LNC,LRI respectively in 2000s. The ensemble results indicate that the elevation of relative risk in East Asia cannot be attributed to dust impact since dust concentration ensemble shows a near background level of dust concentration in that region. The increased anthological emission associated with industrial development and population growth in East Asia is responsible for such elevation and increase between preindustrial times and current years.

There is an obvious increase from 1850 to 2000 in East Asia due to the increasing anthological emission while Saharan or Australia dust effect almost remain the same. Increase is also observed in Arabian Peninsula, which is associated with increasing dust load and a much smaller increase in secondary inorganic and carbonaceous aerosol. (Boys et al., 2014) Multi-ensemble results are very important for depicting the risk distribution in a more accurate way compared with single model. An obvious elevation is observed in Central Australia from the ensemble results.

Short-term health impact from Australia dust storm is proved in Merrifield's study. Australia dust storm has been found to be linked to daily hospital visits in Sydney in Merrifield's study. Asthma risk increased to 1.23 and respiratory risk increased to 1.20 for that period of time. (Merrifield et. al., 2013) Although chronic exposure is hard to prove significant statistically in cohort studies but the model output does depicts the elevation for chronic disease including cardiopulmonary disease and lower respiratory infection for the populated regions including major cities and regional area. The dust concentration ensemble output further indicates the dust peak in the central region of Australia.

The ensemble output of dust concentration is presented in figure 46 for 2000s. The elevation in dust concentration in Mediterranean and Saudi Arabic are very likely to be responsible for the elevated relative risk from ensemble output.

4.6 POPULATION VARIANCE BETWEEN MODELS

Population Variance was calculated and plotted for 1850-1852 (figure 47) and 2000-2002 (figure 48) from four models (MIROC-CHEM, NCAR-CAM3.5, NCAR-CAM5.1 and GISS-E2-R) for gird data. There is relatively a much higher variance for LRI than other diseases between various models.

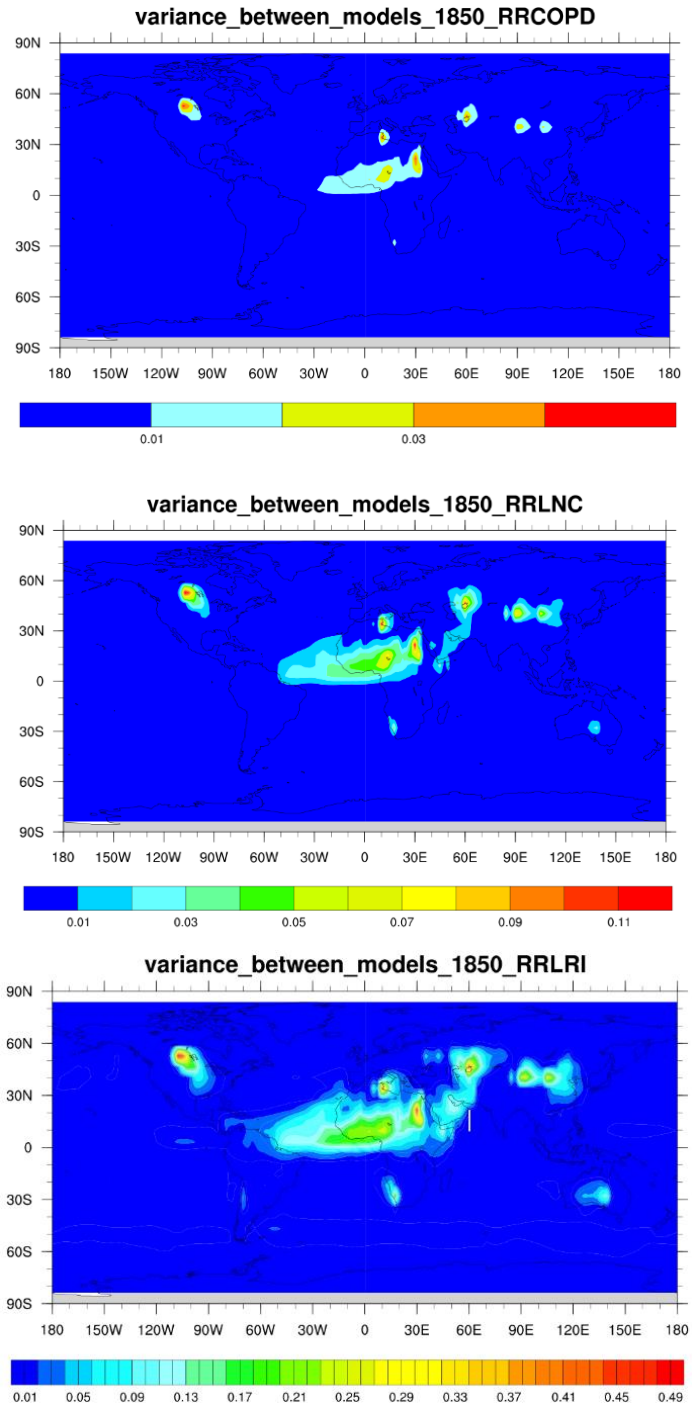


Figure 47 The variance of the prediction of ambient $PM_{2.5}$ concentration derived relative risk for cardiopulmonary disease, lung cancer and lower respiratory infection between various models (MIROC-CHEM,NCAR-CAM3.5,NCAR-CAM5.1,GISS-E2-R) in 1850s. Higher variance value would indicate a more spread out status of various models. It is worth noticing that lower respiratory infection relative risk has a much higher variance level than other disease endpoints, which means that there would be more uncertainty coming from LRI relative risk output from model difference.

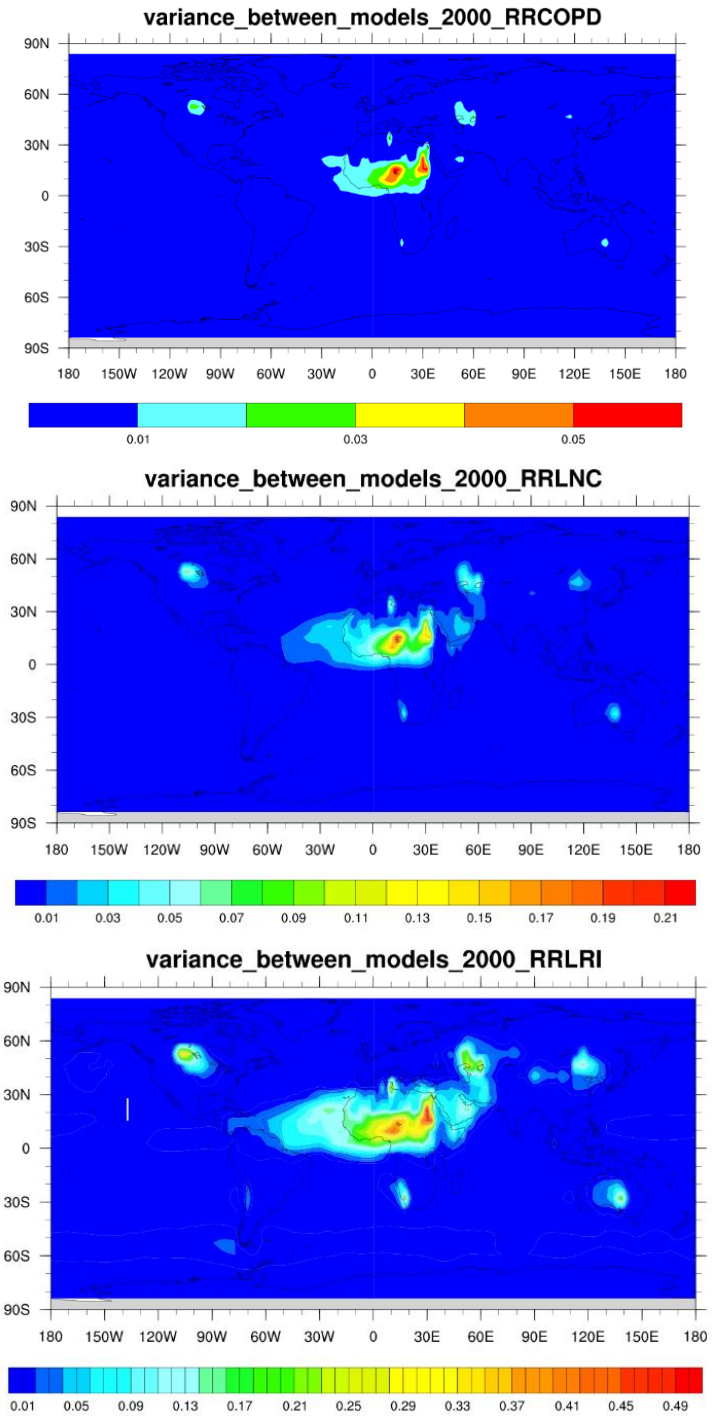


Figure 48 The variance of the prediction of ambient $PM_{2.5}$ concentration derived relative risk for cardiopulmonary disease, lung cancer and lower respiratory infection between various models (MIROC-CHEM,NCAR-CAM3.5,NCAR-CAM5.1,GISS-E2-R) in 2000s. Higher variance value would indicate a more spread out status of various models.

4.7 GRID AVERAGE DATA FROM PRE-INDUSTRIAL TIME TO PRESENT

By calculating the average value of relative risk from each time period, the tendency of risk variation can be derived from the results to measure the exposure change globally speaking. Figure 49 shows the grid average of the relative risk for cardiopulmonary disease from 1850s (pre-industrial) to 2010s (current years). There is a general trend of elevation in grid–averaged relative risk value from1850s to 2010s. The RR value peaks in 1980s.

Figure 76, 77 in the appendix show the grid average of the relative risk for lung cancer and lower respiratory infection respectively from 1850s (pre-industrial) to 2010s (current years).

The variation in LRI relative risk value is relatively high while variation in COPD relative risk value is low.

4.8 POPULATION NORMALIZED OUTPUT

Population normalization is conducted to measure the surface air pollution related to human exposure. Such measure is used as in Apte's study as a way to emphasize the effect of population exposure. (Apte et al., 2015) Regions were divided to analyze the regional distribution related to development level and geography.

The population normalized relative risk value for CIS regions peaks in January and October. Developed countries peak in April. Northern Africa peaks in February and November. Southern Asia peaks in February and December. Latin America and Caribbean peak in January and October. Oceania peaks in September. Western Asia peaks in February and December. Eastern Asia peaks in March. Developed countries peak in April. Sub-Saharan peaks in March.

There is a sudden drop of normalized relative risk value for COPD in December for Northern Africa. (See Table 1) RCP6.0 predicts a relatively higher concentration level while RCP2.6 predicts lower level. There is an increase of predicted normalized surface

$PM_{2.5}$ concentration for developed countries while there is a general decrease trend for other regions.

In SSP2 scenario, CIS regions is predicted with a much lower normalized $PM_{2.5}$ concentration compared with SSP1 while there is not much different between two scenarios for other regions. (See Table 2) Such result indicate that a moderately sustainable population scenario would predict a lower level of population exposure in CIS.

Table 3 shows the population normalized relative risk value for various regions under emission scenarios including RCP2.6,6.0,8.5 and time periods including 2000,2030,2050. The population scenario utilized is SSP1 and the results describe the regional risk distribution from the output of MIROC-CHEM model. For the same population scenario and RCP scenario, MIROC-CHEM actually predicts a much lower normalized $PM_{2.5}$ concentration value level compared with GISS-E2-R.

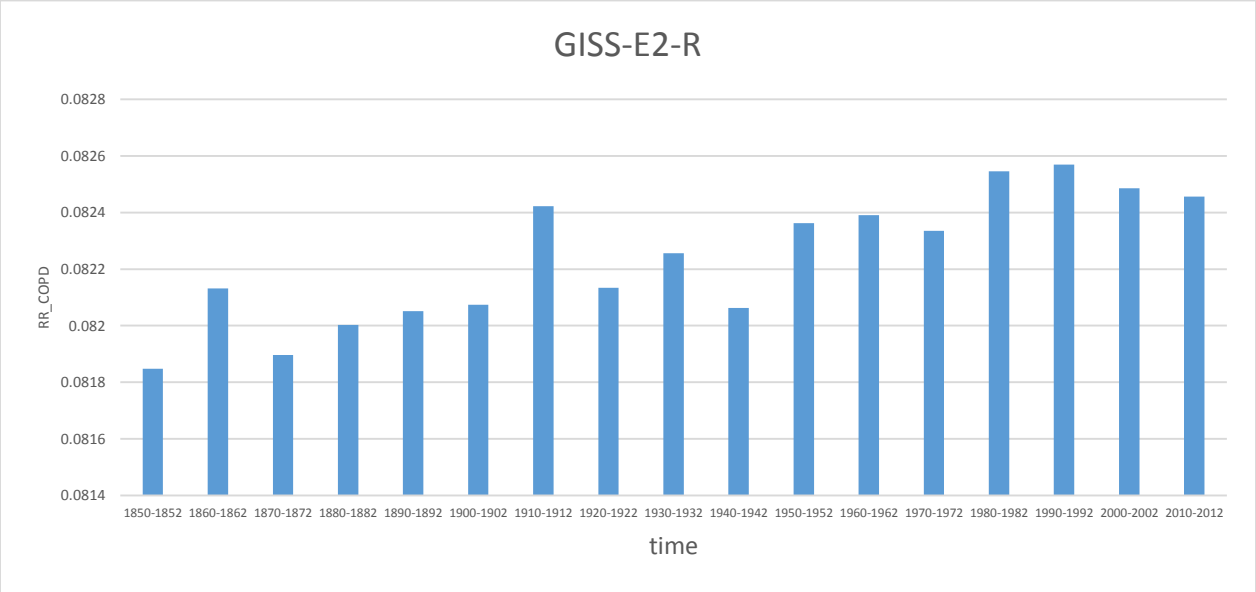


Figure 49 Grid averaged COPD relative risk value for GISS-E2-R from 1850s to 2010s. Grid average is a depiction of how the relative risk level has developed globally since preindustrial times. There is a general increasing trend since pre-industrial times.

TABLE 1 POPULATION NORMALIZED $PM_{2.5}$ CONCENTRATION FOR GISS-E2-R MODEL UNDER POPULATION SCENARIO SSP1 AND DIFFERENT RCP SCENARIOS (RCP2.6, RCP4.5, RCP6.0 and RCP8.5) FOR THE TIME PERIOD OF 2000S,2030S,2050S AS MEASURING THE EFFECT OF BOTH POPULATION SCENARIO AND GREENHOUSE GAS EMISSION SCENARIOS UPON REGIONAL DISTRIBUTION OF POPULATION NORMALIZED RELATIVE RISK.

scenarios / regions	GISS-E2-R								
	SSP1								
	2000	2030				2050			
	hist	RCP2.6	RCP4.5	RCP6.0	RCP8.5	RCP2.6	RCP4.5	RCP6.0	RCP8.5
CIS	9.64	8.841	9.219	9.152	9.01	8.716	8.756	8.872	8.77
developed countries	16.90	17.384	17.899	17.726	17.37	17.54	17.436	17.578	17.493
Sub-Saharan Africa	7.32	6.768	7.293	6.861	6.768	6.7	6.843	7.15	6.779
Eastern Asia	12.04	11.23	11.528	11.665	11.479	11.233	11.033	11.456	11.26
Latin America and the Caribbean	17.45	16.668	16.963	17.576	16.065	16.631	16.693	17.338	17.282
Northern Africa	11.99	13.22	12.902	13.03	13.07	13.196	13.003	12.861	12.938
Oceania	8.84	8.487	8.025	7.936	8.014	8.451	8.012	8.559	8.813
Southern Asia	6.85	6.331	5.999	6.137	5.908	6.288	5.355	5.971	5.884
South-Eastern Asia	8.15	7.669	7.506	8.674	8.425	7.708	6.603	8.584	8.56
Western Asia	13.48	13.001	13.63	13.345	13.12	12.92	12.955	13.332	12.794

TABLE 2 POPULATION NORMALIZED $PM_{2.5}$ CONCENTRATION FOR GISS-E2-R MODEL UNDER POPULATION SCENARIO SSP2 AND DIFFERENT RCP SCENARIOS (RCP2.6, RCP4.5, RCP6.0 and RCP8.5) FOR THE TIME PERIOD OF 2000S,2030S,2050S AS MEASURING THE EFFECT OF BOTH POPULATION SCENARIO AND GREENHOUSE GAS EMISSION SCENARIOS UPON REGIONAL DISTRIBUTION OF POPULATION NORMALIZED RELATIVE RISK.

scenarios / regions	GISS-E2-R								
	SSP2								
	2000	2030				2050			
	hist	RCP2.6	RCP4.5	RCP6.0	RCP8.5	RCP2.6	RCP4.5	RCP6.0	RCP8.5
CIS	9.059	7.703	7.984	8.044	7.885	7.545	7.448	7.68	7.544
developed countries	16.896	17.401	17.92	17.745	17.389	17.547	17.486	17.62	17.55
Sub-Saharan Africa	7.3167	6.76	7.285	6.854	6.757	6.774	6.867	7.154	6.77
Eastern Asia	12.016	11.197	11.504	11.626	11.446	11.204	10.977	11.41	11.20
Latin America and the Caribbean	17.447	16.653	16.954	17.559	16.059	17.265	16.666	17.302	17.26
Northern Africa	13.055	13.223	12.9	13.027	13.069	12.929	12.994	12.85	12.93
Oceania	8.836	8.483	8.02	7.93	8.008	8.806	8.004	8.554	8.806
Southern Asia	6.8832	6.334	5.98	6.132	5.883	5.851	5.315	5.927	5.851
South-Eastern Asia	8.8398	8.504	8.34	9.445	9.156	9.475	7.323	9.324	9.475
Western Asia	13.476	13	13.626	13.34	13.116	12.783	12.945	13.317	12.78

TABLE 3 POPULATION NORMALIZED $PM_{2.5}$ CONCENTRATION FOR MIROC-CHEM MODEL UNDER POPULATION SCENARIO SSP1 AND DIFFERENT RCP SCENARIOS (RCP2.6, RCP6.0 and RCP8.5) FOR THE TIME PERIOD OF 2000S,2030S,2050S AS MEASURING THE EFFECT OF BOTH POPULATION SCENARIO AND GREENHOUSE GAS EMISSION SCENARIOS UPON REGIONAL DISTRIBUTION OF POPULATION NORMALIZED RELATIVE RISK.

region	MIROC-CEHM						
	SSP1						
	2000	2030			2050		
	hist	RCP2.6	RCP6.0	RCP8.5	RCP2.6	RCP6.0	RCP8.5
CIS	1.569	1.069	1.386	1.32	0.934	1.295	1.209
developed countries	7.256	7.909	7.962	8.837	8.219	7.121	9.717
Sub-Saharan Africa	1.073	1.082	1.131	1.077	1.015	1.069	1.146
Eastern Asia	3.973	2.606	3.052	2.342	2.109	2.421	2.053
Latin America and the Caribbean	5.102	5.954	5.877	6.139	4.884	6.608	6.00
Northern Africa	1.672	1.407	1.538	1.531	1.236	1.531	1.461
Oceania	1.927	2.078	1.898	1.772	1.941	1.924	2.121
Southern Asia	4.197	3.422	3.199	3.014	2.595	2.679	2.729
South-Eastern Asia	4.925	0.004	4.576	1.077	4.013	4.317	4.09
Western Asia	1.781	1.331	1.509	1.508	1.226	1.428	1.442

TABLE 4 POPULATION NORMALIZED COPD RELATIVE RISK FOR GISS-E2-R MODEL UNDER POPULATION SCENARIO SSP1 AND DIFFERENT RCP SCENARIOS (RCP2.6, RCP4.5, RCP6.0 AND RCP8.5) FOR THE TIME PERIOD OF 2000S,2030S,2050S AS MEASURING THE EFFECT OF BOTH POPULATION SCENARIO AND GREENHOUSE GAS EMISSION SCENARIOS UPON REGIONAL DISTRIBUTION OF POPULATION NORMALIZED RELATIVE RISK.

scenarios / regions	GISS-E2-R								
	SSP1								
	2000	2030				2050			
	hist	RCP2.6	RCP4.5	RCP6.0	RCP8.5	RCP2.6	RCP4.5	RCP6.0	RCP8.5
CIS	1.0515	1.048	1.05	1.0496	1.049	1.0479	1.048	1.0485	1.048
developed countries	1.0777	1.079	1.081	1.0804	1.0794	1.0799	1.079	1.08	1.08
Sub-Saharan Africa	1.0425	1.04	1.042	1.0408	1.0404	1.0401	1.0408	1.0418	1.04
Eastern Asia	1.0609	1.058	1.059	1.0594	1.0587	1.0578	1.057	1.0586	1.058
Latin America and the Caribbean	1.0788	1.076	1.077	1.0791	1.074	1.076	1.0756	1.0784	1.078
Northern Africa	0.9962	1.065	1.064	1.0646	1.0647	1.0651	1.064	1.0639	1.064
Oceania	1.0485	1.047	1.045	1.045	1.0453	1.047	1.0453	1.0474	1.048
Southern Asia	1.0409	1.039	1.038	1.0381	1.0372	1.037	1.035	1.0374	1.037
South-Eastern Asia	1.0456	1.044	1.043	1.0476	1.0466	1.0439	1.04	1.0472	1.047
Western Asia	1.0662	1.064	1.067	1.0657	1.0648	1.064	1.0642	1.0656	1.064

TABLE 5 POPULATION NORMALIZED COPD RELATIVE RISK FOR GISS-E2-R MODEL UNDER POPULATION SCENARIO SSP2 AND DIFFERENT RCP SCENARIOS (RCP2.6, RCP4.5, RCP6.0 AND RCP8.5) FOR THE TIME PERIOD OF 2000S,2030S,2050S AS MEASURING THE EFFECT OF BOTH POPULATION SCENARIO AND GREENHOUSE GAS EMISSION SCENARIOS UPON REGIONAL DISTRIBUTION OF POPULATION NORMALIZED RELATIVE RISK.

scenarios / regions	GISS-E2-R								
	SSP2								
	2000	2030				2050			
	hist	RCP2.6	RCP4.5	RCP6.0	RCP8.5	RCP2.6	RCP4.5	RCP6.0	RCP8.5
CIS	1.049	1.044	1.045	1.045	1.0447	1.0434	1.043	1.044	1.043
developed countries	1.078	1.079	1.081	1.08	1.0794	1.0799	1.08	1.08	1.08
Sub-Saharan Africa	1.0425	1.040	1.042	1.041	1.0403	1.0404	1.041	1.042	1.04
Eastern Asia	1.0608	1.058	1.059	1.059	1.0586	1.0577	1.057	1.059	1.058
Latin America and the Caribbean	1.0788	1.076	1.077	1.079	1.074	1.0777	1.075	1.078	1.078
Northern Africa	1.0646	1.066	1.064	1.064	1.0647	1.0641	1.064	1.064	1.064
Oceania	1.0485	1.047	1.045	1.045	1.0453	1.0483	1.045	1.047	1.048
Southern Asia	1.041	1.039	1.037	1.038	1.0371	1.037	1.035	1.037	1.037
South-Eastern Asia	1.048	1.047	1.046	1.05	1.0494	1.0505	1.042	1.05	1.050
Western Asia	1.0662	1.064	1.067	1.066	1.0648	1.0635	1.064	1.0656	1.064

Table 4 and table 5 show that the relative risk value for COPD from GISS-E2-R model output with SSP2 has much lower value for CIS region than SSP1. The COPD risk value with SSP2 for south-eastern Asia is much higher than that with SSP1. There is a slight lowering trend from 2000 to 2050 with SSP2 dataset while the different between different RCP scenarios is limited.

For CIS region, relative risk for LRI with SSP2 dataset has lower value than SSP1. The different between SSP1 and SSP2 for relative risk of LRI for other regions is very limited. (See Table 8&9) The LRI relative risk values for regions including CIS, Sub-Saharan Africa, Oceania, South-Eastern Asia are around 1, so the health risk of lower respiratory infection for those regions from surface $PM_{2.5}$ exposure is very limited.

The normalized $PM_{2.5}$ data for CIS, northern Africa, Oceania, Sub-Saharan Africa, south Asia regions with SSP3 is much lower than SSP1 and SSP2 under the same RCP scenarios and models. While normalized concentration or risk value for eastern Asia, east Asia and Latin America and the Caribbean are predicted with much higher values with SSP3.(See Table 10)

TABLE 6 POPULATION NORMALIZED LNC RELATIVE RISK FOR GISS-E2-R MODEL UNDER POPULATION SCENARIO SSP1 AND DIFFERENT RCP SCENARIOS (RCP2.6, RCP4.5, RCP6.0 AND RCP8.5) FOR THE TIME PERIOD OF 2000S,2030S,2050S AS MEASURING THE EFFECT OF BOTH POPULATION SCENARIO AND GREENHOUSE GAS EMISSION SCENARIOS UPON REGIONAL DISTRIBUTION OF POPULATION NORMALIZED RELATIVE RISK.

scenarios / regions	GISS-E2-R								
	SSP1								
	2000	2030				2050			
	hist	RCP2.6	RCP4.5	RCP6.0	RCP8.5	RCP2.6	RCP4.5	RCP6.0	RCP8.5
CIS	1.0625	1.057	1.059	1.06	1.0586	1.0566	1.0573	1.0579	1.0571
developed countries	1.0994	1.103	1.11	1.1064	1.1038	1.1037	1.1065	1.1046	1.106
Sub-Saharan Africa	1.0501	1.046	1.047	1.0487	1.0437	1.0454	1.0455	1.0474	1.0422
Eastern Asia	1.046	1.069	1.07	1.074	1.0403	1.0688	1.0705	1.0727	1.0711
Latin America and the Caribbean	1.1	1.095	1.103	1.103	1.0985	1.0952	1.098	1.1013	1.1082
Northern Africa	1.0094	1.081	1.081	1.0821	1.083	1.0812	1.0816	1.0802	1.0802
Oceania	1.0554	1.055	1.051	1.0525	1.052	1.0552	1.0516	1.057	1.0576
Southern Asia	1.046	1.042	1.0403	1.0418	1.0403	1.0421	1.0361	1.0409	1.0387
South-Eastern Asia	1.0538	1.048	1.05	1.0583	1.05256	1.0484	1.0445	1.0563	1.0498
Western Asia	1.0856	1.082	1.085	1.0848	1.0827	1.0812	1.081	1.0833	1.079

TABLE 7 POPULATION NORMALIZED LNC RELATIVE RISK FOR GISS-E2-R MODEL UNDER POPULATION SCENARIO SSP2 AND DIFFERENT RCP SCENARIOS (RCP2.6, RCP4.5, RCP6.0 AND RCP8.5) FOR THE TIME PERIOD OF 2000S,2030S,2050S AS MEASURING THE EFFECT OF BOTH POPULATION SCENARIO AND GREENHOUSE GAS EMISSION SCENARIOS UPON REGIONAL DISTRIBUTION OF POPULATION NORMALIZED RELATIVE RISK.

scenarios / regions	GISS-E2-R								
	SSP2								
	2000	2030				2050			
	hist	RCP2.6	RCP4.5	RCP6.0	RCP8.5	RCP2.6	RCP4.5	RCP6.0	RCP8.5
CIS	1.059	1.051	1.052	1.053	1.0518	1.05	1.05	1.051	1.05
developed countries	1.099	1.103	1.11	1.106	1.104	1.1063	1.107	1.105	1.106
Sub-Saharan Africa	1.0501	1.046	1.047	1.049	1.1044	1.0422	1.045	1.047	1.042
Eastern Asia	1.0768	1.068	1.072	1.074	1.0708	1.0707	1.07	1.073	1.0707
Latin America and the Caribbean	1.1	1.095	1.103	1.103	1.0985	1.1081	1.1	1.101	1.108
Northern Africa	1.079	1.082	1.081	1.082	1.083	1.08	1.082	1.08	1.08
Oceania	1.055	1.055	1.051	1.052	1.052	1.0575	1.051	1.057	1.058
Southern Asia	1.046	1.042	1.04	1.042	1.04	1.0385	1.036	1.041	1.038
South-Eastern Asia	1.058	1.052	1.055	1.063	1.0568	1.0545	1.049	1.061	1.0545
Western Asia	1.0856	1.082	1.085	1.085	1.0827	1.0789	1.081	1.083	1.0789

TABLE 8 POPULATION NORMALIZED LRI RELATIVE RISK FOR GISS-E2-R MODEL UNDER POPULATION SCENARIO SSP1 AND DIFFERENT RCP SCENARIOS (RCP2.6, RCP4.5, RCP6.0 AND RCP8.5) FOR THE TIME PERIOD OF 2000S,2030S,2050S AS MEASURING THE EFFECT OF BOTH POPULATION SCENARIO AND GREENHOUSE GAS EMISSION SCENARIOS UPON REGIONAL DISTRIBUTION OF POPULATION NORMALIZED RELATIVE RISK.

scenarios / regions	GISS-E2-R								
	SSP1								
	2000	2030				2050			
	hist	RCP2.6	RCP4.5	RCP6.0	RCP8.5	RCP2.6	RCP4.5	RCP6.0	RCP8.5
CIS	0.9871	0.975	0.981	0.9795	0.978	0.9737	0.9742	0.976	0.9744
developed countries	1.0836	1.09	1.096	1.0933	1.0897	1.0918	1.0896	1.093	1.0911
Sub-Saharan Africa	0.9535	0.946	0.953	0.947	0.946	0.9446	0.9473	0.951	0.9458
Eastern Asia	1.0221	1.011	1.015	1.0167	1.014	1.0107	1.0078	1.014	1.0109
Latin America and the Caribbean	1.0871	1.077	1.079	1.0879	1.0694	1.077	1.0746	1.0853	1.0827
Northern Africa	0.9669	1.038	1.034	1.0358	1.0362	1.038	1.0351	1.0332	1.0342
Oceania	0.9759	0.971	0.964	0.9627	0.964	0.97	0.9639	0.9718	0.9753
Southern Asia	0.9475	0.94	0.935	0.9371	0.9339	0.939	0.9258	0.9346	0.9335
South-Eastern Asia	0.9651	0.958	0.956	0.9724	0.9687	0.959	0.9432	0.9709	0.9703
Western Asia	1.0417	1.035	1.044	1.04	1.0367	1.034	1.0343	1.04	1.032

TABLE 9 POPULATION NORMALIZED LRI RELATIVE RISK FOR GISS-E2-R MODEL UNDER POPULATION SCENARIO SSP2 AND DIFFERENT RCP SCENARIOS (RCP2.6, RCP4.5, RCP6.0 AND RCP8.5) FOR THE TIME PERIOD OF 2000S,2030S,2050S AS MEASURING THE EFFECT OF BOTH POPULATION SCENARIO AND GREENHOUSE GAS EMISSION SCENARIOS UPON REGIONAL DISTRIBUTION OF POPULATION NORMALIZED RELATIVE RISK.

scenarios / regions	GISS-E2-R								
	SSP2								
	2000	2030				2050			
	hist	RCP2.6	RCP4.5	RCP6.0	RCP8.5	RCP2.6	RCP4.5	RCP6.0	RCP8.5
CIS	0.9788	0.959	0.963	0.964	0.962	0.9568	0.9554	0.9588	0.9568
developed countries	1.0836	1.09	1.096	1.094	1.09	1.092	1.09	1.0935	1.0917
Sub-Saharan Africa	0.9535	0.945	0.953	0.947	0.945	0.9457	0.947	0.951	0.9457
Eastern Asia	1.022	1.01	1.014	1.016	1.014	1.0101	1.007	1.0137	1.01
Latin America and the Caribbean	1.087	1.077	1.079	1.088	1.069	1.0825	1.074	1.0848	1.0824
Northern Africa	1.0359	1.039	1.034	1.036	1.036	1.0341	1.035	1.0331	1.034
Oceania	0.9758	0.97	0.964	0.963	0.964	0.9752	0.964	0.9717	0.9752
Southern Asia	0.948	0.94	0.935	0.937	0.934	0.933	0.925	0.934	0.933
South-Eastern Asia	0.9749	0.97	0.967	0.983	0.979	0.9832	0.954	0.9814	0.9832
Western Asia	1.0417	1.035	1.044	1.04	1.037	1.0319	1.034	1.0395	1.0319

TABLE 10 POPULATION NORMALIZED $PM_{2.5}$ CONCENTRATION, COPD RISK, LNC RISK, LRI RISK RESPECTIVELY FOR GISS-E2-R MODEL UNDER POPULATION SCENARIO SSP3 FOR THE TIME PERIOD OF 2000S AS MEASURING THE EFFECT OF BOTH POPULATION SCENARIO AND GREENHOUSE GAS EMISSION SCENARIOS UPON REGIONAL DISTRIBUTION OF POPULATION NORMALIZED RELATIVE RISK.

GISS-E2-R SSP3				
Regions	2000			
	hist			
	$PM_{2.5}$	COPD	LNC	LRI
CIS	7.984	1.045	1.052	0.963
DC	17.921	1.081	1.11	1.096
EA	11.504	1.059	1.072	1.014
LAC	16.954	1.077	1.103	1.079
NA	12.9	1.064	1.081	1.034
O	8.02	1.045	1.051	0.964
SA	5.979	1.037	1.04	0.935
SEA	8.34	1.046	1.055	0.967
SSA	7.285	1.042	1.047	0.953
WA	13.626	1.067	1.085	1.044

TABLE 11 POPULATION NORMALIZED $PM_{2.5}$ CONCENTRATION, COPD RISK, LNC RISK, LRI RISK RESPECTIVELY FOR GISS-E2-R MODEL UNDER POPULATION SCENARIO SSP3 AND EMISSION SCENARIOS (RCP2.6,RCP4.5,RCP6.0,RCP8.5) FOR THE TIME PERIOD OF 2030S AS MEASURING THE EFFECT OF BOTH POPULATION SCENARIO AND GREENHOUSE GAS EMISSION SCENARIOS UPON REGIONAL DISTRIBUTION OF POPULATION NORMALIZED RELATIVE RISK.

GISS-E2-R SSP3																
Regions	2030															
	RCP2.6				RCP4.5				RCP6.0				RCP8.5			
	$PM_{2.5}$	COPD	LNC	LRI	$PM_{2.5}$	COPD	LNC	LRI	$PM_{2.5}$	COPD	LNC	LRI	$PM_{2.5}$	COPD	LNC	LRI
CIS	7.43	1.043	1.049	0.955	7.68	1.044	1.05	0.959	7.79	1.044	1.052	0.96	7.62	1.044	1.05	0.958
DC	17.40	1.079	1.103	1.09	17.94	1.081	1.11	1.096	17.73	1.08	1.106	1.094	17.4	1.079	1.104	1.09
EA	11.22	1.058	1.069	1.01	11.52	1.059	1.072	1.015	11.66	1.059	1.074	1.017	11.47	1.059	1.071	1.01
LAC	16.61	1.076	1.095	1.077	16.92	1.077	1.103	1.079	17.5	1.079	1.103	1.087	16.04	1.074	1.098	1.069
NA	13.16	1.065	1.081	1.037	12.85	1.064	1.08	1.033	12.96	1.064	1.082	1.035	13.05	1.064	1.083	1.036
O	8.49	1.047	1.055	0.971	8.02	1.045	1.05	0.964	7.94	1.045	1.052	0.963	8.01	1.045	1.052	0.964
SA	6.31	1.039	1.042	0.939	5.95	1.037	1.04	0.935	6.12	1.038	1.042	0.937	5.89	1.037	1.04	0.934
SEA	7.73	1.044	1.048	0.959	7.58	1.043	1.05	0.957	8.74	1.048	1.059	0.973	8.5	1.047	1.053	0.97
SSA	6.84	1.041	1.046	0.946	6.5	0.92	0.924	0.842	6.9	1.041	1.049	0.948	6.031	0.918	0.921	0.835
WA	12.96	1.064	1.081	1.035	13.59	1.067	1.084	1.043	13.29	1.066	1.084	1.039	13.12	1.065	1.082	1.04

TABLE 12 POPULATION NORMALIZED $PM_{2.5}$ CONCENTRATION, COPD RISK, LNC RISK, LRI RISK RESPECTIVELY FOR GISS-E2-R MODEL UNDER POPULATION SCENARIO SSP3 AND EMISSION SCENARIOS (RCP2.6,RCP4.5,RCP6.0,RCP8.5) FOR THE TIME PERIOD OF 2050S AS MEASURING THE EFFECT OF BOTH POPULATION SCENARIO AND GREENHOUSE GAS EMISSION SCENARIOS UPON REGIONAL DISTRIBUTION OF POPULATION NORMALIZED RELATIVE RISK.

GISS-E2-R SSP3																
Regions	2050															
	RCP2.6				RCP4.5				RCP6.0				RCP8.5			
	$PM_{2.5}$	COPD	LNC	LRI	$PM_{2.5}$	COPD	LNC	LRI	$PM_{2.5}$	COPD	LNC	LRI	$PM_{2.5}$	COPD	LNC	LRI
CIS	6.84	1.0406	1.0455	0.9466	6.96	1.041	1.047	0.948	7.235	1.042	1.048	0.952	7.089	1.042	1.047	0.95
DC	17.54	1.0799	1.1061	1.091	17.54	1.08	1.107	1.091	17.68	1.08	1.105	1.094	17.622	1.08	1.107	1.093
EA	11.01	1.0569	1.07	1.007	11	1.057	1.07	1.007	11.43	1.058	1.072	1.013	11.231	1.058	1.071	1.01
LAC	15.12	1.0706	1.089	1.0568	16.55	1.075	1.097	1.073	17.21	1.078	1.1	1.084	17.181	1.077	1.108	1.081
NA	12.63	1.063	1.079	1.03	12.95	1.064	1.081	1.034	12.82	1.064	1.08	1.033	12.891	1.064	1.08	1.033
O	7.69	1.0441	1.049	0.9595	8	1.045	1.051	0.964	8.56	1.047	1.057	0.972	8.812	1.048	1.058	0.975
SA	5.567	1.0358	1.038	0.9288	5.304	1.035	1.036	0.925	5.92	1.037	1.041	0.934	5.831	1.037	1.038	0.933
SEA	8.75	1.0477	1.057	0.9728	6.78	1.04	1.046	0.946	8.77	1.048	1.057	0.974	8.774	1.048	1.051	0.973
SSA	7.06	1.0415	1.046	0.9497	6.905	1.04	1.046	0.948	7.22	1.042	1.048	0.952	6.805	1.04	1.042	0.946
WA	12.77	1.0635	1.079	1.032	12.96	1.064	1.08	1.034	13.28	1.065	1.083	1.039	12.792	1.064	1.079	1.032

Table 11 and table 12 depict population normalized $PM_{2.5}$ concentration, COPD risk, LNC risk, LRI risk for GISS-E2-R model under population scenario SSP3 and emission scenarios (RCP2.6,RCP4.5,RCP6.0,RCP8.5) for the time period of 2030s and 2050s respectively.

With SSP3 as the population scenario, RCP6.0 represents a higher level of normalized value for regions including CIS, DC, EA, LAC, SA, SSA and WA.

From the GISS-E2-R and SSP3, it is shown that there is generally a decreasing trend of population normalized $PM_{2.5}$ concentration and related relative risk from 2000s to 2050s for various scenarios.

Among various emission scenarios, RCP6.0 predicts the highest surface pollution level in the future while RCP2.6 predicts the lowest. From 2000s to 2050s, the equivalent carbon dioxide increase ranks from high to low as RCP8.5, RCP4.5, RCP6.0 and RCP2.6. The reason for such distribution is due to the difference in radiative forcing value settings. Population normalized concentration is more useful in predicting human exposure derived health impact because the relative risk for each grid would be substantially lower if the population for such grid is extremely low. Such calculation would avoid situation of the too high or too low relative risk in regions with low population causing effect on the overall relative risk or concentration.

For regional distribution, developed countries and Latin America have the highest population normalized concentration and associated relative risk with western Asia and Southern Asia come next.

Surface $PM_{2.5}$ exposure has a much lower effect upon chronic lower respiratory infection while has a much higher effect upon LNC and COPD. In Jassen's study (Janssen et al., 2011), black carbon is used as additional predictor for health impact since black carbon is more toxic than the other component in $PM_{2.5}$. In their study, assumption was made about that black carbon is 5 times more toxic than the other components so black carbon mass is multiplied by 5 to adjust the health impact related $PM_{2.5}$ concentration. It was concluded black carbon is a valuable tool to predict health impact.

For further optimizing the output for health risk, black carbon mass adjusted $PM_{2.5}$ mass concentration and derived relative risks are calculated for NACR-CAM5.1 model output for the three year average of surface $PM_{2.5}$ concentration of 2000 to 2002.

The original calculation function for $PM_{2.5}$ mass concentration:

$PM_{2.5}=BC + OA + SO_4 + SOA + NO_3 + NH_4 + 0.25*SS + 0.1*Dust$

The adjusted calculation function for $PM_{2.5}$ mass concentration:

$PM_{2.5}=5*BC + OA + SO_4 + SOA + NO_3 + NH_4 + 0.25*SS + 0.1*Dust$

The point in adjusting relative risk with black carbon concentration is to discover whether it should be necessary to consider the effect from black carbon since IER model or other C-R functions may only take the mass concentration of particulate matter into consideration instead of assessing the health impact regarding the toxicity of all the components.

Different population scenarios might have slight impact on population normalized fine particle surface concentration but the resulted relative risk change is very trivial.

TABLE 13 POPULATION NORMALIZED $PM_{2.5}$ CONCENTRATION, COPD RISK, LNC RISK, LRI RISK RESPECTIVELY FOR NCAR-CAM5.1 MODEL UNDER POPULATION SCENARIO SSP1,SSP2,SSP3 FOR THE TIME PERIOD OF 2000S AS MEASURING THE EFFECT OF BOTH POPULATION SCENARIO AND GREENHOUSE GAS EMISSION SCENARIOS UPON REGIONAL DISTRIBUTION OF POPULATION NORMALIZED RELATIVE RISK.

region	NCAR-CAM 5.1 SSP1				NCAR-CAM 5.1 SSP2				NCAR-CAM 5.1 SSP3			
	2000				2000				2000			
	$PM_{2.5}$	COPD	LNC	LRI	$PM_{2.5}$	COPD	LNC	LRI	$PM_{2.5}$	COPD	LNC	LRI
CIS	4.018	1.0299	1.0294	0.9064	3.954	1.03	1.029	0.9054	3.924	1.03	1.0288	0.905
developed countries	16.75	1.0698	1.091	1.0476	16.75	1.07	1.091	1.0476	16.75	1.07	1.091	1.048
Sub-Saharan Africa	7.489	1.0433	1.0484	0.9566	7.489	1.043	1.048	0.9565	7.581	1.044	1.0488	0.958
Eastern Asia	6.2	1.0384	1.0417	0.9384	6.238	1.038	1.0419	0.939	6.2	1.038	1.04169	0.938
Latin America and the Caribbean	10.712	1.0554	1.0666	1.001	10.712	1.055	1.0666	1.001	10.71	1.055	1.0666	1.001
Northern Africa	6.409	1.0392	1.0435	0.9415	6.409	1.039	1.0435	0.9415	6.382	1.039	1.0433	0.941
Oceania	9.178	1.0499	1.0584	0.9811	9.177	1.05	1.058	0.9811	9.178	1.04989	1.0584	0.981
Southern Asia	7.244	1.0425	1.0476	0.9534	7.245	1.042	1.0477	0.9534	7.244	1.0425	1.0476	0.953
South-Eastern Asia	14.166	1.0682	1.0877	1.049	13.573	1.066	1.0846	1.041	14.166	1.0682	1.0877	1.049
Western Asia	6.302	1.0388	1.0426	0.9399	6.302	1.0388	1.0426	0.9399	6.378	1.0391	1.043	0.941

TABLE 14 POPULATION NORMALIZED BLACK CARBON ADJUSTED NEW $PM_{2.5}$ CONCENTRATION, COPD RISK, LNC RISK, LRI RISK RESPECTIVELY FOR NCAR-CAM5.1 MODEL UNDER POPULATION SCENARIO SSP1 FOR THE TIME PERIOD OF 2000S AS MEASURING THE EFFECT OF BOTH POPULATION SCENARIO AND GREENHOUSE GAS EMISSION SCENARIOS UPON REGIONAL DISTRIBUTION OF POPULATION NORMALIZED RELATIVE RISK.

region	NCAR-CAM 5.1 SSP1			
	2000			
	NEW$PM_{2.5}$	RRCOPD	RRLNC	RRLRI
CIS	4.11	1.0302	1.0300	0.9078
developed countries	17.03	1.0708	1.0925	1.0511
Sub-Saharan Africa	7.52	1.0434	1.0485	0.957
Eastern Asia	6.33	1.0389	1.0425	0.9403
Latin America and the Caribbean	11.8	1.0593	1.0728	1.0159
Northern Africa	6.437	1.0394	1.0437	0.942
Oceania	9.41	1.0508	1.0598	0.9844
Southern Asia	7.737	1.0444	1.0505	0.9605
South-Eastern Asia	14.62	1.0699	1.0902	1.055
Western Asia	6.345	1.0390	1.0428	0.9405

From table 13 and table 14, the comparison between original $PM_{2.5}$ and derived relative risk and black carbon adjusted value is made to test whether the approach of black carbon adjustment of relative risk would be necessary to alter the current methodology of only taking mass concentration into consideration when measuring health impact. If the difference between non-adjustment and adjustment is big enough, the toxicity of black carbon should also be regarded when calculating relative risk.

The increase in COPD relative risk for various regions from SSP1 scenarios:

CIS:0.03%; DC:0.09%; SSA:0.01%; EA:0.05%; LAC:0.37%; NA:0.02%; O:0.086%; SA:0.2%; SEA:0.16%, WA:0.02%

From the increase in black carbon adjusted relative risk for COPD disease, it is shown that Latin America and the Caribbean and southern Asia would be facing relatively higher COPD exposure risk with the black carbon influence while there is not much black carbon COPD risk in Sub-Saharan Africa, western Asia or CIS.

The increase in LNC relative risk for various regions from SSP1 scenarios:

CIS:0.06%; DC:0.14%; SSA:0.01%; EA:0.39%; LAC:0.58%; NA:0.02%; O:0.13%; SA:0.28%; SEA:0.23%, WA:0.02%

From the increase in black carbon adjusted relative risk for LNC disease, it is shown that Latin America and the Caribbean and Eastern Asia would be facing relatively higher LNC exposure risk with the black carbon influence while there is not much black carbon LNC risk in Sub-Saharan Africa, western Asia or Northern Africa. It is worth noting that there is large increase in LNC risk compared with COPD risk for eastern Asia. LNC derived relative risk might be much more sensitive for black carbon compared with COPD or LRI.

The increase in LRI relative risk for various regions from SSP1 scenarios:

CIS:0.15%; DC:0.33%; SSA:0.04%; EA:0.2%; LAC:1.49%; NA:0.05%; O:0.34%; SA:0.74%; SEA:0.57%, WA:0.06%

From the increase in black carbon adjusted relative risk for LRI disease, it is shown that southern Asia and South-eastern Asia would be facing relatively higher LRI exposure risk with the black carbon influence while there is not much black carbon LRI risk in South-eastern Africa or western Asia. There is an extremely high increase in the relative risk for LAC. LAC region is more sensitive to black carbon surface pollution compared with other regions.

Table 15 and 16 depict the COPD mortality from GISS-E2-R output under population scenario SSP1, SSP2 and SSP3 for the time period of 2000s and 2050s respectively.

For lower respiratory infection premature mortality, the difference is much higher and should take black carbon toxicity into consideration for higher accuracy since lower respiratory infection risk would be higher than other two diseases when $PM_{2.5}$ exceeds 20.2 $\mu g/m^3$.

Mortality in eastern Asia is Southern Asia are highest among all regions in current days or near future. There is an obvious increase in mortality in Southern Asia while slightly decreased mortality in Eastern Asia. There is a very slight decrease in the population

average risk value so the relatively large population base in eastern and southern Asia might contribute to the mortality increase and the dominant mortality among all regions.

From the population information from table 17 and 18, it can be said that population variance for Sub-Saharan Africa is hugely varied among different population scenarios. A highly-fragmented scenario would predict a much higher population in Sub-Saharan region in the future especially as Sub-Saharan would have higher population amount than eastern Asia in SSP3. There is a substantial increase in Sub-Saharan Africa from 2000 to 2030. The population normalized relative risk for COPD disease is not largely changed with the value at 1.04, so the population exposure to Saharan dust would increase due to population growth alone.

It is calculate that there is 460,548,477(unit: person) estimated COPD mortality under SSP1, SSP2, SSP3 scenarios respectively at 2000 and 520,637,581(unit: person) estimated COPD mortality under SSP1, SSP2, SSP3 scenarios respectively at 2030 under emission scenario RCP2.6.

TABLE 15 COPD MORTALITY FROM GISS-E2-R OUTPUT UNDER POPULATION SCENARIO SSP1, SSP2 and SSP3 FOR THE TIME PERIOD OF 2000S

region	COPD mortality GISS-E2-R 2000		
	Unit: person per year		
	SSP1	SSP2	SSP3
CIS	14.67	15.17	14.42
developed countries	33.00	33.00	33.00
Sub-Saharan Africa	26.25	26.25	37.33
Eastern Asia	230.50	282.75	230.50
Latin America and the Caribbean	20.17	20.17	20.17
Northern Africa	6.67	6.67	9.17
Oceania	0.42	0.42	0.42
Southern Asia	95.08	124.92	95.08
South-Eastern Asia	24.67	30.17	24.67
Western Asia	8.50	8.50	11.75

TABLE 16 COPD MORTALITY FROM GISS-E2-R OUTPUT UNDER POPULATION SCENARIO SSP1, SSP2 AND SSP3 FOR THE TIME PERIOD OF 2030S UNDER THE RCP2.6 EMISSION SCENARIO

region	COPD mortality GISS-E2-R RCP2.6 2030		
	Unit: person per year		
	SSP1	SSP2	SSP3
CIS	14.17	15.17	14.67
developed countries	38.58	38.25	36.17
Sub-Saharan Africa	48.08	50.92	76.50
Eastern Asia	219.75	275.08	225.17
Latin America and the Caribbean	24.50	25.42	26.75
Northern Africa	8.92	9.25	13.42
Oceania	0.58	0.58	0.67
Southern Asia	123.33	172.92	135.83
South-Eastern Asia	27.08	34.50	29.08
Western Asia	14.58	15.33	22.58

TABLE 17 POPULATION FOR VARIOUS REGIONS IN 2000 PREDICTED BY POPULATION SCENARIOS INCLUDING SSP1, SSP2 AND SSP3

region	population 2000		
	Unit: million		
	SSP1	SSP2	SSP3
CIS	236.17	255.25	246
developed countries	798.56	798.56	798.56
Sub-Saharan Africa	443.73	443.73	619
Eastern Asia	1049.39	1288.95	1049.39
Latin America and the Caribbean	374.85	374.85	374.85
Northern Africa	89.8	89.8	123.68
Oceania	4.4	4.4	4.4
Southern Asia	1048.04	1373.02	1048.4
South-Eastern Asia	408.94	472.92	408.94
Western Asia	99.32	99.32	138.07

TABLE 18 POPULATION FOR VARIOUS REGIONS IN 2030 PREDICTED BY POPULATION SCENARIOS INCLUDING SSP1, SSP2 AND SSP3

region	population 2030		
	Unit: million		
	SSP1	SSP2	SSP3
CIS	243.43	285.96	283.18
developed countries	912.29	904.42	854.74
Sub-Saharan Africa	854.88	906.66	1351.49
Eastern Asia	1053.63	1321.93	1080.27
Latin America and the Caribbean	470.42	489	516.06
Northern Africa	118.66	123.28	179.24
Oceania	6.54	6.90	7.19
Southern Asia	1433.07	2008.63	1580.92
South-Eastern Asia	468.57	556.26	500.48
Western Asia	175.68	183.88	271.93

CHAPTER FIVE
CONCLUSION AND RECOMMENDATIONS

This study illustrates the continuous data from pre-industrial times and the future. Integrated exposure–response (IER) functions are used rather than concentration-response functions in light of global mortality assessment to reduce the uncertainty derived from health impact assessment function. Black carbon adjusted $PM_{2.5}$ concentration is also applied to the health risk analysis. There is comparison between various models, Representative Concentration Pathways and Socioeconomic pathways scenarios to assess the impact of various scenarios.

For model comparison, NCAR-CAM3.5 has much lower prediction than other models and the population-normalized value are much lower for MIROC-CHEM model than the others. Multi-model ensemble is conducted to integrate the output from various models. Ensemble results show that there is obvious increase from 1850 to 2000 in East Asia and Arabian Peninsula. Variation related to various emission, population scenarios and regional distribution are extensively discussed in this paper. Seasonal and time series of relative risk variation are calculated and discussed in this paper as well.

In further related study, it would be interesting to see into the mortality variation with more accurate baseline mortality data since the current available studies use country level baseline mortality data instead of state or county level, which can be problematic for the spatial analysis for large countries since the spatial distribution is going to be the same over all a large terrain. Persistent peak of $PM_{2.5}$ concentration and relative risk in northern Africa regions might be attributed to the Saharan dust storm contribution, which is also consistent with ensemble dust concentration output. Australia dust storm also contributes to the elevation of relative risk. Eastern and south-eastern Asia would be dominant in mortality compared with other regions.

There is a high increase (1.49%) in the lower respiratory infection relative risk for Latin America and Caribbean region. it might be reasonable to take the black carbon toxicity into consideration when addressing COPD mortality.

Population normalized COPD premature mortality is calculated and compared in this paper. There is 460,548,477 (unit: person) estimated COPD mortality under SSP1, SSP2, SSP3 scenarios respectively at 2000 and 520,637,581 (unit: person) at 2030 under the emission scenario RCP2.6. The population exposure to Saharan dust would increase due to population growth alone. The relatively large population base in eastern and southern Asia might contribute to the mortality increase and the dominant mortality of Asia among all regions.

LIST OF REFERENCES

Anenberg, S. C., Horowitz, L. W., Tong, D. Q., & West, J. J. (2010). An estimate of the global burden of anthropogenic ozone and fine particulate matter on premature human mortality using atmospheric modeling. *Environmental Health Perspectives*, *118*(9), 1189–95. doi:10.1289/ehp.0901220

Apte, J. S., Marshall, J. D., Cohen, A. J., & Brauer, M. (2015). Addressing Global Mortality from Ambient PM 2.5. *Environmental Science & Technology*, *49*, 8057–8066. doi:10.1021/acs.est.5b01236

Arden Pope, C., Burnett, R. T., Turner, M. C., Cohen, A., Krewski, D., Jerrett, M., … Thun, M. J. (2011). Lung cancer and cardiovascular disease mortality associated with ambient air pollution and cigarette smoke: Shape of the exposure-response relationships. *Environmental Health Perspectives*, *119*(11), 1616–1621. doi:10.1289/ehp.1103639

Atkinson, R. W., Mills, I. C., Walton, H. a, & Anderson, H. R. (2014). Fine particle components and health—a systematic review and meta-analysis of epidemiological time series studies of daily mortality and hospital admissions. *Journal of Exposure Science and Environmental Epidemiology*, *25*(2), 208–214. doi:10.1038/jes.2014.63

Bill, F., & Foundation, M. G. (2015). Global, regional, and national incidence, prevalence, and years lived with disability for 301 acute and chronic diseases and injuries in 188 countries, 1990–2013: a systematic analysis for the Global Burden of Disease Study 2013. *The Lancet*, *6736*(15), 1990–2013. doi:10.1016/S0140-6736(15)60692-4

Boys, B. L., Martin, R. V, van Donkelaar, A., MacDonell, R. J., Hsu, N. C., Cooper, M. J., … Wang, S. W. (2014). Fifteen-Year Global Time Series of Satellite-Derived Fine Particulate Matter. *Environmental Science & Technology*, *48*(19), 11109–11118. Retrieved from http://pubs.acs.org/doi/abs/10.1021/es502113p

Brauer, M., Amann, M., Burnett, R. T., Cohen, A., Dentener, F., Ezzati, M., … Thurston, G. D. (2012). Exposure assessment for estimation of the global burden of disease attributable to outdoor air pollution. *Environmental Science & Technology*, *46*(2),

652–60. doi:10.1021/es2025752

Burnett, R. T., Arden Pope, C., Ezzati, M., Olives, C., Lim, S. S., Mehta, S., … Cohen, A. (2014a). An integrated risk function for estimating the global burden of disease attributable to ambient fine particulate matter exposure. *Environmental Health Perspectives*, *122*, 397–403. doi:10.1289/ehp.1307049

Burnett, R. T., Arden Pope, C., Ezzati, M., Olives, C., Lim, S. S., Mehta, S., … Cohen, A. (2014b). An integrated risk function for estimating the global burden of disease attributable to ambient fine particulate matter exposure. *Environmental Health Perspectives*, *122*(4), 397–403. doi:10.1289/ehp.1307049

Cao, J., Yang, C., Li, J., Chen, R., Chen, B., Gu, D., & Kan, H. (2011). Association between long-term exposure to outdoor air pollution and mortality in China: A cohort study. *Journal of Hazardous Materials*, *186*(2-3), 1594–1600. doi:10.1016/j.jhazmat.2010.12.036

Cohen, A. J., Ross Anderson, H., Ostro, B., Pandey, K. D., Krzyzanowski, M., Künzli, N., … Smith, K. (2006). The global burden of disease due to outdoor air pollution. *Journal of Toxicology and Environmental Health. Part A*, *68*(13-14), 1301–1307. doi:10.1080/15287390590936166

Crouse, D. L., Peters, P. a., van Donkelaar, A., Goldberg, M. S., Villeneuve, P. J., Brion, O., … Burnett, R. T. (2012). Risk of nonaccidental and cardiovascular mortality in relation to long-term exposure to low concentrations of fine particulate matter: A canadian national-level cohort study. *Environmental Health Perspectives*, *120*(5), 708–714. doi:10.1289/ehp.1104049

de Longueville, F., Hountondji, Y.-C., Ozer, P., Marticorena, B., Chatenet, B., & Henry, S. (2013). Saharan Dust Impacts on Air Quality: What Are the Potential Health Risks in West Africa? *Human and Ecological Risk Assessment: An International Journal*, *19*(6), 1595–1617. doi:10.1080/10807039.2012.716684

EANET. (2015). *Review on the state of air pollution in East Asia*. Retrieved from http://www.eanet.asia/product/RSAP/RSAP.pdf

Fang, Y., Naik, V., Horowitz, L. W., & Mauzerall, D. L. (2013). Air pollution and associated human mortality: The role of air pollutant emissions, climate change and methane concentration increases from the preindustrial period to present. *Atmospheric Chemistry and Physics*, *13*(3), 1377–1394. doi:10.5194/acp-13-1377-2013

Goudie, A. S., & Middleton, N. J. (2001). Saharan dust storms: Nature and consequences. *Earth-Science Reviews*, *56*(1-4), 179–204. doi:10.1016/S0012-8252(01)00067-8

Janssen, N. A. H., Hoek, G., Simic-Lawson, M., Fischer, P., van Bree, L., ten Brink, H., … Cassee, F. R. (2011). Black Carbon as an Additional Indicator of the Adverse Health Effects of Airborne Particles Compared with PM10 and PM2.5. *Environmental Health Perspectives*, *119*(12), 1691–1699. doi:10.1289/ehp.1003369

Jiang, L. (2014). Internal consistency of demographic assumptions in the shared socioeconomic pathways. *Population and Environment*, *35*(3), 261–285. doi:10.1007/s11111-014-0206-3

Jie, W. U., Ying, X. U., & Bing, Z. (2016). Projection of PM 2 . 5 and Ozone Concentration Changes over the Jing-Jin-Ji Region in China, *8*(3), 143–146. doi:10.3878/AOSL20140102.The

Kan, H., London, S. J., Chen, G., Zhang, Y., Song, G., Zhao, N., … Chen, B. (2007). Differentiating the effects of fine and coarse particles on daily mortality in Shanghai, China. *Journal of Environ Int.*, *33*(3), 376–384.

Karanasiou, A., Moreno, N., Moreno, T., Viana, M., Leeuw, F. De, & Querol, X. (2012). Health effects from Sahara dust particles. *The European Topic Centre on Air Pollution and Climate Change Mitigation (ETC/ACM) Is*.

KC, S., & Lutz, W. (2014). The human core of the shared socioeconomic pathways: Population scenarios by age, sex and level of education for all countries to 2100. *Global Environmental Change*. doi:10.1016/j.gloenvcha.2014.06.004

Krewski, D., Jerrett, M., Burnett, R. T., Ma, R., Hughes, E., Shi, Y., … Tempalski, B. (2009). Extended follow-up and spatial analysis of the American Cancer Society study linking particulate air pollution and mortality. *Research Report (Health Effects Institute)*, (140), 5–114; discussion 115–136.

Lamarque, J.-F., Shindell, D. T., Josse, B., Young, P. J., Cionni, I., Eyring, V., … Zeng, G. (2013). The Atmospheric Chemistry and Climate Model Intercomparison Project (ACCMIP): overview and description of models, simulations and climate diagnostics. *Geoscientific Model Development*, *6*(1), 179–206. doi:10.5194/gmd-6-179-2013

Lelieveld, J., Evans, J. S., Fnais, M., Giannadaki, D., & Pozzer, A. (2015). The contribution of outdoor air pollution sources to premature mortality on a global scale. *Nature*, *525*(7569), 367–71. doi:10.1038/nature15371

Lepeule, J., Laden, F., Dockery, D., & Schwartz, J. (2012). Chronic exposure to fine particles and mortality: An extended follow-up of the Harvard six cities study from 1974 to 2009. *Environmental Health Perspectives*, *120*(7), 965–970. doi:10.1289/ehp.1104660

Lutz, W., & Striessnig, E. (2015). Demographic aspects of climate change mitigation and adaptation. *Population Studies*, *69*(sup1), S69–S76. doi:10.1080/00324728.2014.969929

Merrifield, A., Schindeler, S., Jalaludin, B., & Smith, W. (2013). Health effects of the September 2009 dust storm in Sydney, Australia: did emergency department visits and hospital admissions increase? *Environmental Health : A Global Access Science Source*, *12*(September 2009), 32. doi:10.1186/1476-069X-12-32

Miller, R. L., & Tegen, I. (1998). Climate response to soil dust aerosols. *Journal of Climate*, *11*(12), 3247–3267. doi:10.1175/1520-0442(1998)011<3247:CRTSDA>2.0.CO;2

Murray, C. J. L., & Lopez, A. D. (1997). Alternative projections of mortality and disability by cause 1990-2020: Global Burden of Disease Study. *Lancet*, *349*(9064), 1498–

1504. doi:10.1016/S0140-6736(96)07492-2

Murray, C. J. L., & Lopez, A. D. (2013). Measuring the Global Burden of Disease. *New England Journal of Medicine*, *369*(5), 448–457. doi:10.1056/NEJMra1201534

Pope, C. A., Muhlestein, J. B., May, H. T., Renlund, D. G., Anderson, J. L., & Horne, B. D. (2006). Ischemic heart disease events triggered by short-term exposure to fine particulate air pollution. *Circulation*, *114*(23), 2443–8. doi:10.1161/CIRCULATIONAHA.106.636977

Schwartz, J. (2000). Harvesting and long term exposure effects in the relation between air pollution and mortality. *American Journal of Epidemiology*, *151*(5), 440–448.

Shi, L., Zanobetti, A., Kloog, I., Coull, B. a., Koutrakis, P., Melly, S. J., & Schwartz, J. D. (2015). Low-Concentration PM2.5 and Mortality: Estimating Acute and Chronic Effects in a Population-Based Study. *Environmental Health Perspectives*, (August 2014). doi:10.1289/ehp.1409111

Silva, R. a, West, J. J., Zhang, Y., Anenberg, S. C., Lamarque, J.-F., Shindell, D. T., … Zeng, G. (2013). Global premature mortality due to anthropogenic outdoor air pollution and the contribution of past climate change. *Environmental Research Letters*, *8*(3), 034005. doi:10.1088/1748-9326/8/3/034005

Tager, I. B., Balmes, J., Lurmann, F., Ngo, L., Alcorn, S., & K??nzli, N. (2005). Chronic Exposure to Ambient Ozone and Lung Function in Young Adults. *Epidemiology*, *16*(6), 751–759. doi:10.1097/01.ede.0000183166.68809.b0

Tebaldi, C., & Knutti, R. (2007). The use of the multi-model ensemble in probabilistic climate projections. *Philosophical Transactions. Series A, Mathematical, Physical, and Engineering Sciences*, *365*(1857), 2053–2075. doi:10.1098/rsta.2007.2076

Toggweiler, J., & Key, R. (2001). Multi-model ensemble estimates of climate change impacts on UK seasonal precipitation extremes. *Encyclopedia of Atmospheric Sciences*, *4*(December 2007), 1549–1555. doi:10.1002/joc

van Donkelaar, A., Martin, R. V., Brauer, M., & Boys, B. L. (2014). Use of Satellite Observations for Long-Term Exposure Assessment of Global Concentrations of

Fine Particulate Matter. *Environmental Health Perspectives*, *110*(October), A174. doi:10.1289/ehp.1408646

APPENDIX

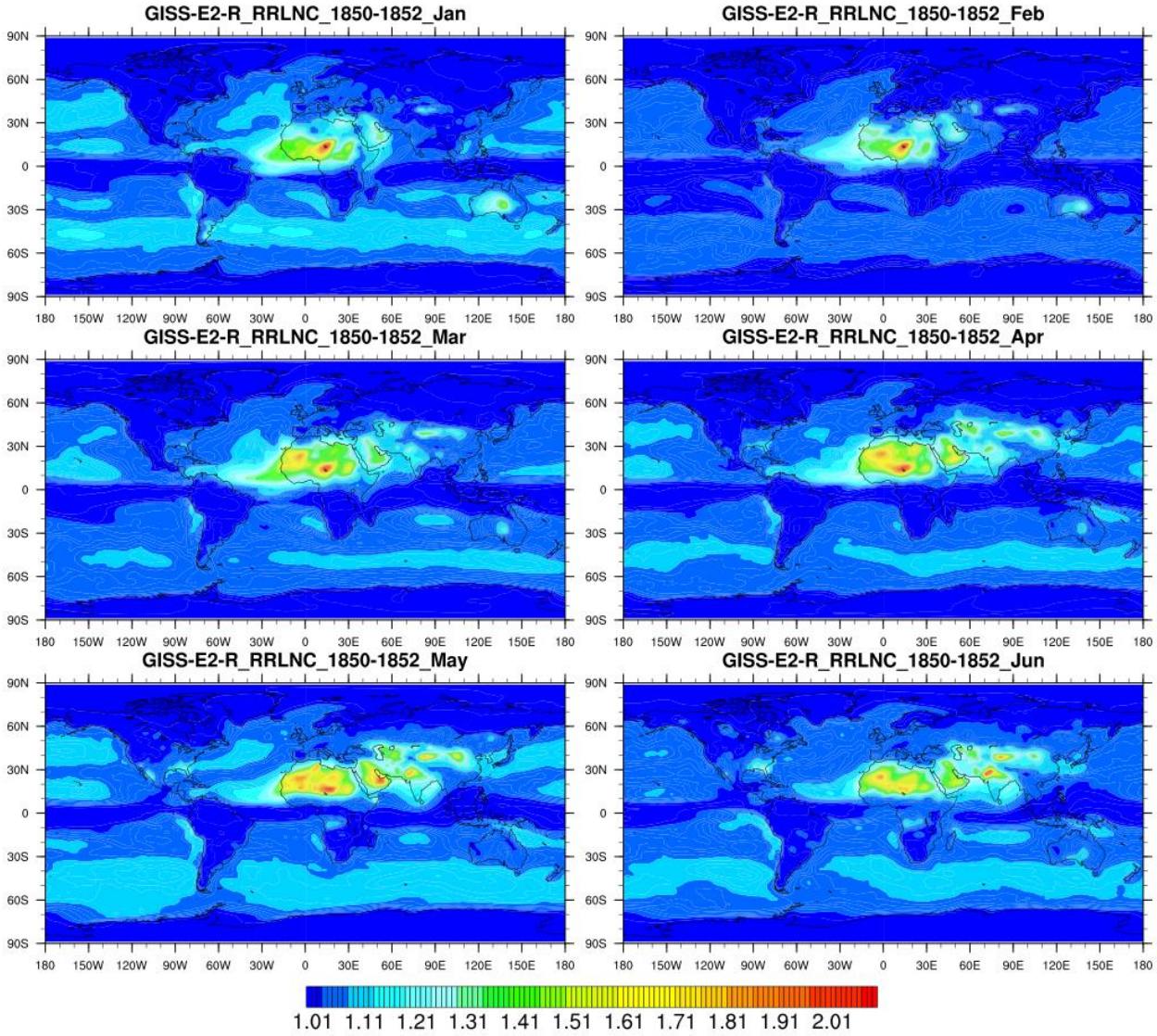


Figure 50 Global relative risk for lung cancer from January to June of the three year average data from 1850 to 1852 with the ambient $PM_{2.5}$ concentration output from GISS-E2-R model based on the integrated risk function developed for GBD(Burnett et al., 2014b) for each figure, vertical axes indicate latitude and horizontal axes indicate longitude. The map plot indicate the monthly level of relative risk over a global terrain by applying the concentration-risk function from IER model for LNC disease endpoint.

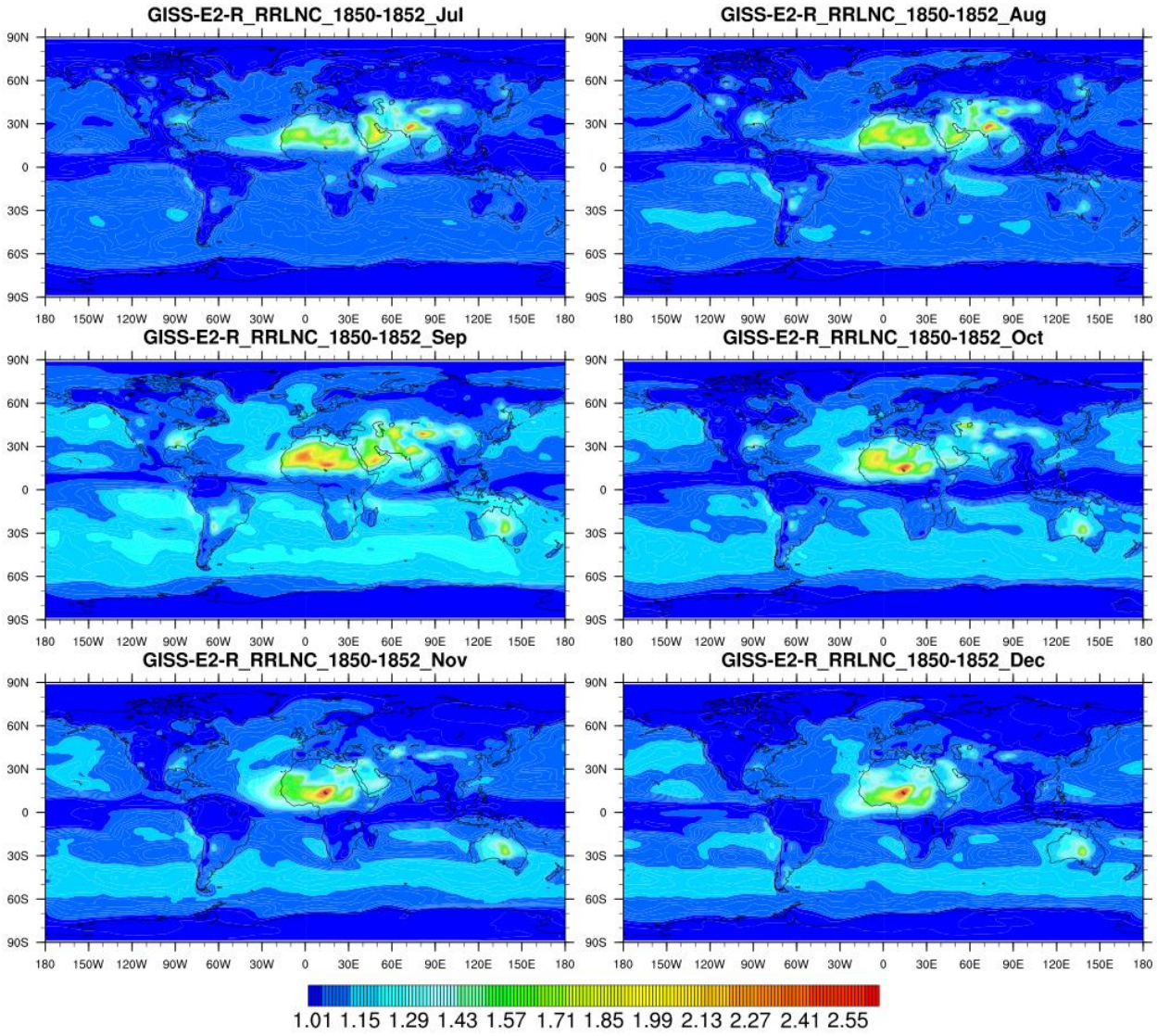


Figure 51 Global relative risk for lung cancer from July to December of the three year average data from 1850 to 1852 with the ambient $PM_{2.5}$ concentration output from GISS-E2-R model based on the integrated risk function developed for GBD(Burnett et al., 2014b) for each figure, vertical axes indicate latitude and horizontal axes indicate longitude. The map plot indicate the monthly level of relative risk over a global terrain by applying the concentration-risk function from IER model for LNC disease endpoint.

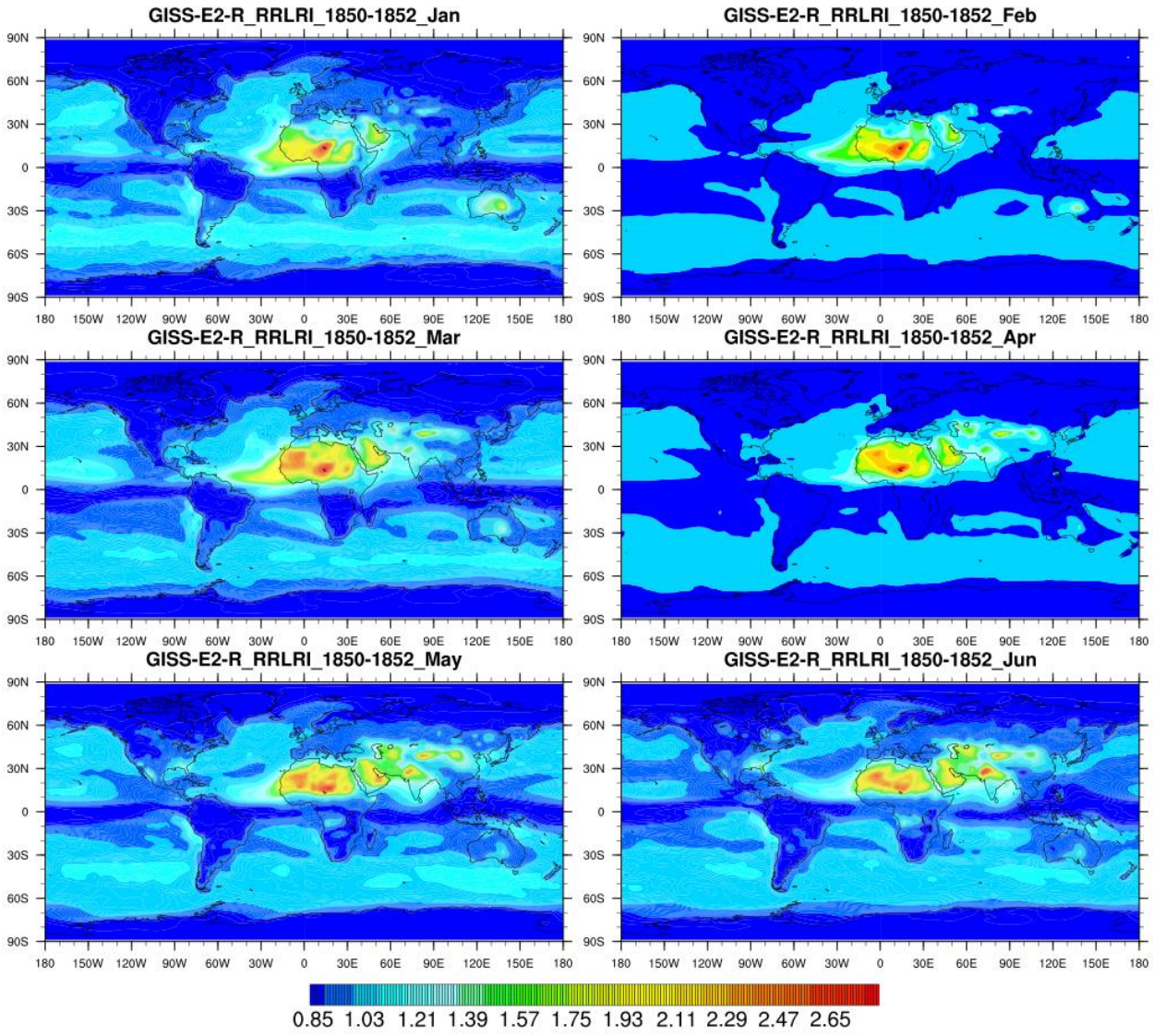


Figure 52 Global relative risk for lower respiratory infection disease from January to June of the three year average data from 1850 to 1852 with the ambient $PM_{2.5}$ concentration output from GISS-E2-R model based on the integrated risk function developed for GBD(Burnett et al., 2014b) for each figure, vertical axes indicate latitude and horizontal axes indicate longitude. The map plot indicate the monthly level of relative risk over a global terrain by applying the concentration-risk function from IER model for LRI disease endpoint.

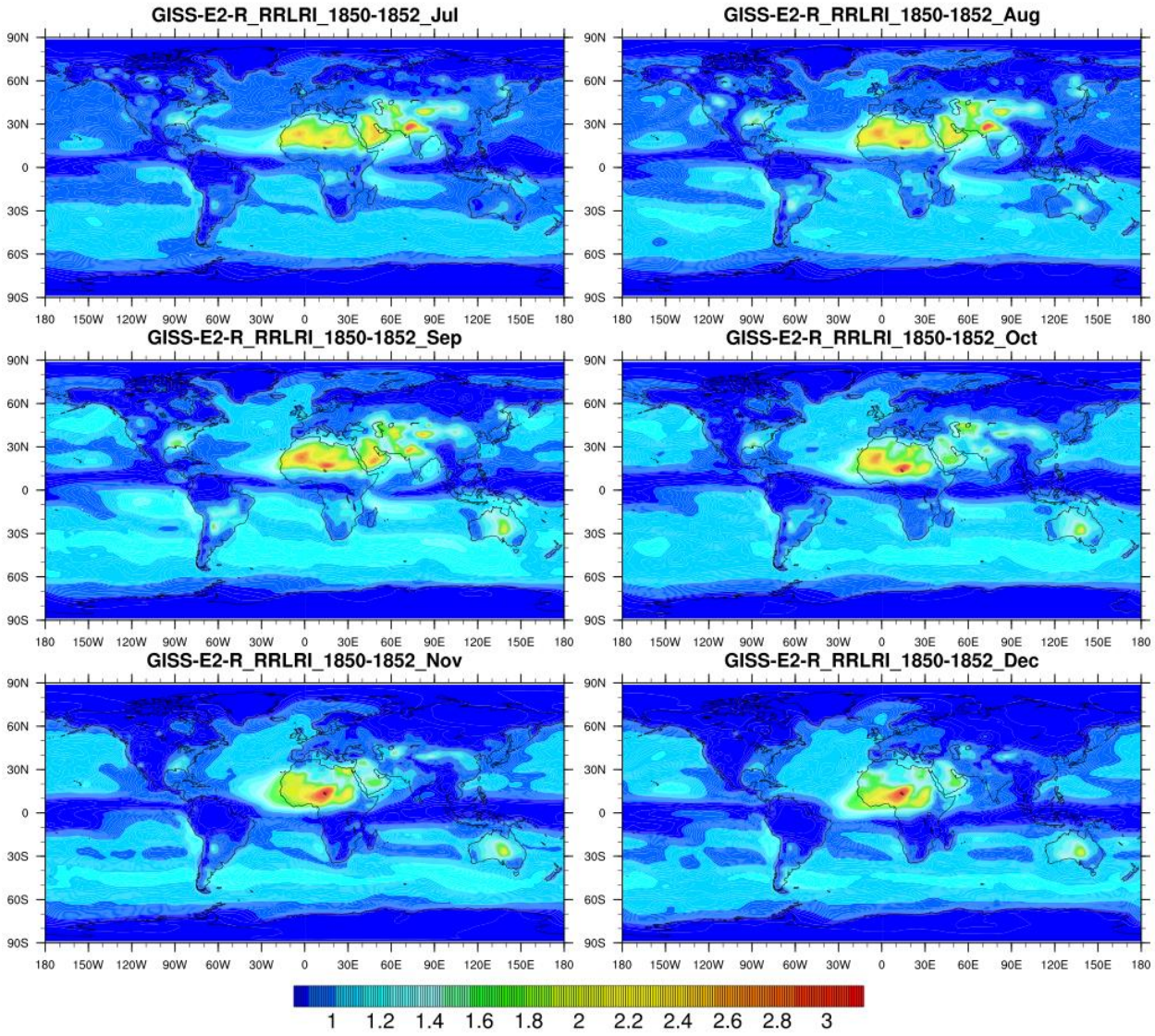


Figure 53 Global relative risk for cardiopulmonary disease from July to December of the three year average data from 1850 to 1852 with the ambient $PM_{2.5}$ concentration output from GISS-E2-R model based on the integrated risk function developed for GBD(Burnett et al., 2014b) for each figure, vertical axes indicate latitude and horizontal axes indicate longitude. The map plot indicate the monthly level of relative risk over a global terrain by applying the concentration-risk function from IER model for LRI disease endpoint.

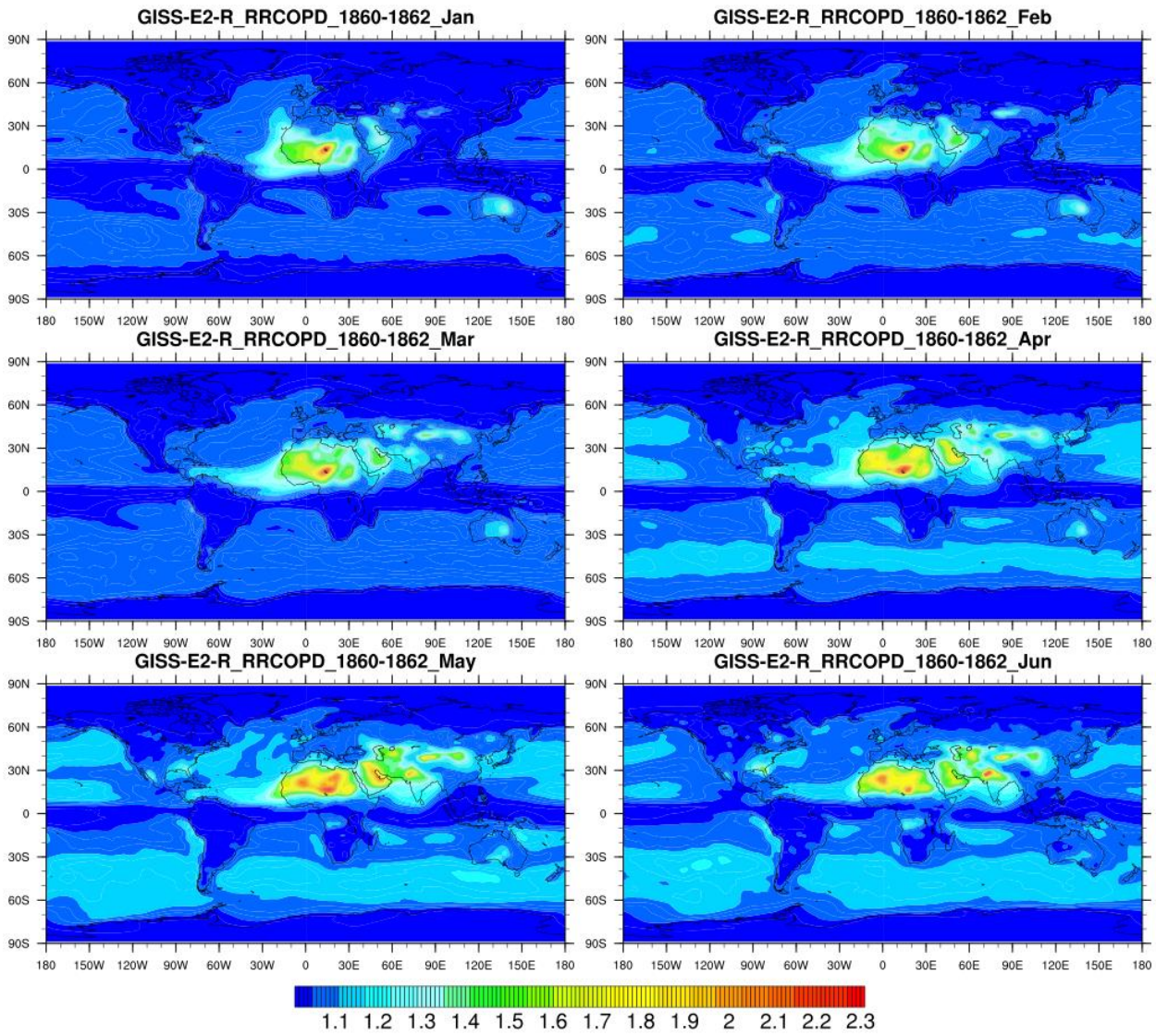


Figure 54 Global relative risk for cardiopulmonary disease from January to June of the three year average data from 1860 to 1862 with the ambient $PM_{2.5}$ concentration output from GISS-E2-R model based on the integrated risk function developed for GBD(Burnett et al., 2014b) for each figure, vertical axes indicate latitude and horizontal axes indicate longitude. The map plot indicate the monthly level of relative risk over a global terrain by applying the concentration-risk function from IER model for COPD disease endpoint.

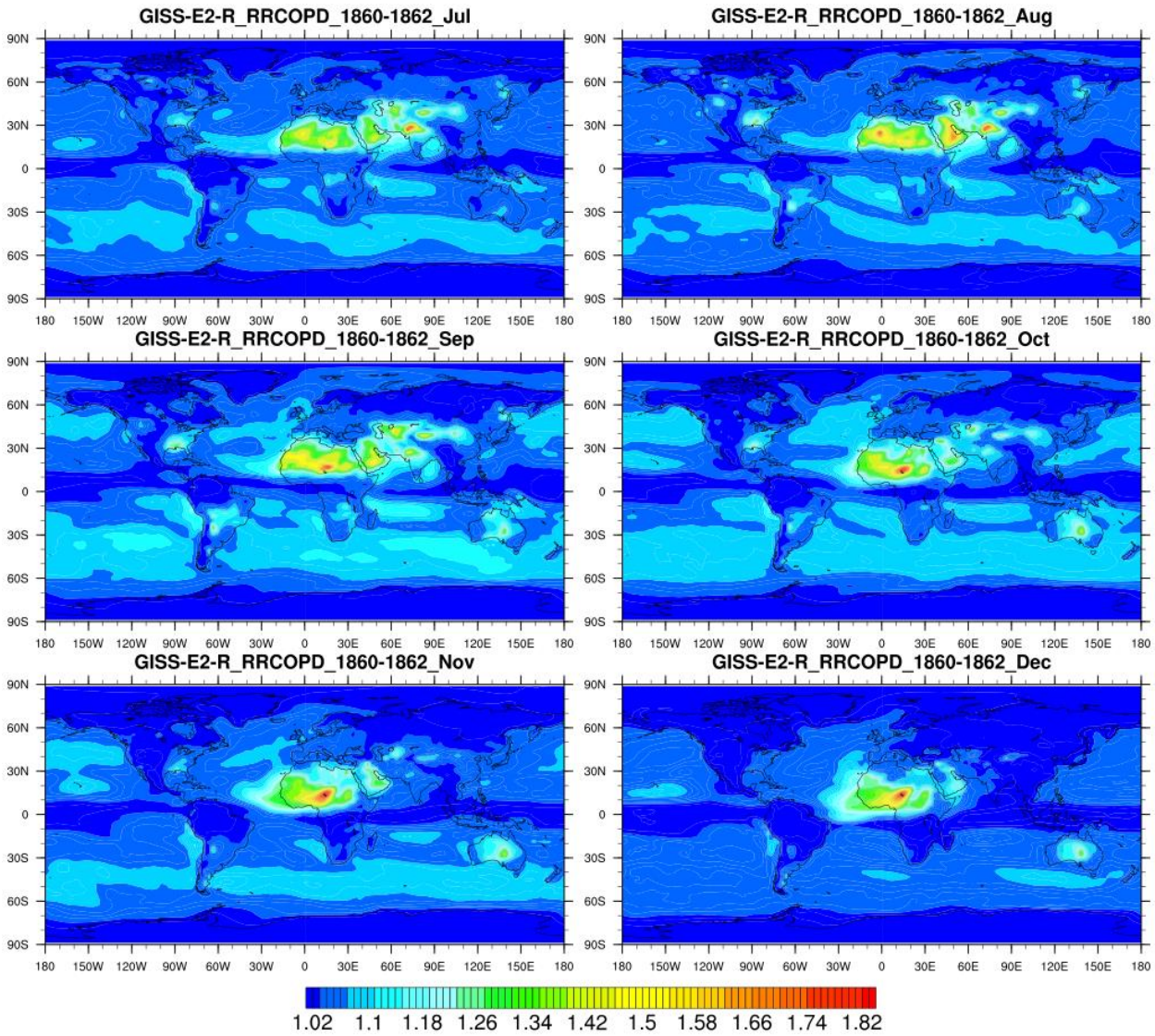


Figure 55 Global relative risk for cardiopulmonary disease from July to December of the three year average data from 1860 to 1862 with the ambient $PM_{2.5}$ concentration output from GISS-E2-R model based on the integrated risk function developed for GBD(Burnett et al., 2014b) for each figure, vertical axes indicate latitude and horizontal axes indicate longitude. The map plot indicate the monthly level of relative risk over a global terrain by applying the concentration-risk function from IER model for COPD disease endpoint.

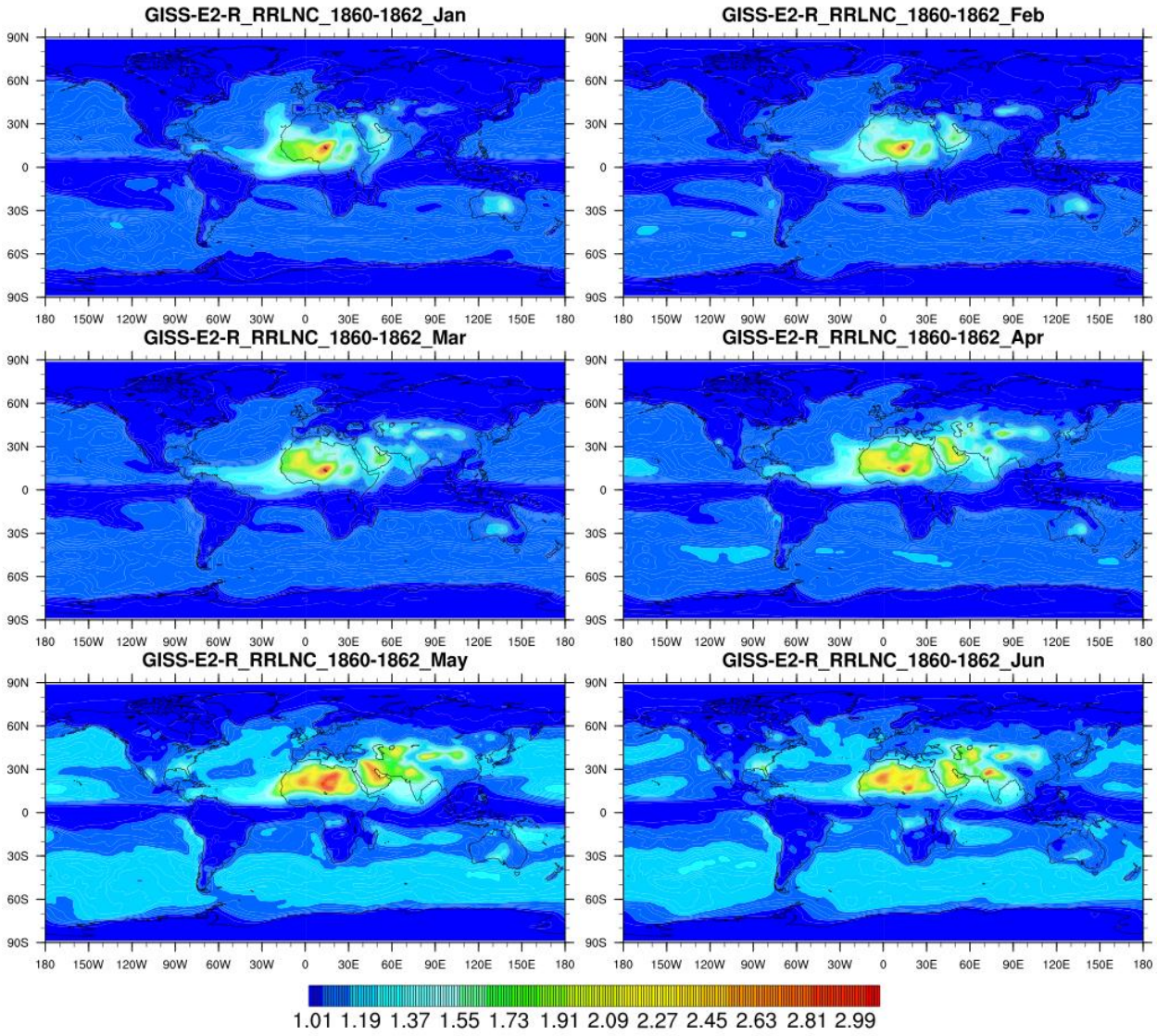


Figure 56 Global relative risk for lung cancer from January to June of the three year average data from 1860 to 1862 with the ambient $PM_{2.5}$ concentration output from GISS-E2-R model based on the integrated risk function developed for GBD(Burnett et al., 2014b) for each figure, vertical axes indicate latitude and horizontal axes indicate longitude. The map plot indicate the monthly level of relative risk over a global terrain by applying the concentration-risk function from IER model for LNC disease endpoint.

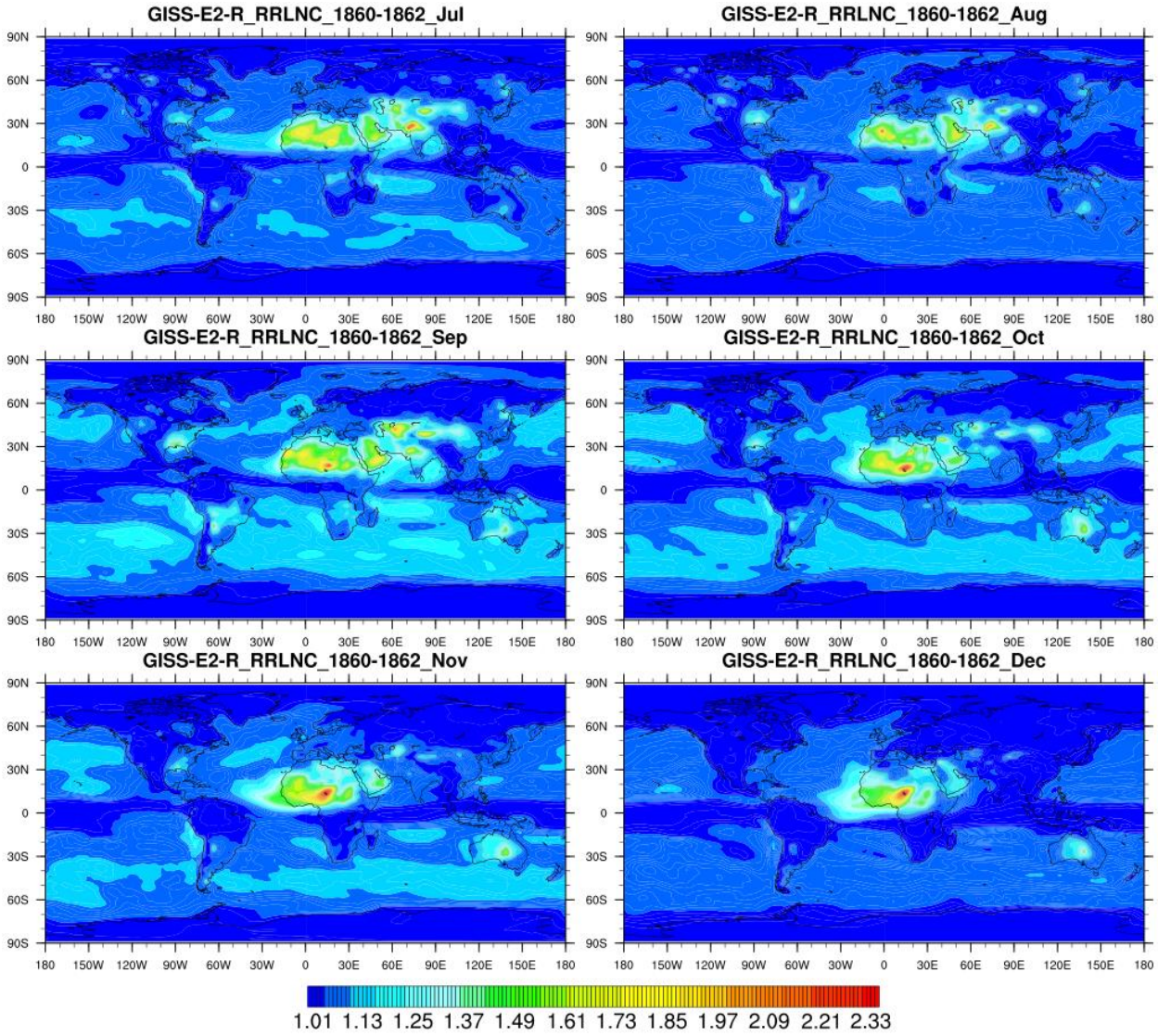


Figure 57 Global relative risk for lung cancer from July to December of the three year average data from 1860 to 1862 with the ambient $PM_{2.5}$ concentration output from GISS-E2-R model based on the integrated risk function developed for GBD(Burnett et al., 2014b) for each figure, vertical axes indicate latitude and horizontal axes indicate longitude. The map plot indicate the monthly level of relative risk over a global terrain by applying the concentration-risk function from IER model for LNC disease endpoint.

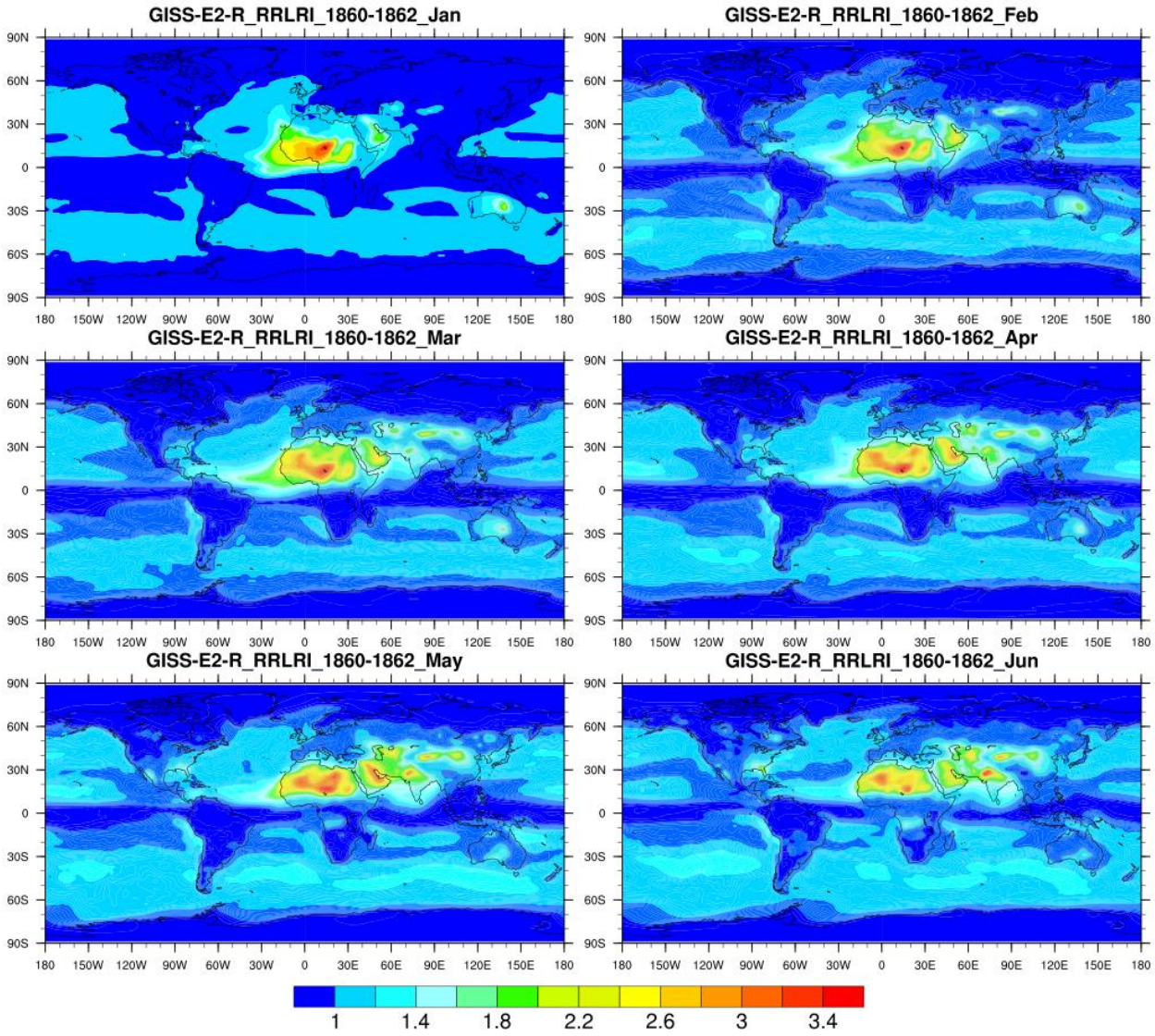


Figure 58 Global relative risk for lower respiratory infection disease from January to June of the three year average data from 1860 to 1862 with the ambient $PM_{2.5}$ concentration output from GISS-E2-R model based on the integrated risk function developed for GBD(Burnett et al., 2014b) for each figure, vertical axes indicate latitude and horizontal axes indicate longitude. The map plot indicate the monthly level of relative risk over a global terrain by applying the concentration-risk function from IER model for LRI disease endpoint.

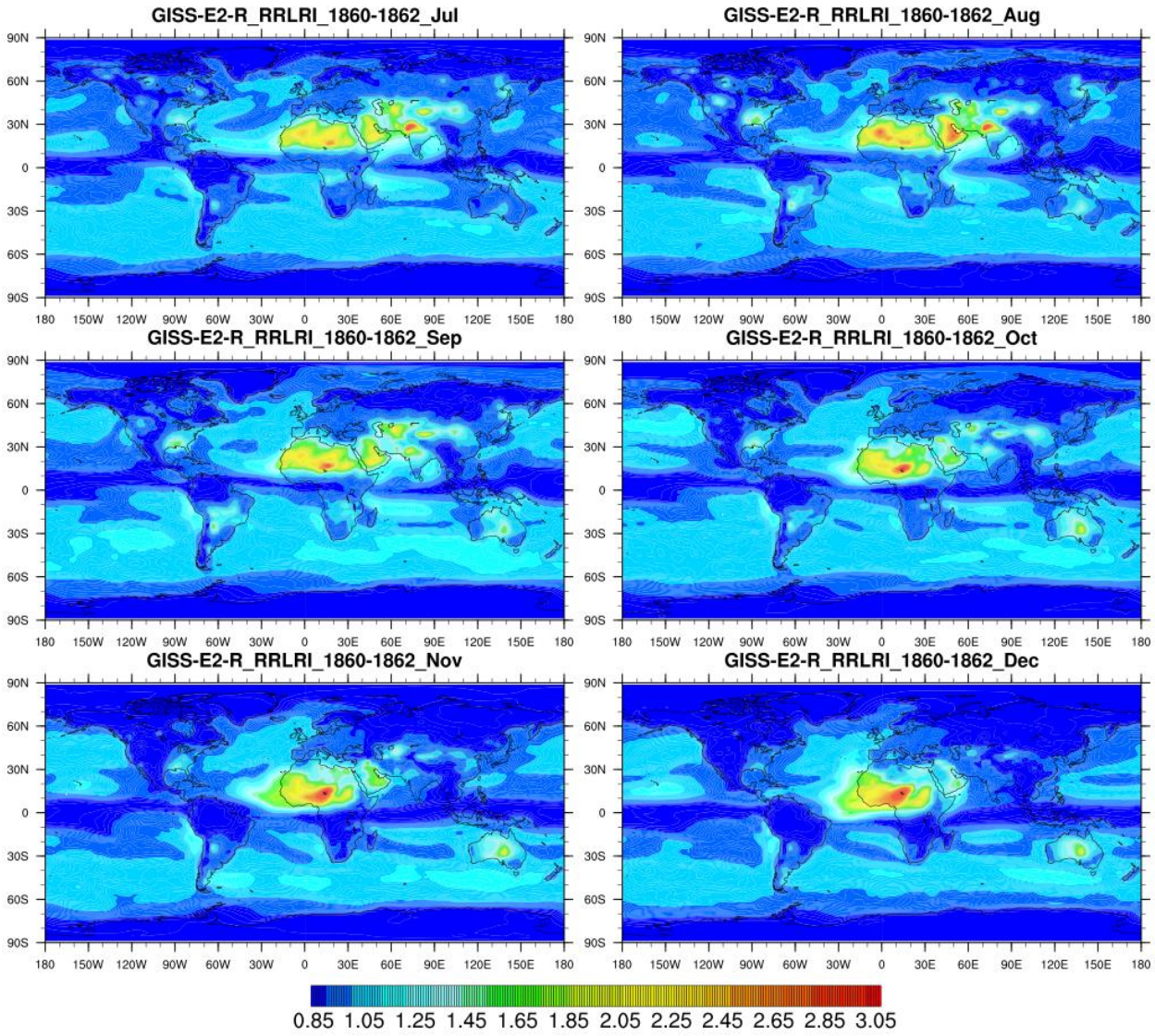


Figure 59 Global relative risk for lower respiratory infection disease from July to December of the three year average data from 1860 to 1862 with the ambient $PM_{2.5}$ concentration output from GISS-E2-R model based on the integrated risk function developed for GBD(Burnett et al., 2014b) for each figure, vertical axes indicate latitude and horizontal axes indicate longitude. The map plot indicate the monthly level of relative risk over a global terrain by applying the concentration-risk function from IER model for LRI disease endpoint.

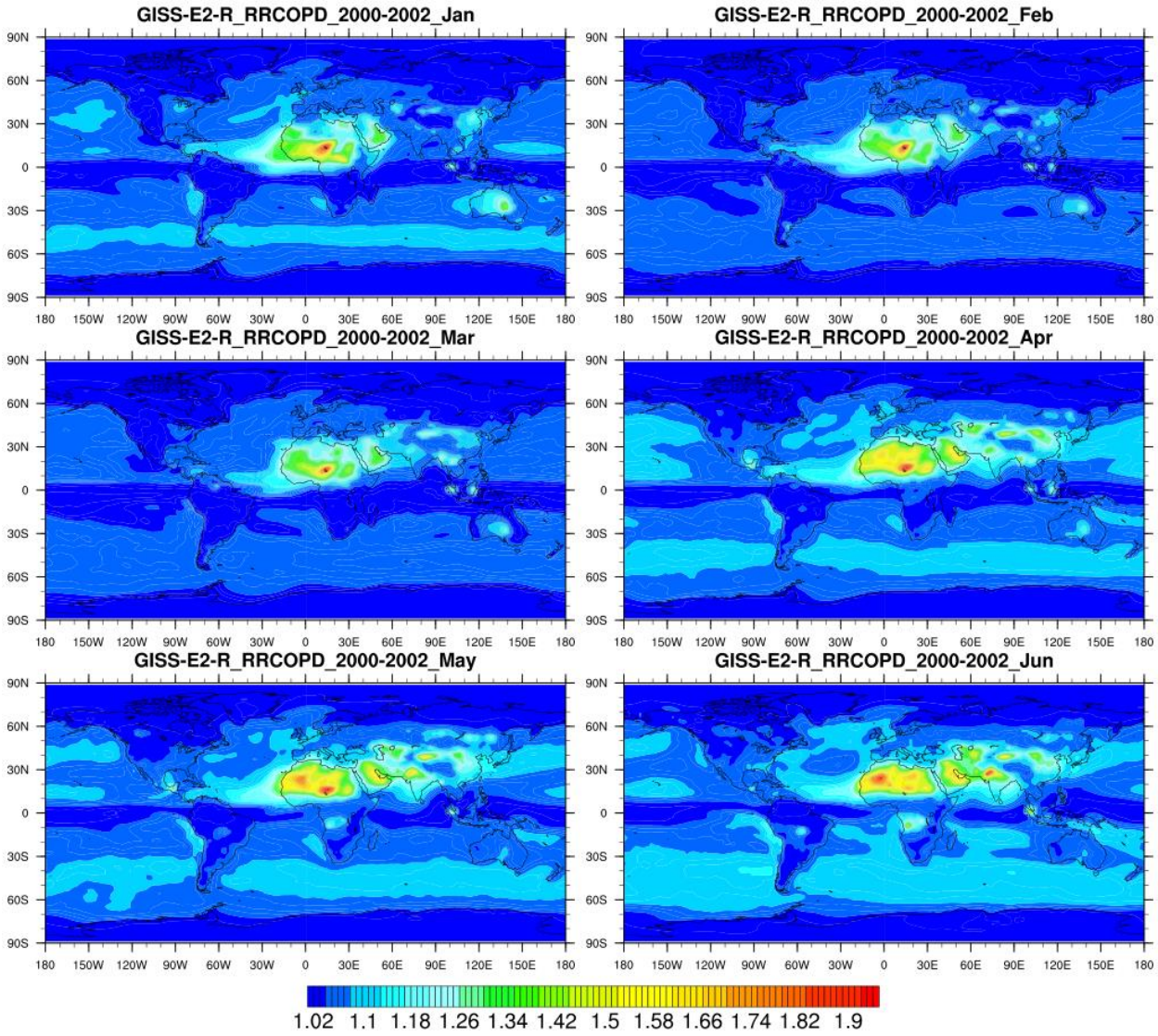


Figure 60 Global relative risk for cardiopulmonary disease from January to June of the three year average data from 2000 to 2002 with the ambient $PM_{2.5}$ concentration output from GISS-E2-R model based on the integrated risk function developed for GBD(Burnett et al., 2014b) for each figure, vertical axes indicate latitude and horizontal axes indicate longitude. The map plot indicate the monthly level of relative risk over a global terrain by applying the concentration-risk function from IER model for COPD disease endpoint.

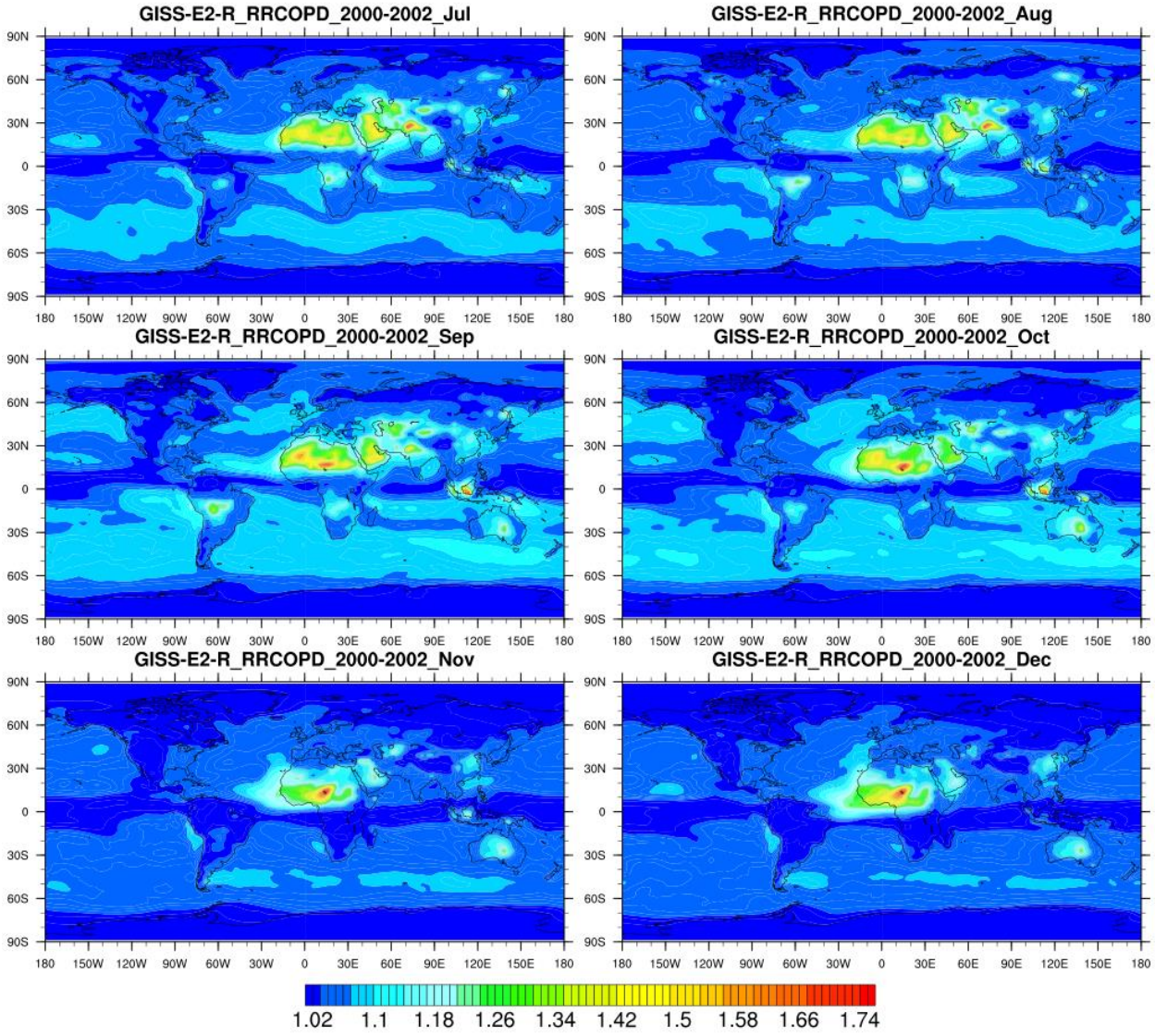


Figure 61 Global relative risk for cardiopulmonary disease from July to December of the three year average data from 2000 to 2002 with the ambient $PM_{2.5}$ concentration output from GISS-E2-R model based on the integrated risk function developed for GBD(Burnett et al., 2014b) for each figure, vertical axes indicate latitude and horizontal axes indicate longitude. The map plot indicate the monthly level of relative risk over a global terrain by applying the concentration-risk function from IER model for COPD disease endpoint.

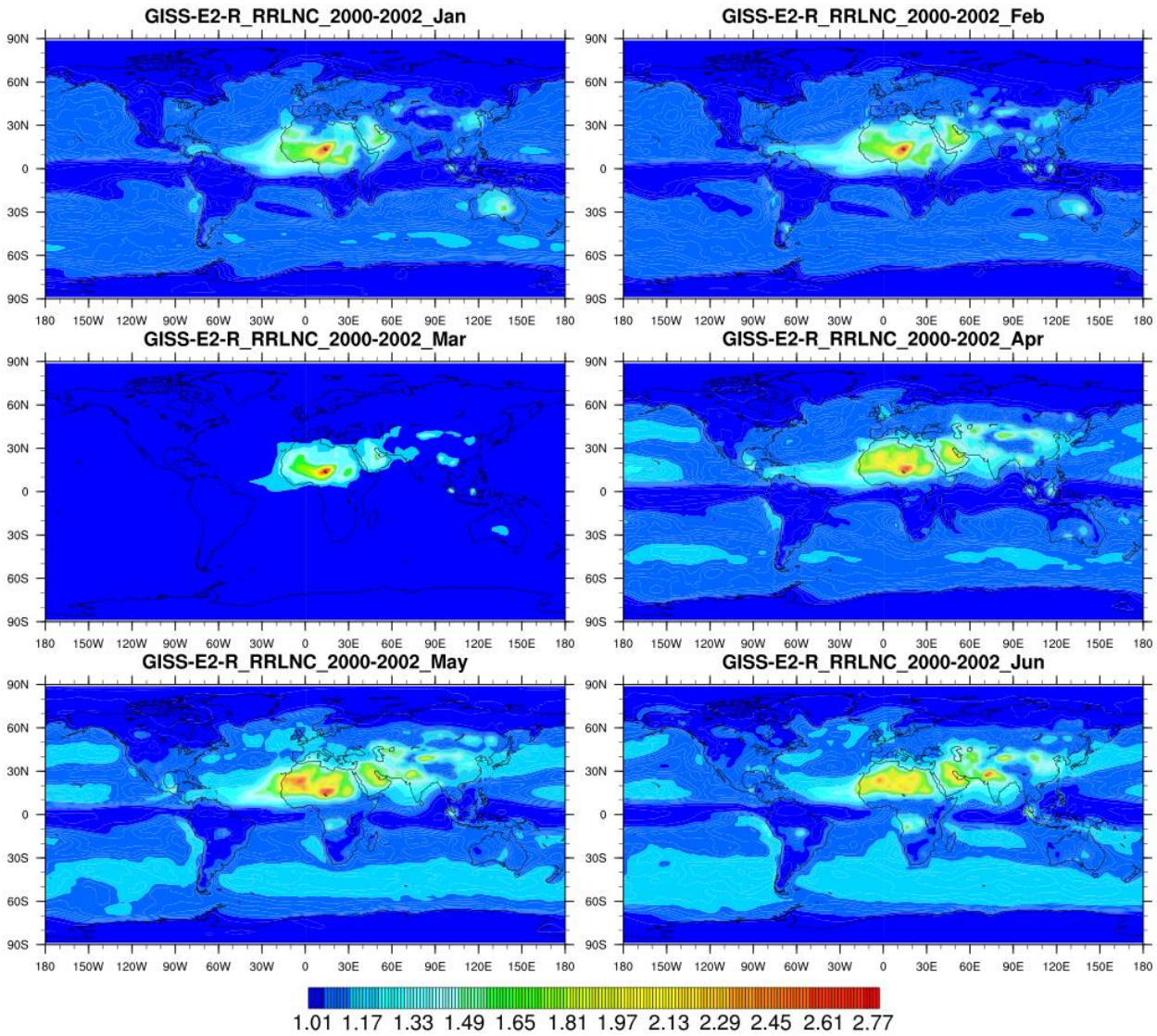


Figure 62 Global relative risk for lung cancer from January to June of the three year average data from 2000 to 2002 with the ambient $PM_{2.5}$ concentration output from GISS-E2-R model based on the integrated risk function developed for GBD(Burnett et al., 2014b) for each figure, vertical axes indicate latitude and horizontal axes indicate longitude. The map plot indicate the monthly level of relative risk over a global terrain by applying the concentration-risk function from IER model for LNC disease endpoint.

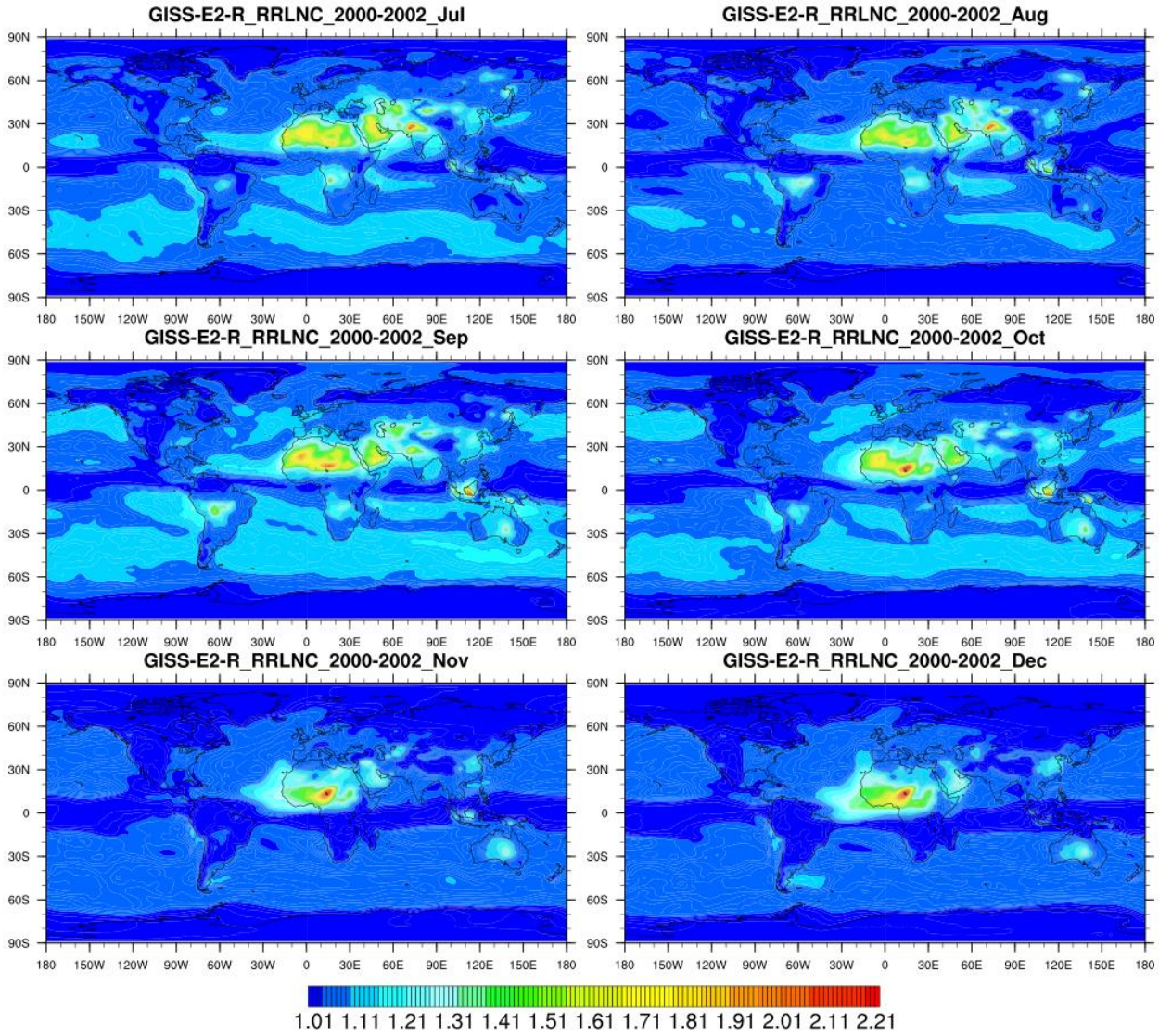


Figure 63 Global relative risk for lung cancer from July to December of the three year average data from 2000 to 2002 with the ambient $PM_{2.5}$ concentration output from GISS-E2-R model based on the integrated risk function developed for GBD(Burnett et al., 2014b) for each figure, vertical axes indicate latitude and horizontal axes indicate longitude. The map plot indicate the monthly level of relative risk over a global terrain by applying the concentration-risk function from IER model for LNC disease endpoint.

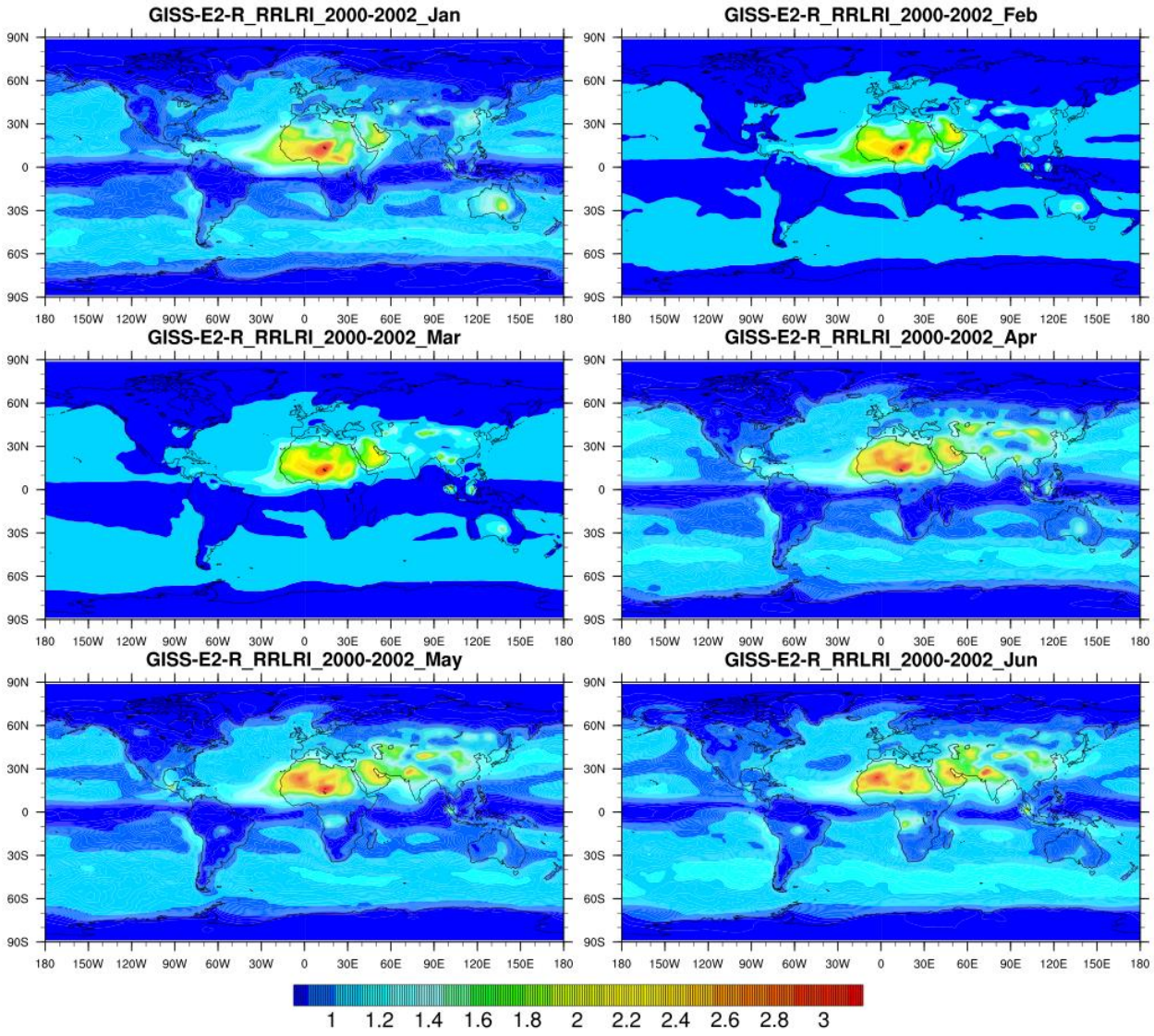


Figure 64 Global relative risk for lower respiratory infection from January to June of the three year average data from 2000 to 2002 with the ambient $PM_{2.5}$ concentration output from GISS-E2-R model based on the integrated risk function developed for GBD(Burnett et al., 2014b) for each figure, vertical axes indicate latitude and horizontal axes indicate longitude. The map plot indicate the monthly level of relative risk over a global terrain by applying the concentration-risk function from IER model for LRI disease endpoint.

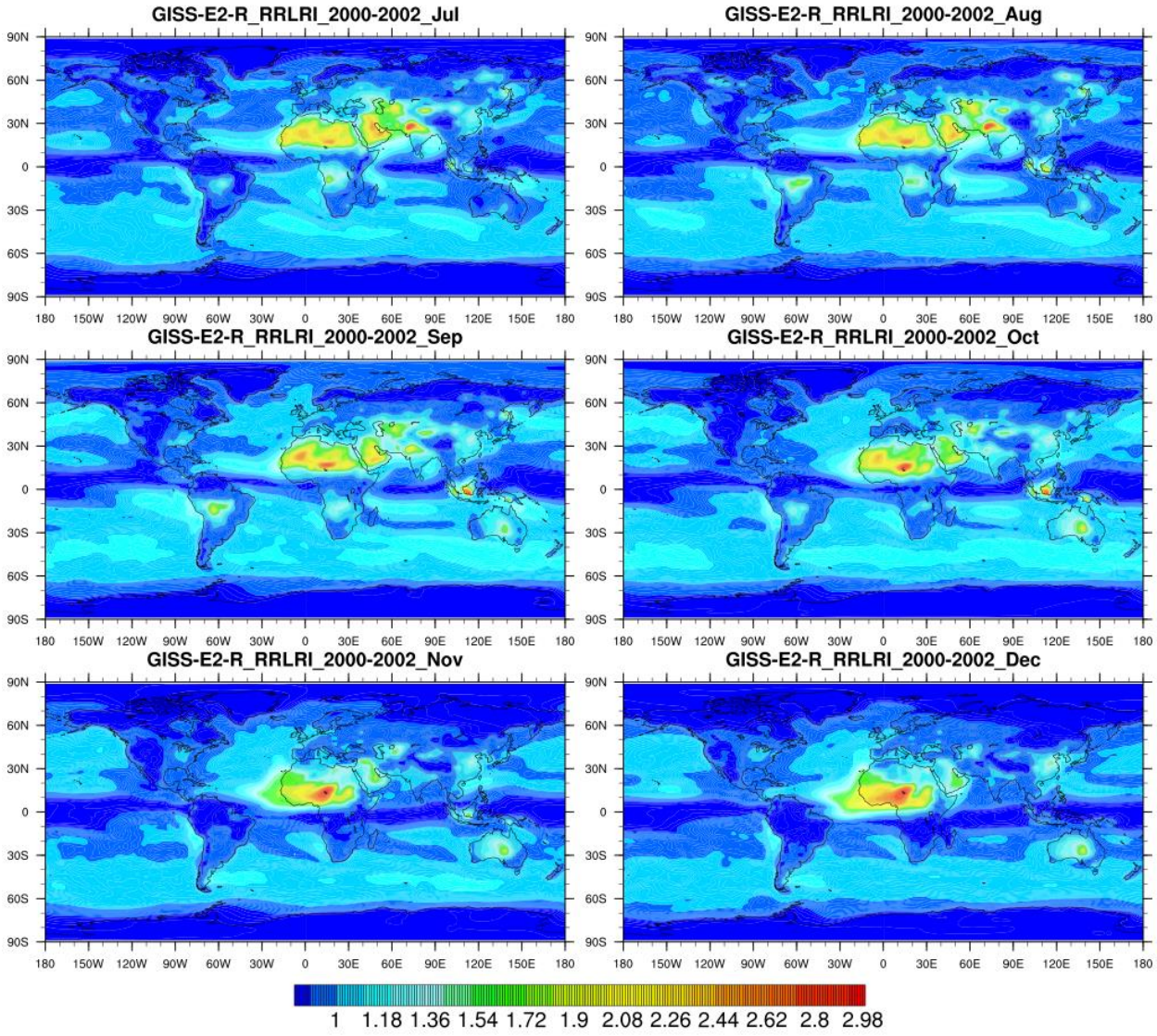


Figure 65 Global relative risk for lower respiratory infection from July to December of the three year average data from 2000 to 2002 with the ambient $PM_{2.5}$ concentration output from GISS-E2-R model based on the integrated risk function developed for GBD(Burnett et al., 2014b) for each figure, vertical axes indicate latitude and horizontal axes indicate longitude. The map plot indicate the monthly level of relative risk over a global terrain by applying the concentration-risk function from IER model for LRI disease endpoint.

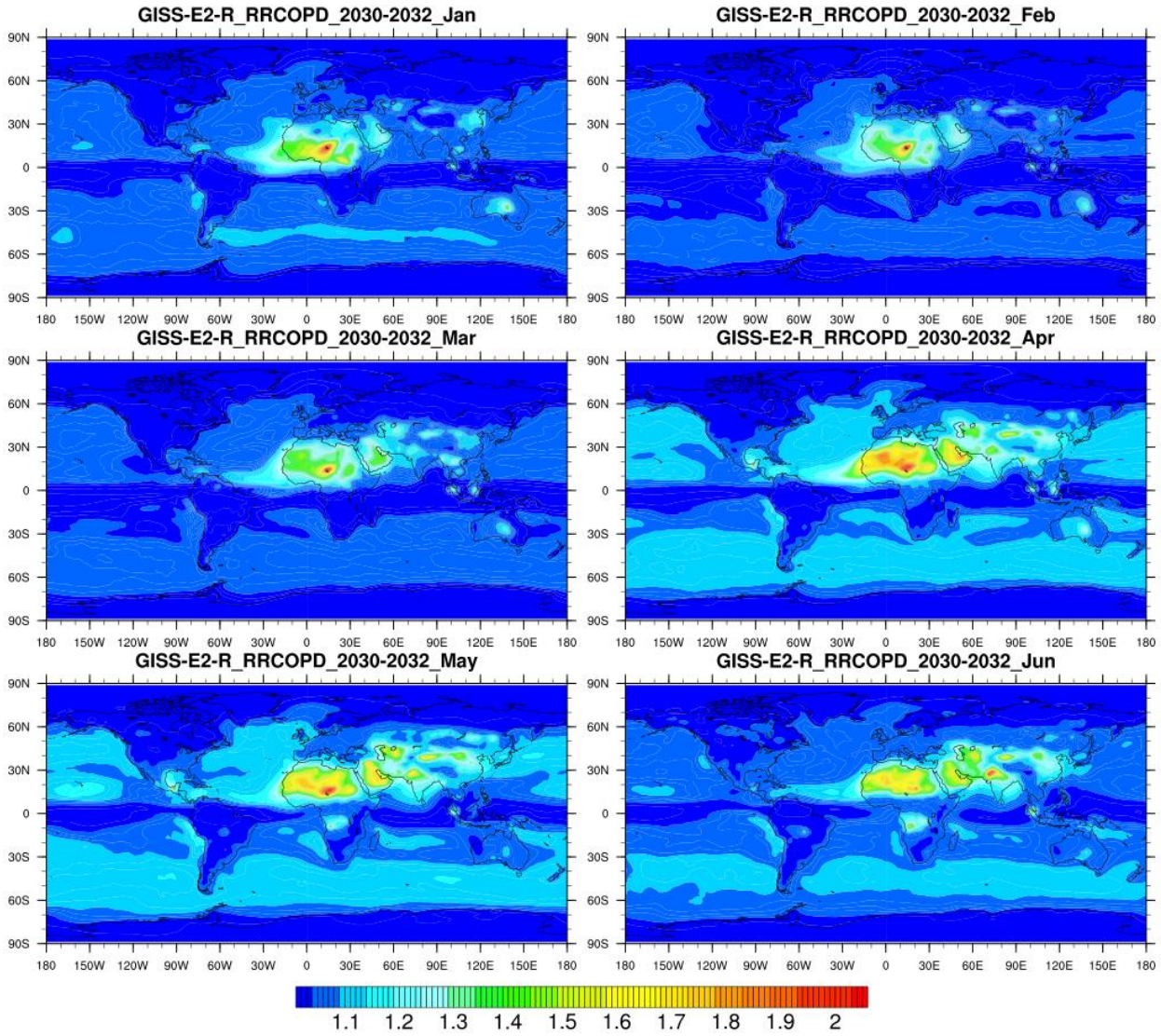


Figure 66 Global relative risk for cardiopulmonary disease from January to June of the three year average data from 2030 to 2032 with the ambient $PM_{2.5}$ concentration output from GISS-E2-R model based on the integrated risk function developed for GBD(Burnett et al., 2014b) for each figure, vertical axes indicate latitude and horizontal axes indicate longitude. The map plot indicate the monthly level of relative risk over a global terrain by applying the concentration-risk function from IER model for COPD disease endpoint.

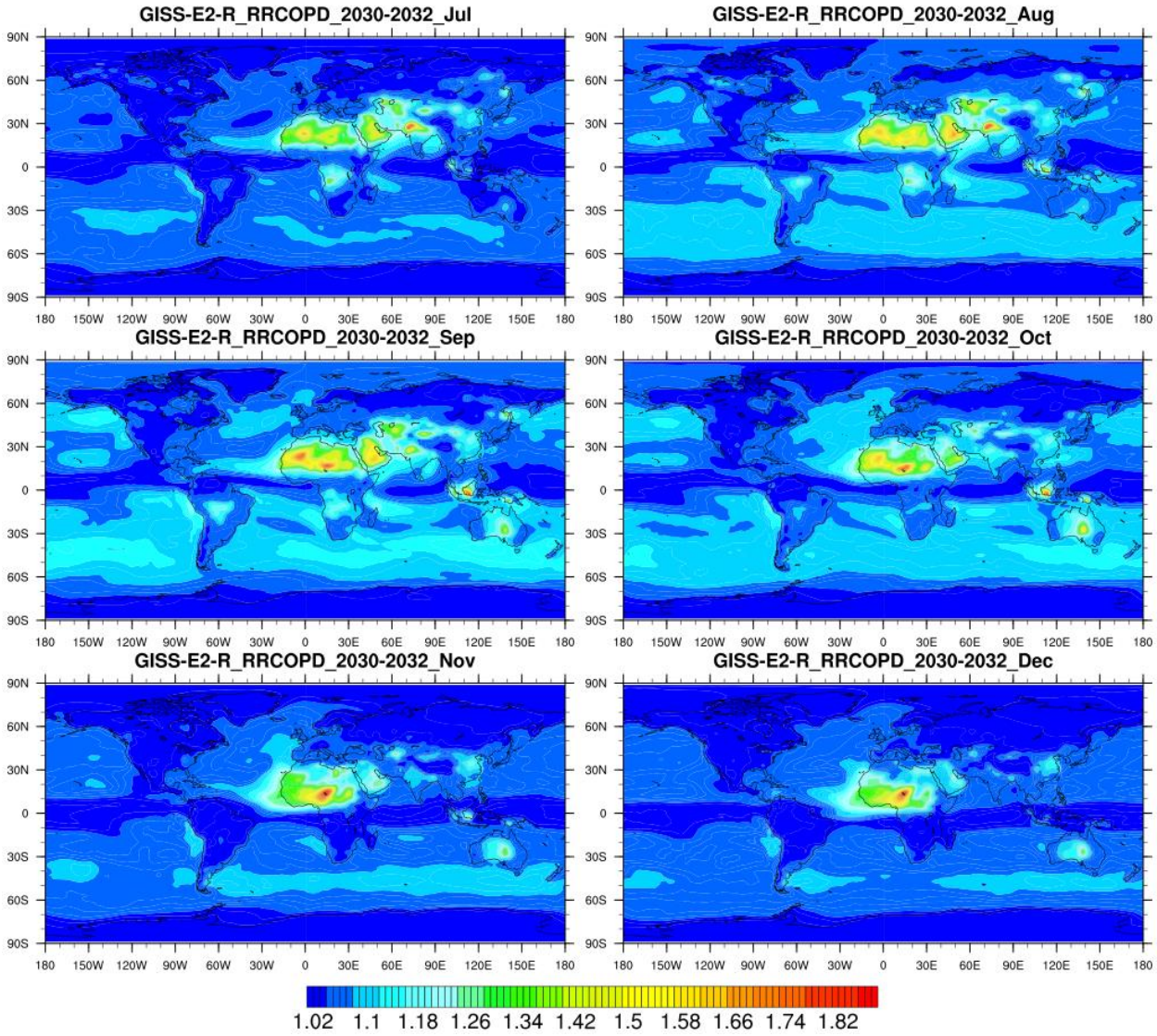


Figure 67 Global relative risk for cardiopulmonary disease from July to December of the three year average data from 2030 to 2032 with the ambient $PM_{2.5}$ concentration output from GISS-E2-R model based on the integrated risk function developed for GBD(Burnett et al., 2014b) for each figure, vertical axes indicate latitude and horizontal axes indicate longitude. The map plot indicate the monthly level of relative risk over a global terrain by applying the concentration-risk function from IER model for COPD disease endpoint.

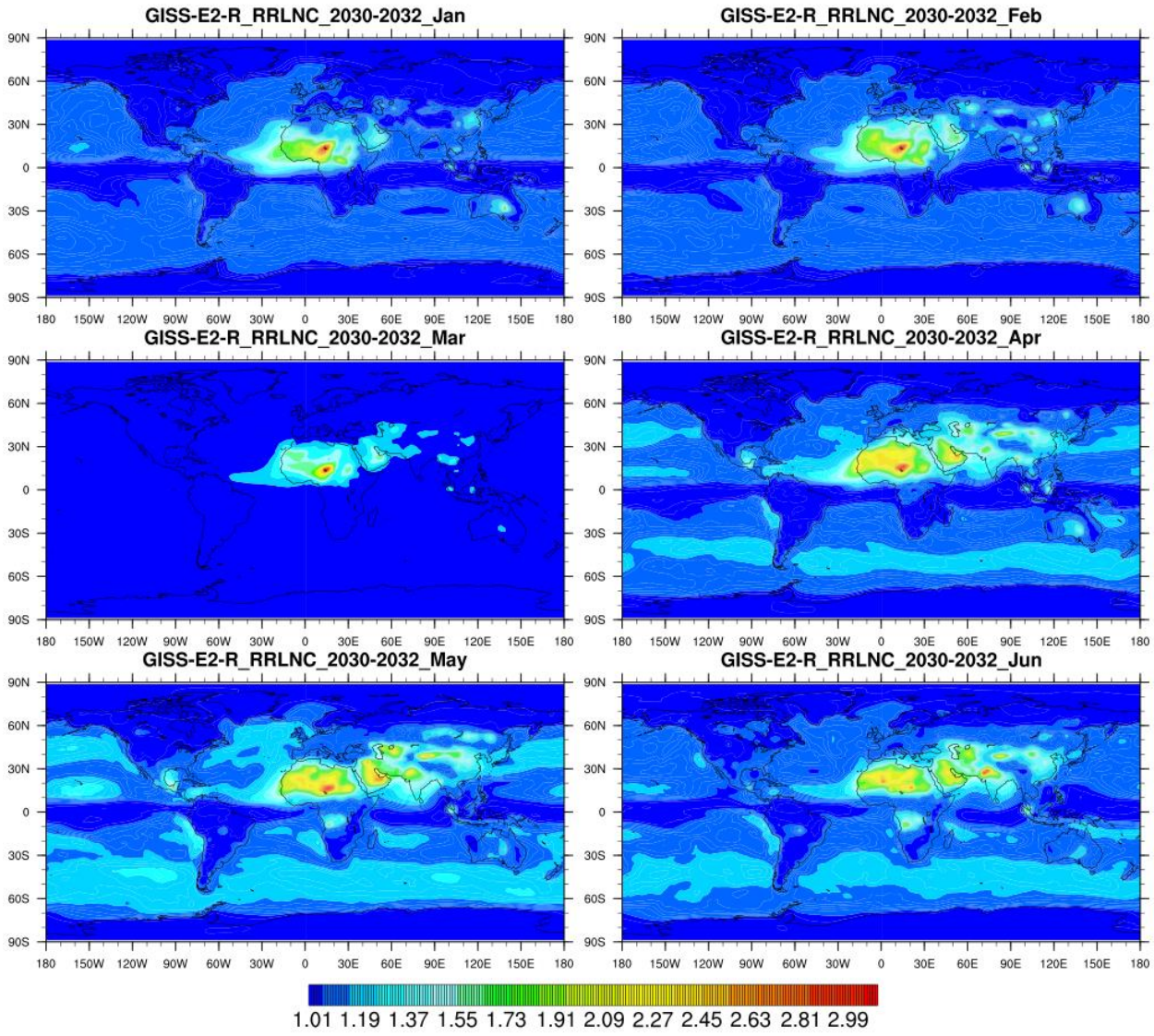


Figure 68 Global relative risk for lung cancer from January to June of the three year average data from 2030 to 2032 with the ambient $PM_{2.5}$ concentration output from GISS-E2-R model based on the integrated risk function developed for GBD(Burnett et al., 2014b) for each figure, vertical axes indicate latitude and horizontal axes indicate longitude. The map plot indicate the monthly level of relative risk over a global terrain by applying the concentration-risk function from IER model for LNC disease endpoint.

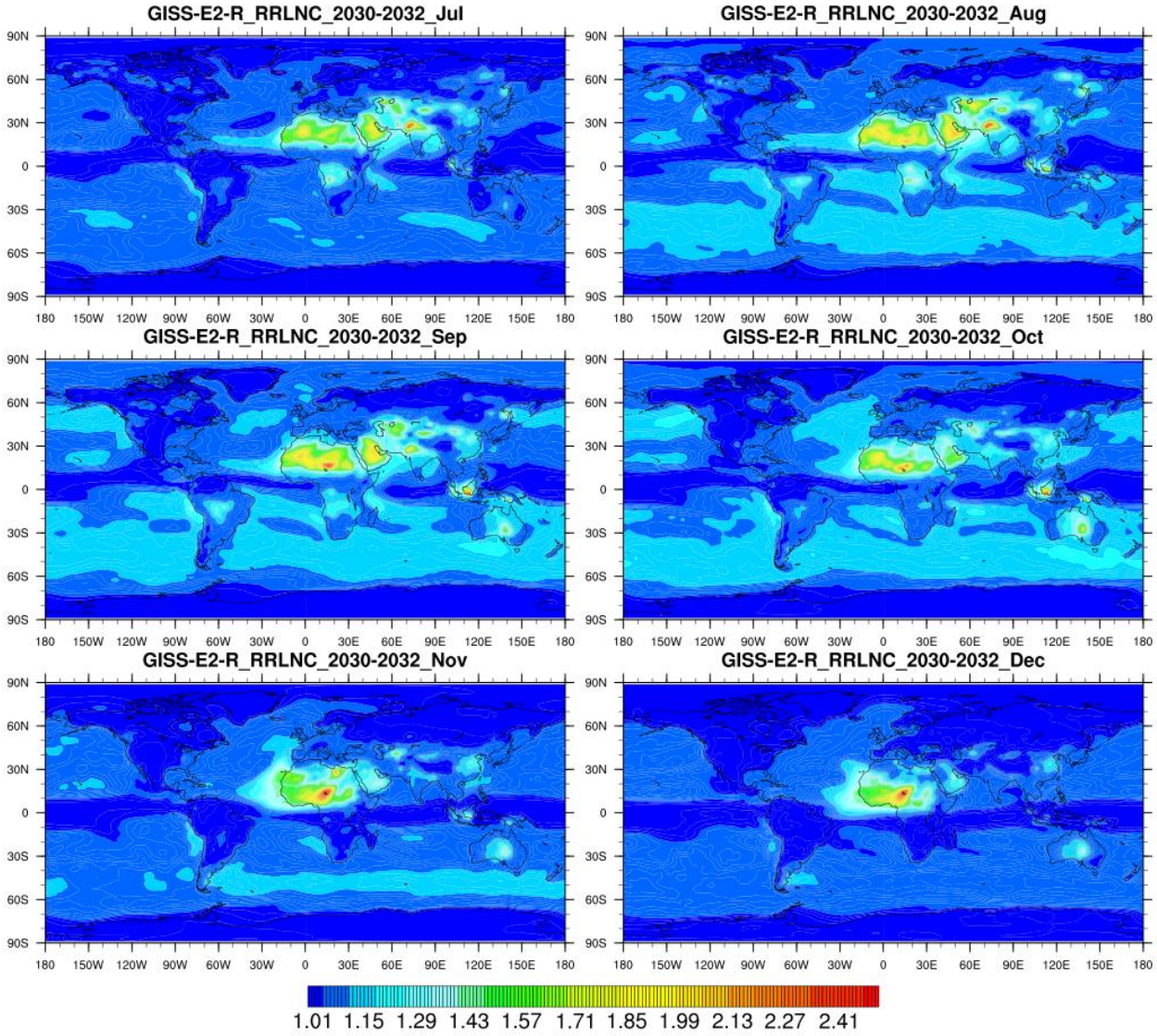


Figure 69 Global relative risk for lung cancer from July to December of the three year average data from 2030 to 2032 with the ambient $PM_{2.5}$ concentration output from GISS-E2-R model based on the integrated risk function developed for GBD(Burnett et al., 2014b) for each figure, vertical axes indicate latitude and horizontal axes indicate longitude. The map plot indicate the monthly level of relative risk over a global terrain by applying the concentration-risk function from IER model for LNC disease endpoint.

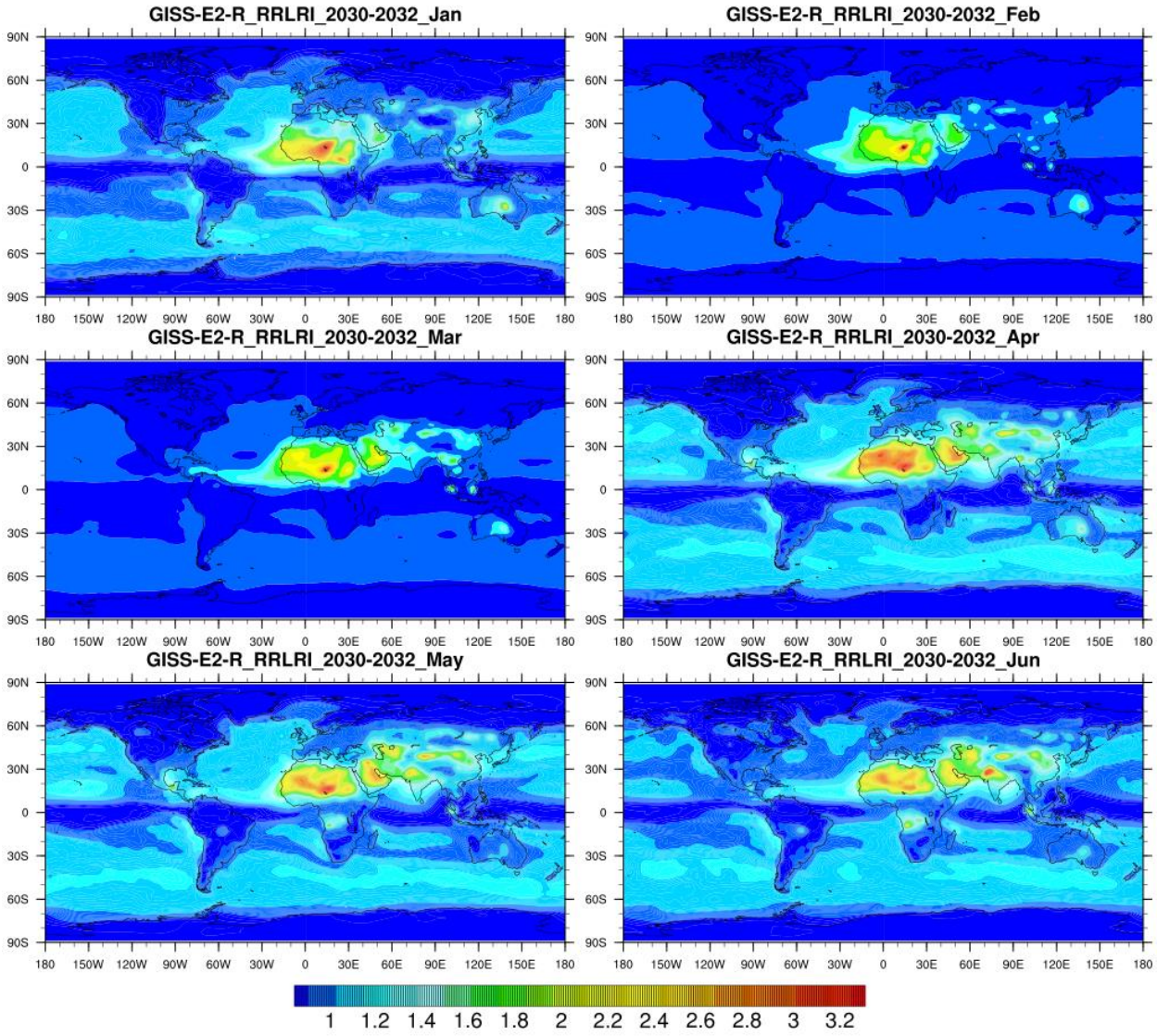


Figure 70 Global relative risk for lower respiratory infection from January to June of the three year average data from 2030 to 2032 with the ambient $PM_{2.5}$ concentration output from GISS-E2-R model based on the integrated risk function developed for GBD(Burnett et al., 2014b) for each figure, vertical axes indicate latitude and horizontal axes indicate longitude. The map plot indicate the monthly level of relative risk over a global terrain by applying the concentration-risk function from IER model for LRI disease endpoint.

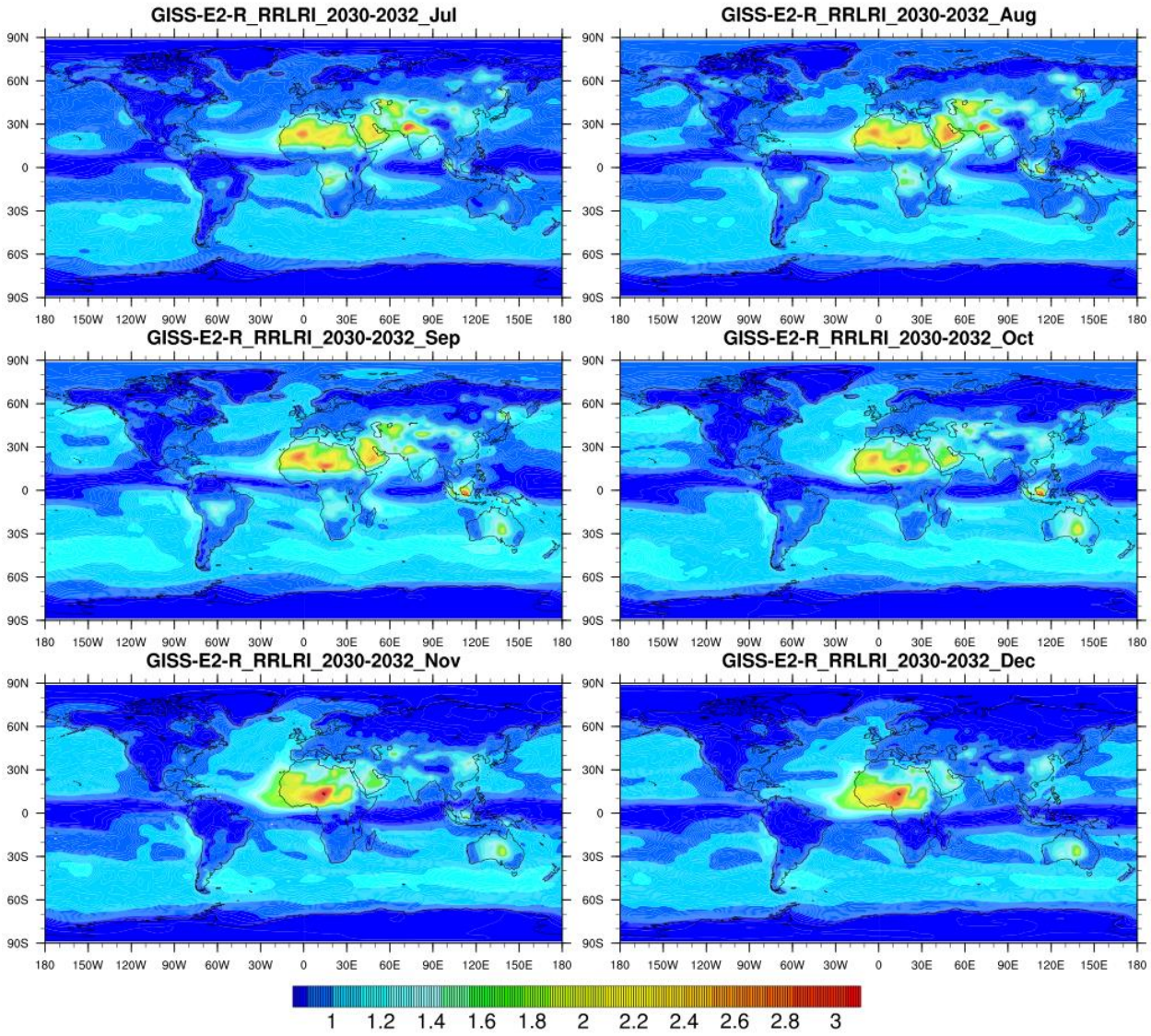


Figure 71 Global relative risk for lower respiratory infection from July to December of the three year average data from 2030 to 2032 with the ambient $PM_{2.5}$ concentration output from GISS-E2-R model based on the integrated risk function developed for GBD(Burnett et al., 2014b) for each figure, vertical axes indicate latitude and horizontal axes indicate longitude. The map plot indicate the monthly level of relative risk over a global terrain by applying the concentration-risk function from IER model for LRI disease endpoint.

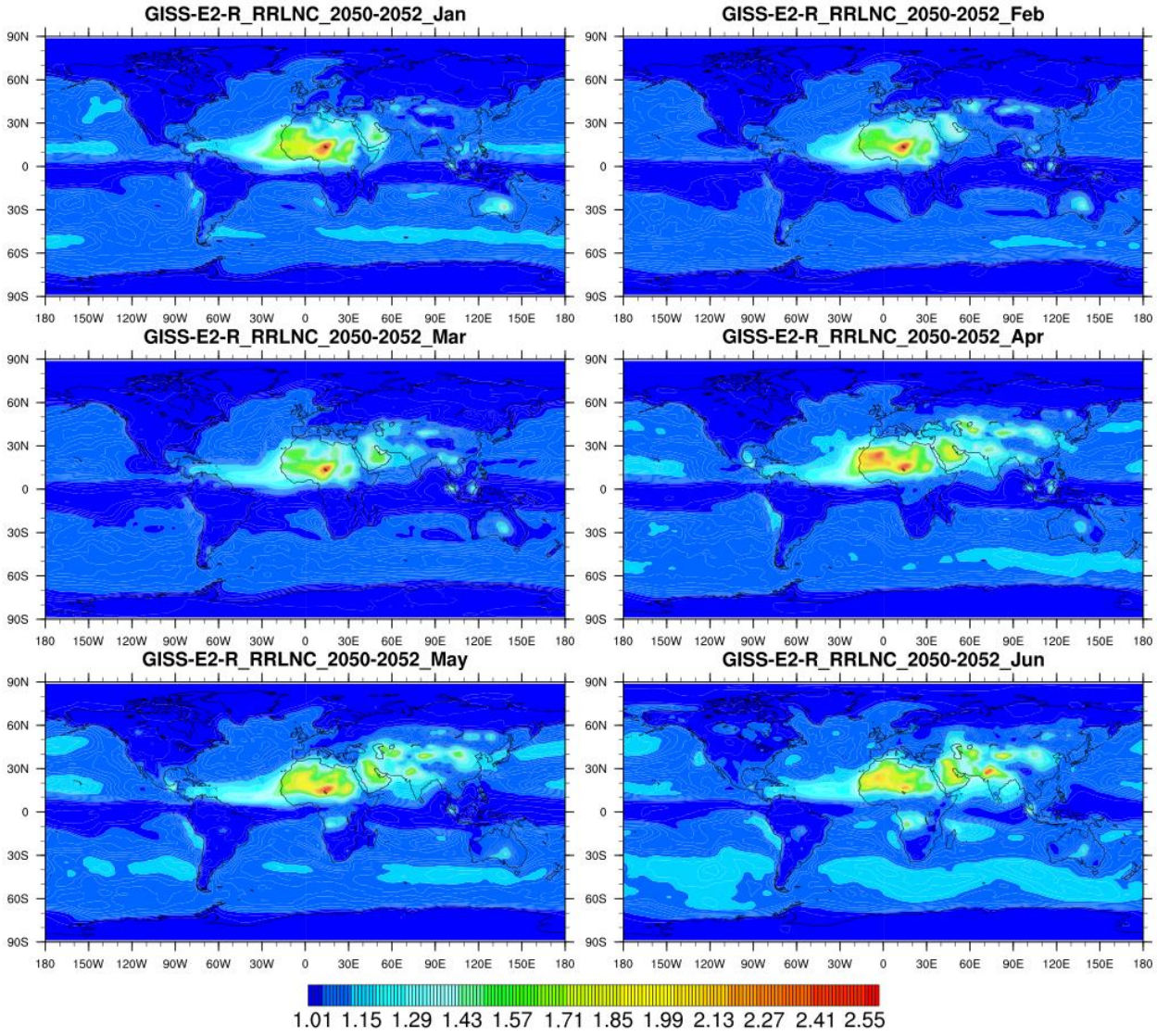


Figure 72 Global relative risk for lung cancer from January to June of the three year average data from 2050 to 2052 with the ambient $PM_{2.5}$ concentration output from GISS-E2-R model based on the integrated risk function developed for GBD(Burnett et al., 2014b) for each figure, vertical axes indicate latitude and horizontal axes indicate longitude. The map plot indicate the monthly level of relative risk over a global terrain by applying the concentration-risk function from IER model for LNC disease endpoint.

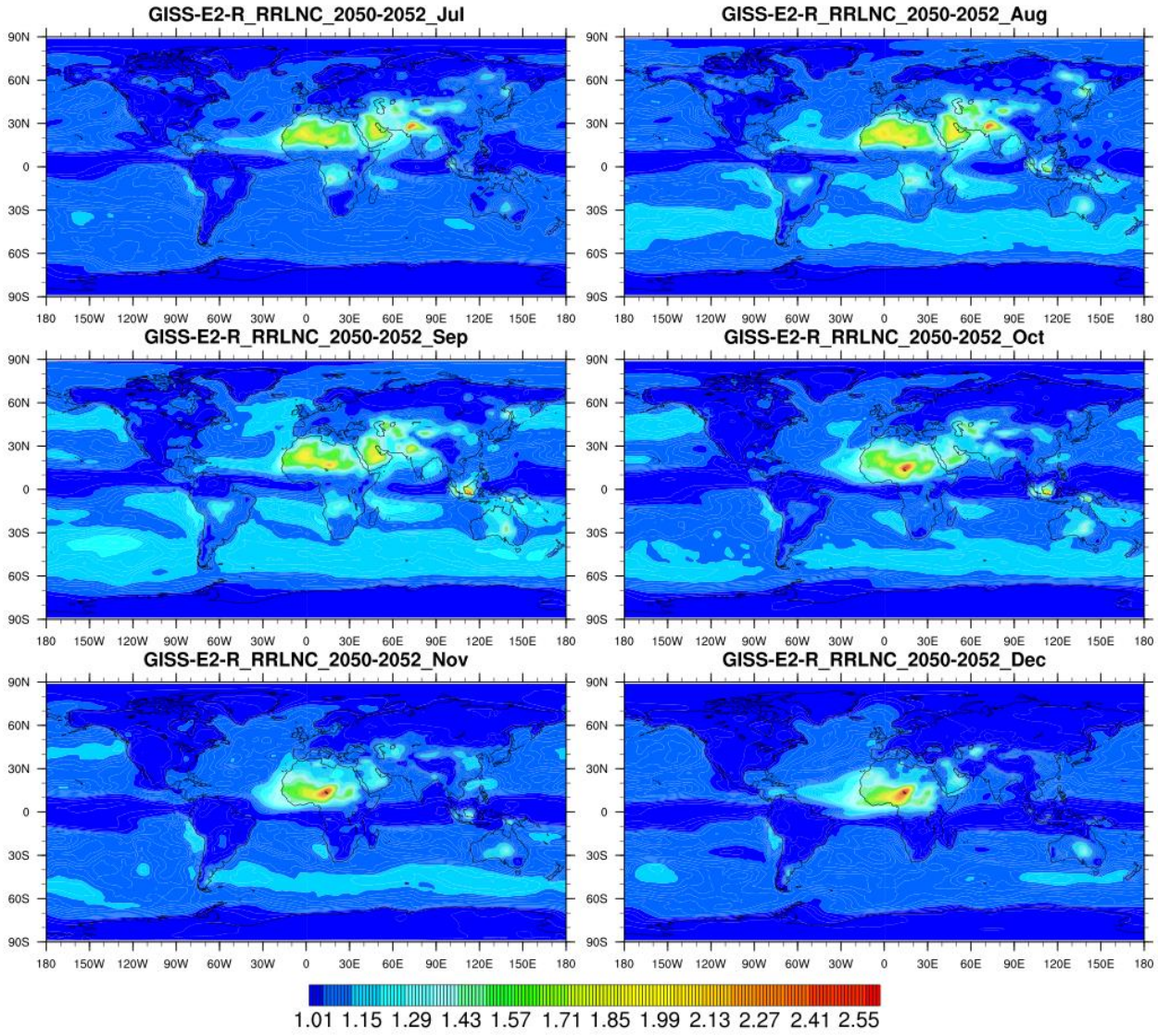


Figure 73 Global relative risk for lung cancer from July to December of the three year average data from 2050 to 2052 with the ambient $PM_{2.5}$ concentration output from GISS-E2-R model based on the integrated risk function developed for GBD(Burnett et al., 2014b) for each figure, vertical axes indicate latitude and horizontal axes indicate longitude. The map plot indicate the monthly level of relative risk over a global terrain by applying the concentration-risk function from IER model for LNC disease endpoint.

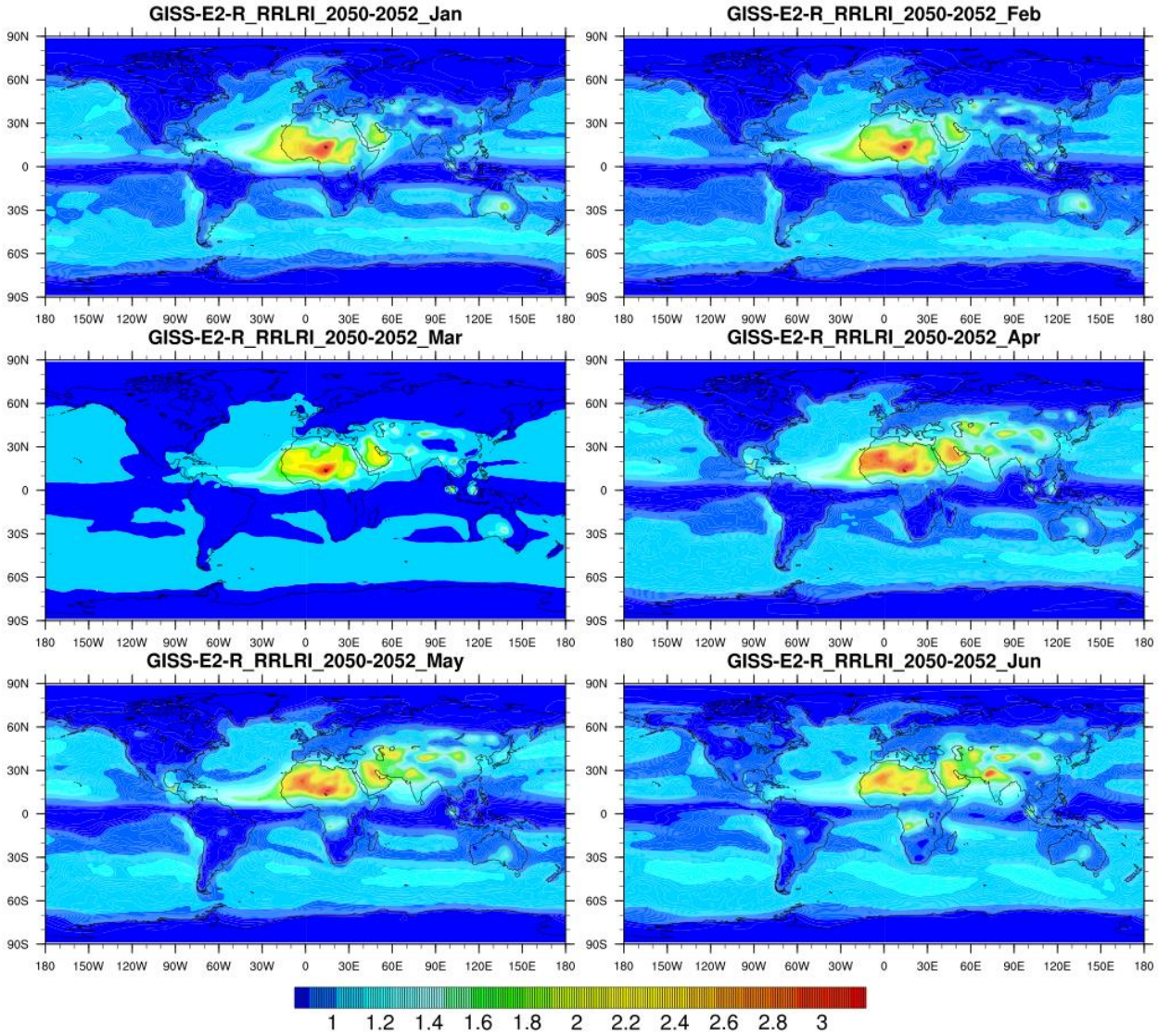


Figure 74 Global relative risk for lower respiratory infection from January to June of the three year average data from 2050 to 2052 with the ambient $PM_{2.5}$ concentration output from GISS-E2-R model based on the integrated risk function developed for GBD(Burnett et al., 2014b) for each figure, vertical axes indicate latitude and horizontal axes indicate longitude. The map plot indicate the monthly level of relative risk over a global terrain by applying the concentration-risk function from IER model for LRI disease endpoint.

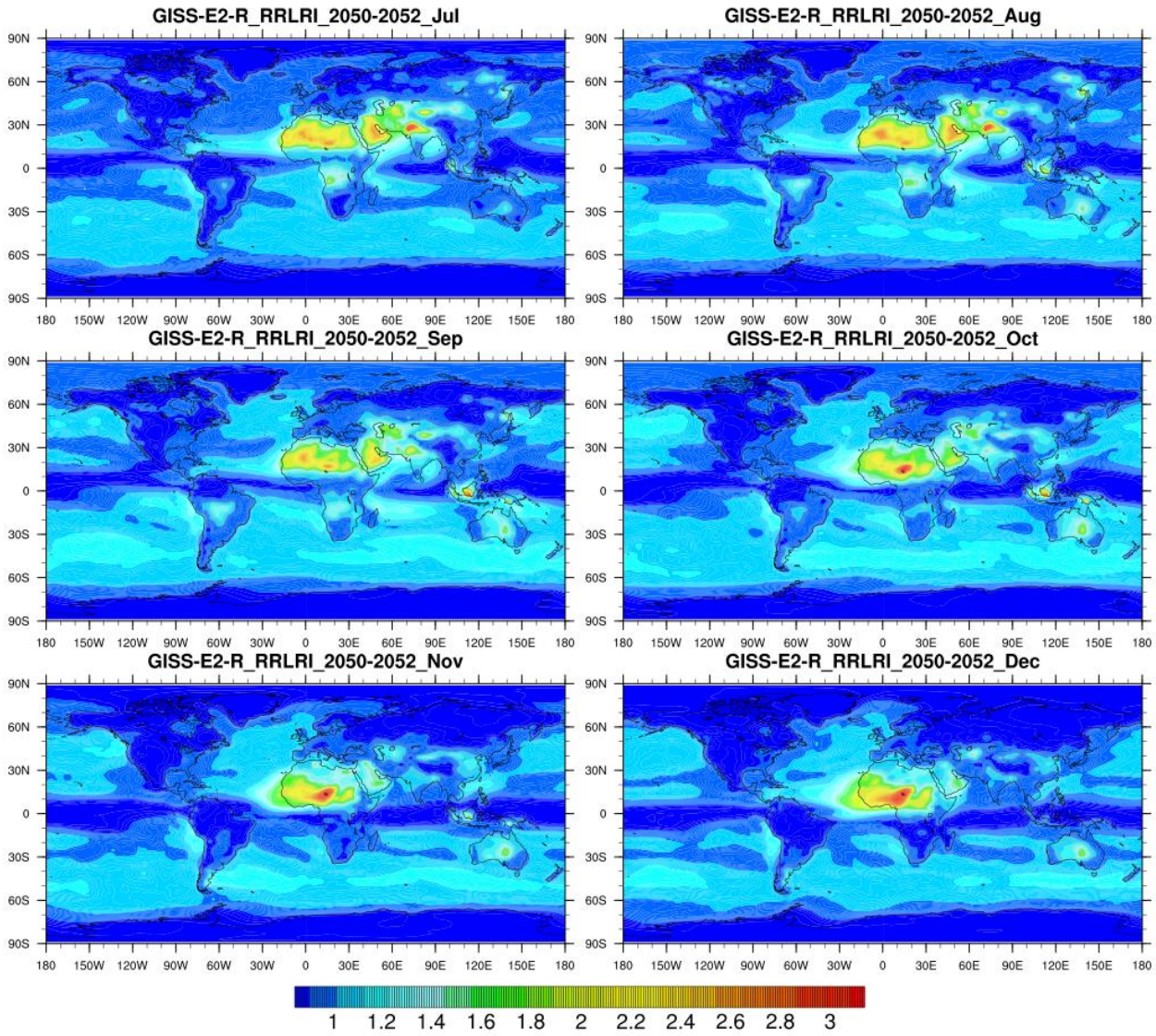


Figure 75 Global relative risk for lower respiratory infection from July to December of the three year average data from 2050 to 2052 with the ambient $PM_{2.5}$ concentration output from GISS-E2-R model based on the integrated risk function developed for GBD(Burnett et al., 2014b) for each figure, vertical axes indicate latitude and horizontal axes indicate longitude. The map plot indicate the monthly level of relative risk over a global terrain by applying the concentration-risk function from IER model for LRI disease endpoint.

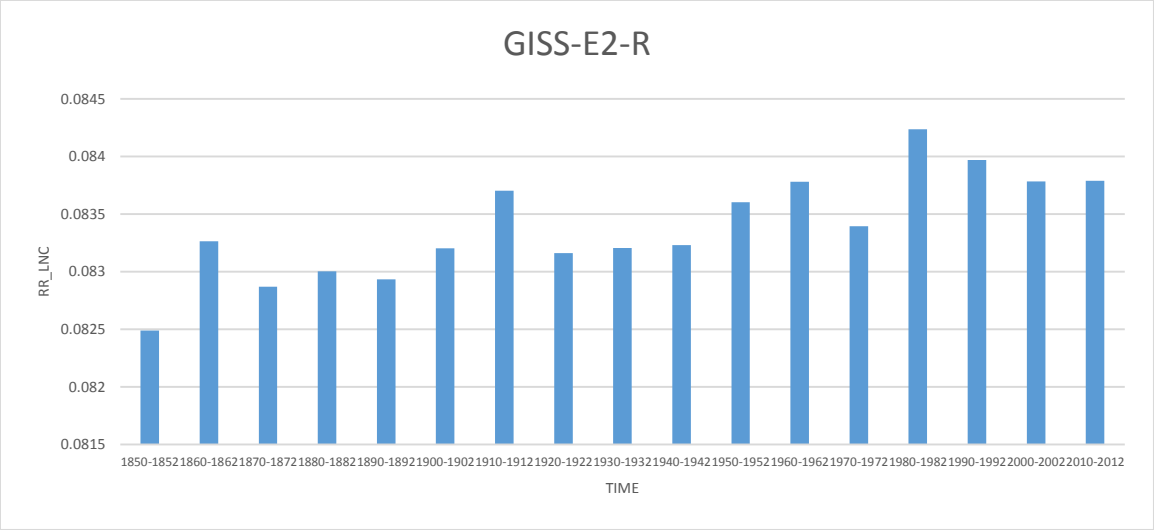


Figure 76 Grid averaged LNC relative risk value for GISS-E2-R from 1850s to 2010s. Grid average is a depiction of how the relative risk level has developed globally since preindustrial times. There is a general increasing trend since pre-industrial times.

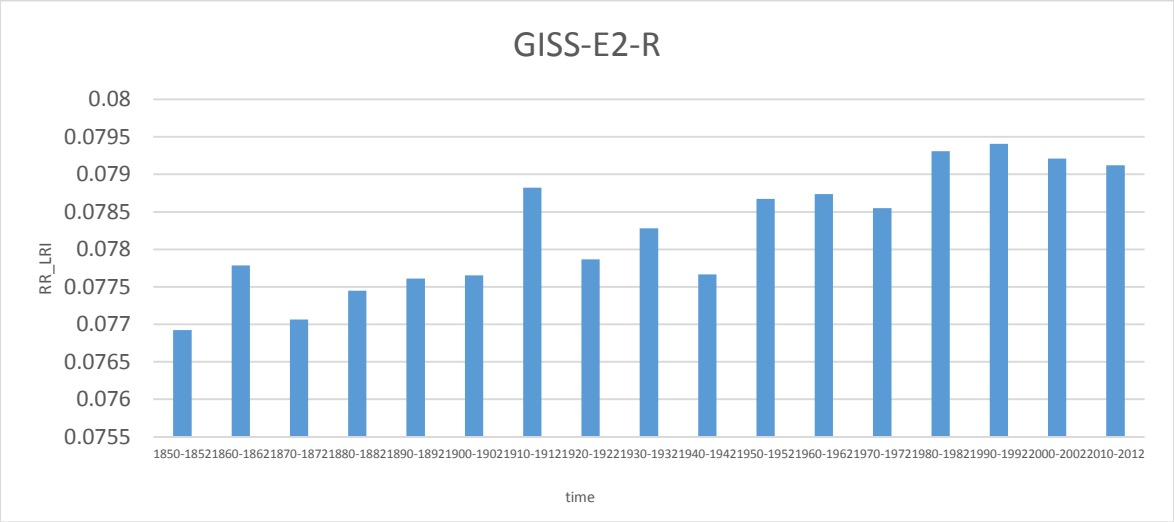


Figure 77 Grid averaged LRI relative risk value for GISS-E2-R from 1850s to 2010s. Grid average is a depiction of how the relative risk level has developed globally since preindustrial times. There is a general increasing trend since pre-industrial times.

EPA	environmental protection agency
GBD	global burden of disease
IHD	ischemic heart disease
BenMAP-CE	Environmental Benefits Mapping and Analysis Program - Community Edition
C-R	concentration-response
ACCMIP	Atmospheric Chemistry and Climate Model Intercomparison Project
$PM_{2.5}$	particle matter with aerodynamic diameter less than 2.5 micrometer
PM_{10}	particle matter with aerodynamic diameter less than 10 micrometer
PM10-2.5	particle matter with aerodynamic diameter between 2.5 and 10 micrometer
EC	elemental carbon
OC	organic carbon
CRFs	concentration-response functions
IER	integrated exposure-response
COPD	chronic obstructive pulmonary disease
YLDs	Years lived with disability
RR	relative risk
SAT	Systematic Approach to Training
WHO	World Health Organization
AOD	aerosol optical depth
BC	black carbon
OA	organic aerosol
SOA	secondary organic aerosol
SS	sea slat
SSP	Shared Socio-economic Pathways
LRI	lower respiratory infection
LNC	lung cancer
DC	developed countries
CIS	Caucasus and Central Asia
NA	Northern Africa
LAC	Latin America and the Carribbean
EA	Eastern Asia
SA	Southern Asia
SEA	South-eastern Asia
WA	Western Asia
O	Oceania

VITA

Xiufen Zhu was born in Shanghai, China. She got her B.S. in environmental science from Fudan University. She is continuing her education with a M.S. in environmental engineering at the University of Tennessee, Knoxville.